Stephan Weixler, BSc

Investigation of the process parameters regarding the uniaxial die compaction of ceramic granules

MASTER'S THESIS

to achieve the university degree of

Diplom-Ingenieur

Master's degree programme: Chemical and Process Engineering

submitted to

Graz University of Technology

Supervisor

Ao.Univ.-Prof. Dipl.-Ing. Dr.techn. Gernot Krammer

Institute of Process and Particle Engineering

Graz, April 2018

AFFIDAVIT

I declare that I have authored this thesis independently, that I have not used other than the declared sources/resources, and that I have explicitly indicated all material which has been quoted either literally or by content from the sources used. The text document uploaded to TUGRAZonline is identical to the present master‘s thesis.

18.5.18

Date

Signature

Abstract

The uniaxial die compaction process for the manufacturing of a ceramic disc electrode, made from lead magnesium niobite, was examined. The influence of a variety of process parameters, ranging from the particle properties, to the die filling equipment as well as the operating conditions of the hydraulic press, have been examined regarding their impact on the properties of the compacted green parts in a controlled experimental context.

The experimental manufacturing runs were carried out by pressing a batch containing 500 parts for each individual experiment, while selectively isolating one or more process parameters. The resulting green parts were analyzed regarding their weight, thickness and their inner and outer diameter, as well as the part-to-part variation of these properties throughout the manufacturing run.

Two different binder formulations were tested, with one of them (PTC) showing more consistent part-to part green part properties as well as no significant volume expansion after ejection from the die. The variation of the particle size distribution of the used granule batches, achieved through varying disk atomizer speeds during spray-drying, was found to have a significant, but non-linear correlation with the properties of the green part. A lower residual moisture content as well as a lower organic content in the granule batches were strongly correlated with reduced part-to-part variation of the green part properties. Furthermore, a lower axial green strength was also correlated with reduced part-to-part variation of the green part properties. The increase of the machine stroke rate from 15 to 20 parts per minute has yielded mixed results, depending on the employed binder system. The impact of the internal force control mechanism of the hydraulic press could not be sufficiently determined, however the standard deviation of the compaction force was shown to strongly correlate with the weight and thickness of the manufactured green parts. Through the comparison of two different filling shoe and feeding funnel designs, it was shown that the shape and geometry of the die filling equipment has a significant influence on the green part properties.

The most significant impact on the green part properties and their part-to-part variation, was achieved by means of a pseudo-sieving process, where the granule batches where either

sieved directly after granulation or prior to pressing with a metal screen (mesh width of 200 µm), that resulted in no leftover particle residue on the screen, or through the implementation of a screen directly into the filling shoe chamber. However, the exact mechanism of action that resulted in the lowered part-to-part variation of the green part properties could not be determined.

Kurzfassung

Der Prozessschritt des uniaxialen Pressens für die Herstellung einer keramischen Scheibenelektrode, bestehend aus Bleimagnesiumniobat, wurde untersucht. Der Einfluss einer Vielzahl von Prozessparametern, ausgehend von den Partikeleigenschaften hin zu den verwendeten Werkzeugen und den Betriebsbedingungen der hydraulischen Presse, wurden hingehend ihrer Auswirkung auf die Eigenschaften der gepressten Grünteile in einem kontrollierten experimentellen Umfeld untersucht.

Bei jedem experimentellen Fertigungslauf wurden jeweils 500 Presslinge angefertigt mit dem Ziel, einen oder mehrere Prozessparameter zu variieren. Die daraus resultierenden Grünteile wurden hinsichtlich Gewicht, Dicke, Innen- und Außendurchmesser vermessen und statistisch ausgewertet, um den Pressling zu charakterisieren und die Streuung innerhalb eines Fertigungslaufs auszuwerten.

Zwei verschiedene Bindemittel wurden getestet, wobei sich bei Einsatz des „PTC“ Binders eine geringere Streuung der Grünteileigenschaften gezeigt hat, zudem trat auch keine signifikante Volumenausdehnung nach Ausstoß aus dem Pressstempel auf. Die Variation der Korngrößenverteilung, durch Anpassung der Drehzahl des Scheibenzerstäubers beim Sprühtrocknungsprozess, zeigte eine signifikante und nichtlineare Korrelation mit den Grünteileigenschaften. Sowohl ein geringerer Restfeuchtegehalt als auch ein geringerer organischer Anteil in den verwendeten Granulatchargen korrelierten stark mit einer niedrigeren Streuung der Grünteileigenschaften. Des Weiteren hat sich gezeigt, dass eine niedrigere axiale Grünteilfestigkeit auch stark mit einer geringeren Streuung der Grünteileigenschaften korreliert. Das Erhöhen der Maschinentaktung von 15 auf 20 Hübe pro Minute hat, je nach Bindemittel, kein eindeutiges Ergebnis nach sich gezogen. Der Einfluss des internen Presskraftregelungsmechanismus der hydraulischen Presse konnte nicht festgestellt werden. Es hat sich jedoch eine starke Korrelation zwischen der Standardabweichung der Presskraft und der Standardabweichung des Gewichts und der Dicke des Grünteils gezeigt. Durch den Vergleich von zwei verschiedenen Füllschuhen und Beschickungstrichtern hat sich gezeigt, dass die Form und Geometrie der Füllwerkzeuge einen signifikanten Einfluss auf die Grünteileigenschaften hat.

Den größten Einfluss auf die Grünteileigenschaften und die Streuung dieser, wurde durch Anwendung eines Pseudo-Siebungsprozesses erreicht. Hierbei wurden die Granulatchargen entweder direkt nach der Granulierung oder kurz vorm Pressen durch ein konventionelles Metallsieb mit einer Sieböffnungsgröße von 200 µm hindurchgesiebt, wobei jedoch keine nennenswerten Rückstände am Sieb zurückblieben. Des Weiteren zeigte sich ein ähnlich gutes Ergebnis hinsichtlich der Grünteileigenschaften beim direkten Einbau eines Metallgitters in den Füllschuh. Es konnte jedoch der exakte Wirkmechanismus, der für die verringerte Streuung der Grünteileigenschaften verantwortlich ist, nicht bestimmt werden.

Acknowledgement

I would like to express my gratitude to all those who supported and guided me during the preparation of this master thesis.

First, I want to give thanks to Ao.Univ.-Prof. Dipl.-Ing. Dr.techn. Gernot Krammer, who has supervised and assessed my master thesis, for his continued support and advice as well as his guiding hand over the course of this thesis.

I would also like to thank my company supervisor Dipl.-Ing Josef Mörth, for his continued support and guidance during the planning, preparation and execution of the experiments.

I would also like to extend gratitude to the EPCOS OHG, especially the Piezo and Protection Devices Business Group, for initiating this thesis and offering me the chance to conduct the experimental part of my master thesis in a leading industry environment.

Furthermore, I would like to thank the RCPE (Research Center Pharmaceutical Engineering GmbH) for allowing me to carry out some measurements with their in-house equipment.

Table of Contents

Nomenclature and abbreviations

Latin Symbols

A	Measured area of the particle projection [µm]
BPP	Break point pressure [MPa]
b/l_3	Aspect ratio [-]
C	Cohesiveness of the green compact [-]
e_a	Green compact radial expansion [-]
f	Mass fraction of the fine material [-]
F	Force which acts on the mechanically driven matrix
ff_c	flow function [-]
g	Mass fraction of the coarse material [-]
GV	Ignition loss [-]
ΔH	Height differential of the mechanically driven matrix
P	Measured circumference of the particle projection [µm]
PMN	Lead magnesium niobate
p_{nc}	Net isostatic pressure for the test compact [MPa]
n_k	Channel wheel rotation speed [rpm]
Q_A	Cumulative density distribution of the feed material [-]
Q_G	Cumulative density distribution of the coarse material [-]
Q_F	Cumulative density distribution of the fine material [-]
r_1, r_2	range from the center of the projected area to the borders in the measuring direction.
$SPHT_3$	Sphericity of particle projection [-]
$Symm_3$	Symmetry of the particle [-]
$\dot{V}_k$	Volume flow ion the channel wheel separator [Nm³/h]
w_{sa}	Axial strength of the test compact [MPa]
X_{10}	Max. particle diameter of the lowest decile [µm]
X_{50}	Median particle diameter [µm]
X_{90}	Min. diameter of the highest decile [µm]
$x_{c\,min}$	particle width of the shortest chord [µm]
$x_{Fe\,max}$	longest Feret diameter [µm]

Greek Symbols

β	Angle of repose [°]
σ_1	Major Principal Stress [MPa]
σ_c	Unconfined Yield Strength [MPa]

1. Introduction

New developments in the field of ceramics over the last few decades have led to the emergence of so called high performance ceramics, which allow for unique property profiles and use cases that cannot be achieved with traditional metal- or synthetic-based materials. They are usually classified by their composition into oxide-based ceramics, where metal oxides, such as aluminum oxide, form the basis of the ionic bond dominant crystalline structure, and into non-oxide ceramics, such as carbides, nitrides and borides which display a higher degree of covalent bonding. Depending on the composition and type, advanced ceramic materials offer a multitude of exceptional properties, for example an immense heat resistance that is utilized in heating elements and furnace tiles. They also offer a high degree of electrical insulation used for ceramic capacitors and other electronic components, several compositions display piezoelectric properties which are used in the manufacturing of quartz crystals, sensors and actuators. Ceramic materials with a high hardness and notable resistance to abrasion and wear find use in many industrial applications such as bearings, sealings, cutting materials and nozzles. Another field of use is in the area of medical technology, where certain ceramic materials, e.g. zirconium dioxide, are used as implants because of their high durability and bio-inert properties. [1] [2]

But there are also other medical applications that involve the usage of high performance ceramics, such as so-called tumor treating fields therapy (TTFields). This novel treatment modality allows for a non-invasive therapy option that utilizes low-intensity and alternating electric fields at an intermediate frequency of 100-300 kHz to disrupt the critical phase of mitosis and organelle assembly in cancerous cells. These non-uniform electrical fields are transduced by an array of insulated disk-shaped ceramic electrodes and exert a dipole alignment as well as dielectrophoretic forces on the targeted cells to achieve the desired therapeutic effect. Said disc electrodes are manufactured out of lead magnesium niobate, which is characterized by its common ABO_3 cubic perovskite structure with a mixed B-site, distinct relaxor ferroelectric properties and its very high dielectric constant. At the beginning of the manufacturing process, the basic raw material is grinded down to ensure consistent baseline conditions, afterwards a water-based slurry is prepared before undergoing a spray-drying process to form proper granules. A dry uniaxial die compaction process, powered by hydraulics, is used to shape and compact the ceramic granules into the desired compacted green bodies. Subsequently the compacts undergo the thermal process of decarburization

and debinding before sintering at high temperatures to fuse the ceramic particles into a solid mass. Lapping is afterwards used to machine the parts to their geometric specifications regarding thickness and surface. Finally, one end face of the disk is metallized via screen printing and the following thermal curing. [3] [4]

The aim of this thesis is to establish the pivotal process parameters of the uniaxial die compaction and to quantify their influence on the compacted green body results in terms of weight and geometry as well as part-to-part variation. This will be achieved by selectively varying particle properties, die filling parameters as well as the operating conditions of the hydraulic presses in order to impact the various stages of the compaction cycle. The hereby manufactured compacted green bodies will be analyzed regarding their weight and geometry to allow for statistical comparison and evaluation. These findings will be used to devise recommendations for further process optimization and increased product quality.

2. Product background

The focus of this thesis is to examine the influence parameters of the uniaxial die compaction process that is part of the *EPCOS* manufacturing process for the *Novocure* NC-Disc. The NC-Disc, as shown in Figure 1, is a ceramic disc with an outer diameter of 19 mm and an inner diameter of 3,2 mm and a height of 1 mm. One side of the disc is metallized with a conductive silver plating with a margin of 1mm to both the inner and outer contour of the part. This ceramic disc is a key component for a novel cancer treatment method, known as tumor treating fields (TTFields). This therapy uses low intensity electric fields that are non-uniform and alternate at a specific frequency, with the aim of blocking the cell reproduction and interfering with the organelle assembly of a variety of tumor types. These electrical fields are emitted from transducer arrays that consists of 9 insulated ceramic discs each, and are placed onto the skin of the patient. This therapy has already been proven to be effective in the case of a tumor type known as glioblastoma. [3]

Figure 1: The finished Novocure NC-Disc [5]

2.1. Process flow

The following chapter gives a brief overview of the entire manufacturing process, as depicted in Figure 2, of the ceramic disc, beginning with the granule production and ending with the optical inspection and subsequent delivery of the finished ceramic product.

The sourced raw material, lead magnesium niobate, is at first grinded down into a submicron powder to prepare to produce a water based suspension. This slurry is containing the primary material, lead magnesium niobate and the various ceramic additives that are added with the

aim of improving the granule production process. This slurry is then agglomerated in a controlled manner by the means of a spray-drying process. The finished granule batches are then stored until they are further processed.

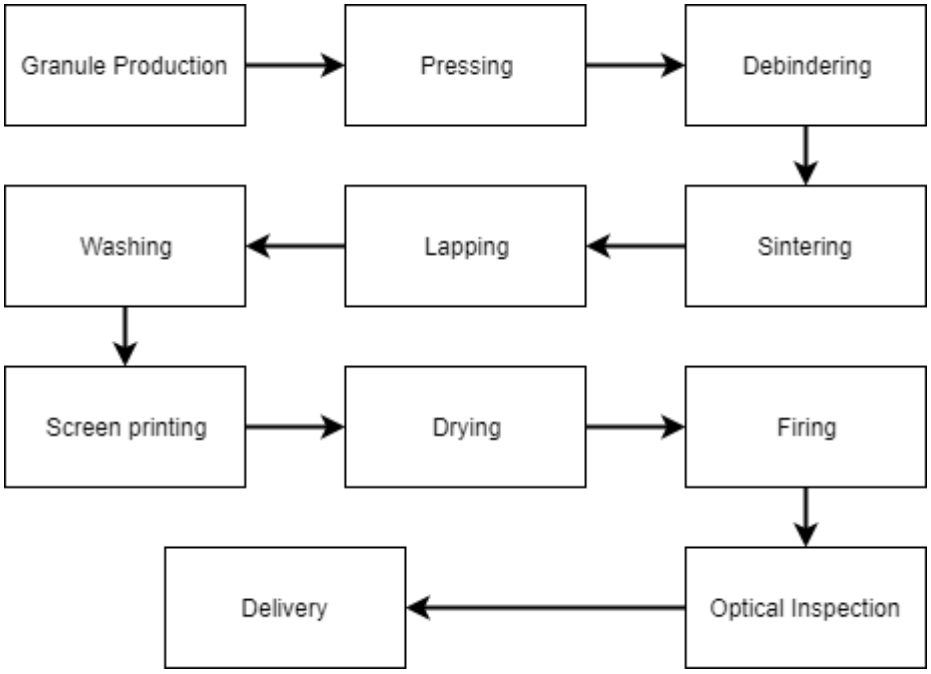

Figure 2: Schematic depiction of the entire manufacturing process of the ceramic "NC-Disc"

In the next processing step, the granulate is densified into a solid mass of material, known as the green part, by using a dry uniaxial die pressing process. This is achieved by using a hydraulic press with a two-sided pressing configuration. In this case, the densification is carried out by the upper punch and a mechanically driven matrix that is lowered concurrently during compaction and a fixed lower punch. The ejected green parts are then stacked onto a tray and prepared for the debindering process.

The stacked tray full of green parts is then put into a batch furnace to burn out the organic residue, caused by the ceramic additives, and effectively decarburize the ceramic discs. Afterwards they are placed into another batch furnace for the firing process at high temperature to sinter the green part into the finished ceramic microstructure. During this process the parts lose a significant amount of volume, due to the process of grain growth and pore elimination. This is also the process step where the electrical properties of the ceramic material pronounce themselves.

The ceramic disc is then undergoing a process of hard machining, namely lapping. This process step is necessary to achieve the final thickness and to ensure a smooth surface. Afterwards they are washed by the means of an ultrasonic cleaning equipment to remove any residue that remained on the surface of the ceramic disc.

To transform the ceramic disc into an electrode, the plating of one of the end sides is necessary. A metallic screen printing process is used to apply a silver paste onto the disc. After an appropriate amount of drying the printed disc is going through a tunnel furnace to sinter the silver paste into a solid plating.

Now the finished ceramic discs are examined for visual defects, the desired electrical properties, the geometrical characteristics and the adhesion of the silver plating before they are packed and prepared for delivery.

3. Theoretical background

This chapter lays out the theoretical foundation of this thesis. At first, there is a broader description of technical ceramics and the various materials and manufacturing processes that are employed as well as the different applications. Afterwards there is a deeper examination of how the ceramic green parts are formed and shaped, with closer look at the dry uniaxial die compaction and its influencing parameters, which is the centerpiece of the experimental setup of this thesis. In addition, the influence of the granulation process on the particle compaction and green parts is further detailed.

3.1. Technical ceramics

Ceramics materials have been established for a wide array of use cases, and are characterized by their exceptional hardness, wear and corrosion resistance, endurance for high temperatures as well as their unique electrical properties. They are generally defined as inorganic and non-metallic and are usually shaped from raw material and then undergo a high temperature firing process. Technical ceramics usually refers to ceramic materials and products that are designed for specific engineering applications. Such as cutting tool ceramics that are selected for their wear and temperature resistance, construction ceramics that rely on their ability to withstand mechanical stresses. Electrical ceramics display highly unique behaviors in relation to conductivity, non-linear resistance, ionic conduction and ferroelectricity. [6] [1]

3.1.1. Material description

Technical ceramics can be divided and classified into distinct subgroups by using various parameters. One of them is their mineralogical and chemical composition, by which ceramic materials are clustered into the three following groups:

- Silicate ceramics
- Oxide ceramics
- Non-oxide ceramics

Silicate ceramics represent the oldest group amongst ceramic materials and occupy the largest proportion of fine ceramic products. From the chemical point of view, silicon and oxygen forms the major building blocks of these materials and these are commonly sourced from minerals like clay, kaolin, feldspar and soapstone. In addition, components like alumina and zircon are used to reinforce the properties of these materials, e.g. higher strength. Silicate ceramics themselves can be further subdivided into different groups based on their chemical composition and source material. Technical porcelain is understood to mainly consist out of silica and alumina (alkaline alumina silicate porcelain) and displays high mechanical strength, excellent dielectric properties as well as a high chemical resistance. Magnesium silicates consist mainly of silica, magnesia an alumina and show high mechanical strength, good dielectric properties and a low loss factor. The loss factor is a measure of the rate of energy that is lost due to oscillation in a dissipative system. Mullite ceramics consist of mullite ($3AL_2O_3*SiO_2$), alumina and silica and are characterized by their high strength, high thermal shock resistance and good creep resistance. Typical use cases for silicate ceramic products are insulators, fuse cartridges, catalysts, enclosures and refractory materials. [1] [6]

Oxide ceramics are generally understood as materials that are composed of a single phase and majority component metal oxide with little to no glass phase. The raw materials are usually synthetically derived with a high degree of purity. Therefore, a highly uniform microstructure can be achieved through high-temperature sintering. Oxide ceramics can be further subdivided into single-material systems such as aluminum oxide, magnesium oxide, zirconium oxide and titanium oxide. Aluminum oxide is the most prevalent oxide ceramic material for engineering purposes and is commonly used in a wide range of applications. It is characterized by a high strength and hardness, temperatures stability, and a high wear and corrosion resistance while still maintaining a favorable price/performance ratio. There are also multi-material systems, such as lead zirconium titanate which is known for its pronounced piezoelectric properties that are employed in various electronic parts and components that act as transducers, actuators or sensors. [1] [6]

Non-oxide ceramics are based on components such as boron, carbon nitrogen and silicon. Their high proportion of covalent compounds, which enables truly unusual properties, allows

for usage at very high temperatures, furthermore they display very high elastic modulus, high strength and hardness, while still maintaining strong resistance to corrosion and wear. The manufacturing process for non-oxide ceramics is generally considered to be more expensive in comparison to their oxide counterparts, because the raw materials must be extremely fine grained, and an inert oxygen-free sintering process of up to 2000 °C is required. The most used non-oxide ceramics are silicon carbide, silicon nitride, aluminum nitride, boron carbide and boron nitride. They are used for the manufacturing of cutting tools (wolfram carbide), rocket nozzles (TiB_2), heating elements ($MoSi_2$) and as super-hard abrasives (B_4C). [1] [6]

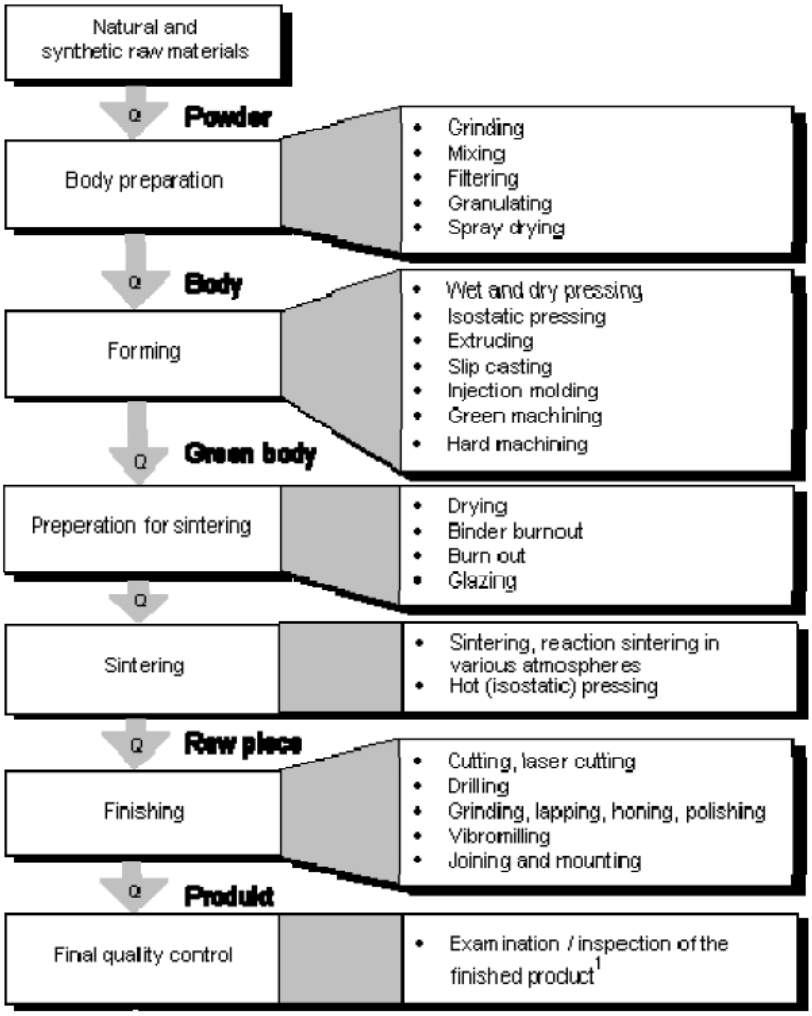

Figure 3: Scheme of the ceramic manufacturing process [6]

The properties of a given ceramic product are primarily influenced by the sourcing and processing of the raw materials and the body preparation, the forming of the compacted green part and the firing process known as sintering. The entire manufacturing process, as depicted in Figure 3 is more complex, but these three process steps determine the

microstructure of the finished ceramic body, which in turn determines the mechanical, chemical, thermal and electrical properties that are displayed. [1] [6]

3.1.2. Raw material and body preparation

The raw material can be derived from both natural and synthetic sources, and is usually chosen in terms of economic feasibility and product specifications regarding the purity, type, grain size and surface area. The sourced raw material usually is grinded down to achieve a desired grain size and distribution to prepare and mix the slurry. In addition to the raw material, ceramic additives, that serve a wide range of purposes, are added into the mixture at this stage. These organic or inorganic aids impact the various stages of the manufacturing process, such as sintering, forming and granulation. Depending on the forming process, the prepared slurry mixture is then used for casting, or further processed into granules or plastic material for pressing or extrusion. Granulated material is commonly created by the means of a spray drying process, with the goal to achieve high flowability and compressibility for the finished granular material. [1] [6]

3.1.3. Forming

The prepared material is then formed into a coherent shape, that is ideally resilient enough to withstand the subsequent handling further down the manufacturing chain. This shaped, but still unsintered mass is commonly referred to as a green body or green part. The different methods of forming said green bodies can be divided into three different groups that are defined by the mechanical act of forming and the used source material. [1] [6]

- Pressing
- Plastic forming
- Casting

The most used pressing methods are dry pressing, moist pressing and isostatic pressing. Dry pressing is used for the mass-manufacturing of ceramic products with a high precision. For this, non-clumping granulates with a very low moisture content (<4%) are compressed in appropriately designed dies that reflect the desired geometry of the green part. The compression is usually carried out in a single axis direction by either on ore two rigid

punches in a single or double ended fashion. The advantages of this forming method include the ease of automation, good reproducibility, high dimensional accuracy and its ability to easily scale to high-volume manufacturing. The costly manufacturing of the pressing tools and the granular material, the limitations of the possible part geometries and the unavoidable density gradients can be considered distinct disadvantages of this method. [1] [6]

Wet pressing is methodically the same as dry pressing except for the moisture content of the used powders. The higher moisture content of the granules allows the granular material to flow more freely, therefore more complex and intricate geometries, such as screw threads, recesses and undercuts can be manufactured. Additionally, this results in a more uniform density distribution of the green bodies. These advantages, that result from the higher moisture content, are counter acted by the fact that wet pressing materials usually can only accept lower compressive strains than dry pressing materials and warrant the introduction of an additional drying period before further processing. [1] [6]

Isostatic pressing is a forming process that is characterized by its equal application of compaction pressure in all directions by utilizing a pressured container and an elastic mould that encloses the green body. Through this process an exceptional high degree of uniformity of density and the underlying microstructure is achieved and simultaneously removing the geometrical limitations of uniaxial pressing. Isostatic pressing can be performed at ambient temperatures (cold isostatic pressing) but also at elevated temperatures and gas pressures (hot isostatic pressing) to further eliminate porosity and density gradients. The main disadvantage of this pressing method is the slow cycle time in comparison to the very high cycle times of up to 100 cycles per minute that are possible with uniaxial pressing. [1] [6]

Extrusion and injection moulding are the two commonly used plastic forming methods. The process of extrusion works by pressing homogenized plasticized mass through a nozzle by using a piston or vacuum screw as a feeding mechanism. The nozzle forms the material into a certain geometry, ideally rotationally symmetrical parts of indefinite lengths. Injection moulding utilizes the high-pressure injection of plasticized mass (a shot) to fill the geometry of the mould and is principally suited for the mass production of very complex parts. [1] [6]

Slip casting is a relatively simple forming method, that is mostly used for the manufacturing of parts with complex geometries, large dimensions or for prototyping. Forming is achieved by pouring a stable suspension, referred to as the slip, onto a porous, absorbent plaster mould. Extraction of the resulting suspended liquid causes thin layers of particles to develop on the mould walling. This process is selectively repeated until the part is fully cast. In a process called tape casting, a ceramic slip is continuously poured from a reservoir onto an endless steel strip carrier. This flow can be regulated by an adjustable strip and is subsequently dried by hot air which results in a flexible tape of green ceramics. This tape can then be further processed through cutting, punching, stamping or other similar methods. [1] [6]

The choice of the appropriate forming process is often decided by a myriad of different factors. These factors range from the requirements of the source material and the subsequent handling of the particles to the geometry and tolerances of the desired parts. Furthermore, economic factors such as the process costs and the lot sizes should be considered as well. [1] [6]

3.1.4. Preparation for sintering

Formed green bodies usually carry a significant amount of moisture and often organic additives such as plasticizers, binder and deflocculants. Since the firing process takes place at temperatures, depending on the material, in the range of 1250 – 2500 °C, all materials that are prone to vaporize or decompose at these temperatures should be removed beforehand, due to the negative effect on the sintering process. [1] [6]

Particles in a formed moist body are surrounded by a thin film of water. A drying process is therefore employed to drastically lower the residual moisture content of the green body. During the water removal, the individual particles move closer together and this results in a reduction of volume that is referred to as the drying shrinkage. Another pre-sintering process is known as burnout or burning out. During this process the organic additives that are present in the green bodies are either completely burned out of the green body (decarbonization) or they are converted into carbon which remains in the structure (carbonizing) that is then incorporated into the ceramic structure during the firing process. It should be noted that because of the drying and burnout process the green body loses a significant amount of the

cohesive forces that hold the part together and should therefore be handled appropriately until it is fired. [1] [6]

3.1.5. Sintering

Sintering is understood as a process to compact and form particle packs into a solid mass of material through the means of exerting heat or pressure without melting the material. During this process, the atoms of the individual particles diffuse across the particle boundaries, thereby fusing the particles together in one solid mass. This phenomenon is referred to as grain growth and pore elimination, and the driving force behind is, that a system always seeks the state of lowest free enthalpy. This material transport is greatly enhanced through the very high temperatures that are employed for sintering process as well as the high surface area and surface energy of the particles. [1] [6]

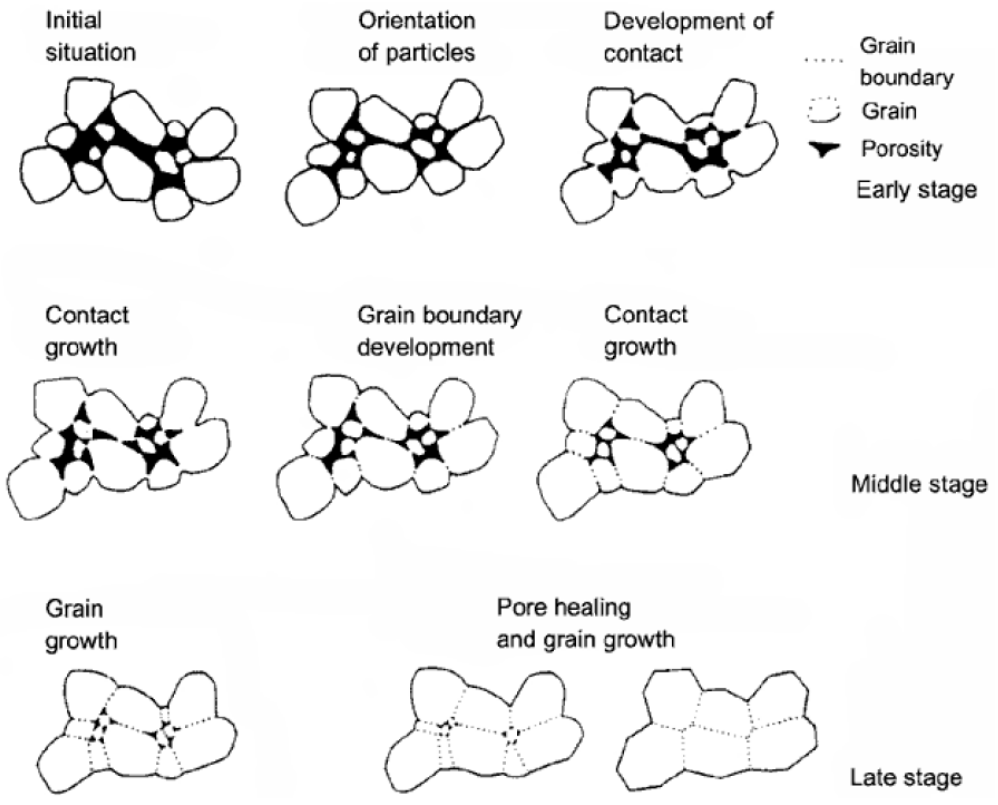

Figure 4: The different stages of grain growth during the sintering process [6]

The kinetics of the sintering process and grain growth can be divided into three different stages, the early, middle and late stage. The early stage of grain growth is characterized by the initial development of contact and the neck formation between the individual particles.

As depicted in Figure 4, adjacent particles form grain boundaries at the point of contact by diffusion. Further neck formation is then driven by the energy gradient that results through the different curvatures of the particle and the neck. Surface diffusion is the dominant driving force during this early stage of the neck formation. This point contact and initial neck formation does not translate into dimensional changes as well as a reduction in porosity yet. [1] [6]

The intermediate phase starts to begin, when adjacent neck formations start to impinge upon each other. During this phase, the interconnected networks and channels of pores start getting broken up by the continued neck formation. This process of densification and grain growth is accelerated by the creation of new contact points between the particles and it is responsible for the majority of densification during the sintering process, as depicted in Figure 5. The driving forces during this stage of sintering are bulk transport mechanisms such as grain boundary diffusion and volume diffusion that causes the migration of material from the inside of the individual particles to the surface and consequently the contact points. [1] [6]

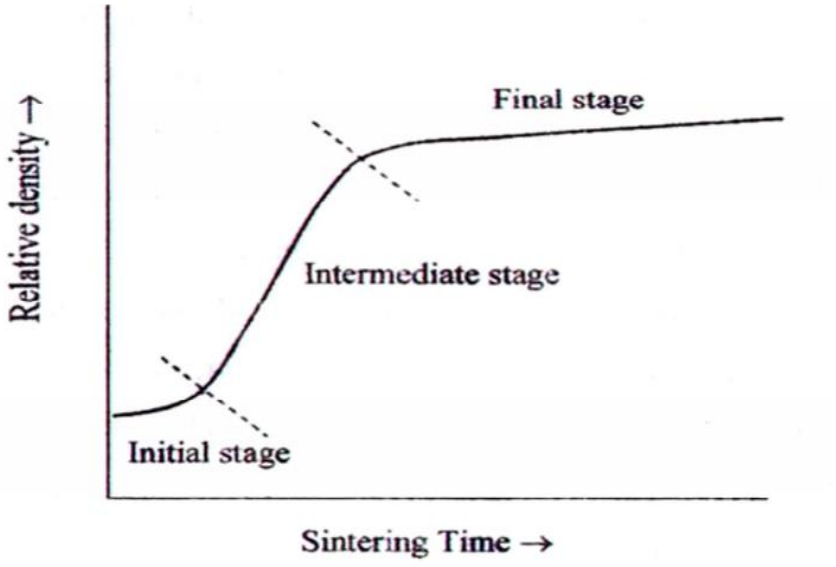

Figure 5: typical densification curve of the sintering process [7]

The final stage of the sintering process is reached when most pores are closed and the remaining ones are isolated from one another. The kinetic during this stage slows down dramatically, as depicted in Figure 5, in comparison to the early and intermediate stage of the process. Pore shrinkage is the defining characteristic of this stage and is caused by the continuous growth of the grains and the escape of the trapped gas in the pores. This results

in a shrinkage of body volume, depending on the material, of up to 30%. For this reason, the initial geometry of the green body should be over-sized in an appropriate manner to compensate for this loss in volume. [1] [6]

3.1.6. Machining and part finishing

In some cases, the sintered or unsintered ceramic body does not yet conform to the desired specifications regarding the geometry, shape and surface of the finished product. Therefore, a variety of different machining process are employed to either improve the dimensions and tolerances of the part or create entire geometries and shapes that are not achievable with the forming process alone. This refinement is not necessarily confined to already sintered parts, but can also be applied directly after the shaping of the green body (green machining) or after it has undergone drying and burning out (white machining). Machining that takes place before the firing process consists usually of cutting, stamping, drilling, turning, sawing and grinding and is mostly used to create more complex shapes and geometries to overcome the limitations of the forming method. Hard machining, that takes place after sintering, however is mostly used to achieve the final dimensional tolerances and surface qualities. Methods such as laser cutting, grinding, honing, lapping and polishing are commonly employed for this process step and due to the hardness of the fired ceramic, diamond based tooling is used almost exclusively. Depending on the requirements of the ceramic product, additional finishing steps such as metallization, glazing, enameling and coating can also be employed. [6] [1]

3.2. Influencing parameters on the dry uniaxial die compaction

This chapter presents the different uniaxial powder pressing techniques and their problems and objectives, as well as the parameters that describe the behavior of the particles during the various pressing steps and the spread of the pressure throughout the powder column.

The manufacturing of a sintered ceramic component begins with the densification of the prepared loose material into the desired contour. In the case of uniaxial die pressing, the

powdered material is filled into a rigid die, upon which a substantial amount of pressure is then exerted via one or more compacting punches in the axial direction. Under the influence of these compacting forces, the individual powder particles are shoved together in such a way that their surfaces start to interlock with each other. Through this mechanism a sufficient amount of cohesive forces are build up to form a green part that can withstand the subsequent processing without damage.[2] [8]

The first distinction between uniaxial die compaction processes can be drawn, by the configuration of the upper and lower punch, as well as the role of the matrix. In the case of a solid non-moving matrix, there are two commonly employed configurations, as shown in Figure 6. The first one is referred to as one-sided pressing or unilateral pressing. This means that for example the lower punch and the matrix are both in fixed position during the compaction, and the densification is only exerted through the upper punch. This results in a density gradient from the top of the part to the bottom. In a two-sided configuration both the lower and upper punch perform the compaction. This allows for the propagation of pressure throughout the compact from both sides which results in a more uniform density distribution, as depicted by different color gradients in Figure 6. One-sided pressing is mostly used for the manufacturing of very flat parts or for the calibration of the machinery for more complex compaction cycles. [2] [8]

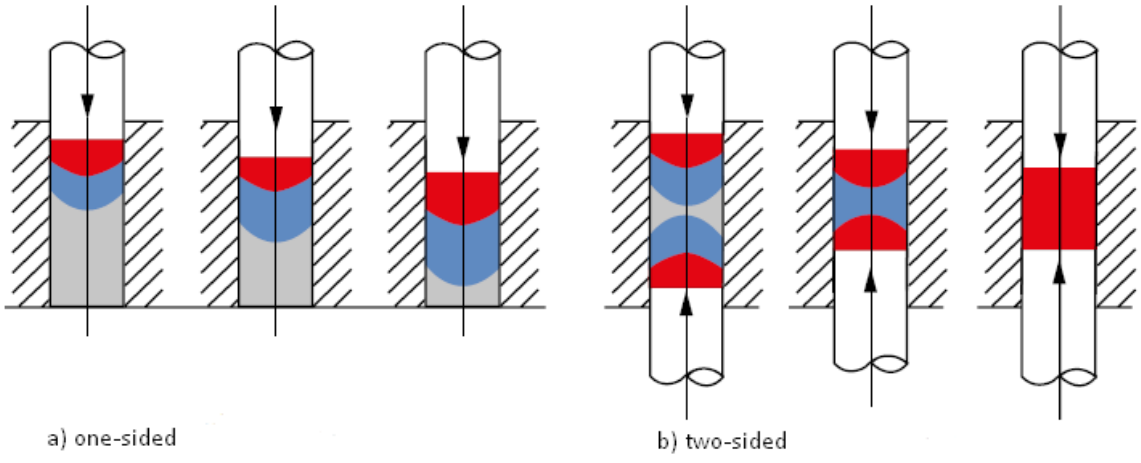

Figure 6: Principle of uniaxial pressing in a solid matrix: a) one-sided compaction b) two-sided compaction [2]

Through the introduction of a movable matrix, the efficiency of the compaction can be further improved. Such a movable matrix is usually integrated into a one-sided pressing configuration with the aim to reduce the friction forces between the powder and the die wall

by lowering alongside with the upper punch. There are mainly two mechanisms that allow for the lowering of the matrix during the compaction itself. The first one being referred to as a floating matrix, as depicted in Figure 7, which intermediates a spring with an appropriate stiffness between the matrix and the rigid mounting. Once the friction forces between the powder and the matrix rise to a sufficient level during compaction, the floating matrix will move alongside the compacting part. A common problem that occurs during the usage of a floating matrix, is that the friction forces that build between the die and powder fluctuate because of the inhomogeneous distribution of material and lubricant. This leads to more difficulty in controlling the exact movement of the matrix as well as additional wear on the surface of the die. This problem can be mitigated through the replacement of the floating matrix, that merely reacts in accordance to the friction forces between the part and the die, with a mechanically driven matrix that allows for the precise configuration of the motion during the entire compaction cycle. Such a matrix is not impacted by the nonuniform friction forces and is therefore capable of achieving a much more controlled and reproducible movement. Because of this advantage, pressing processes that utilize a mechanically driven matrix are the market-dominating configurations. [2] [8] [9]

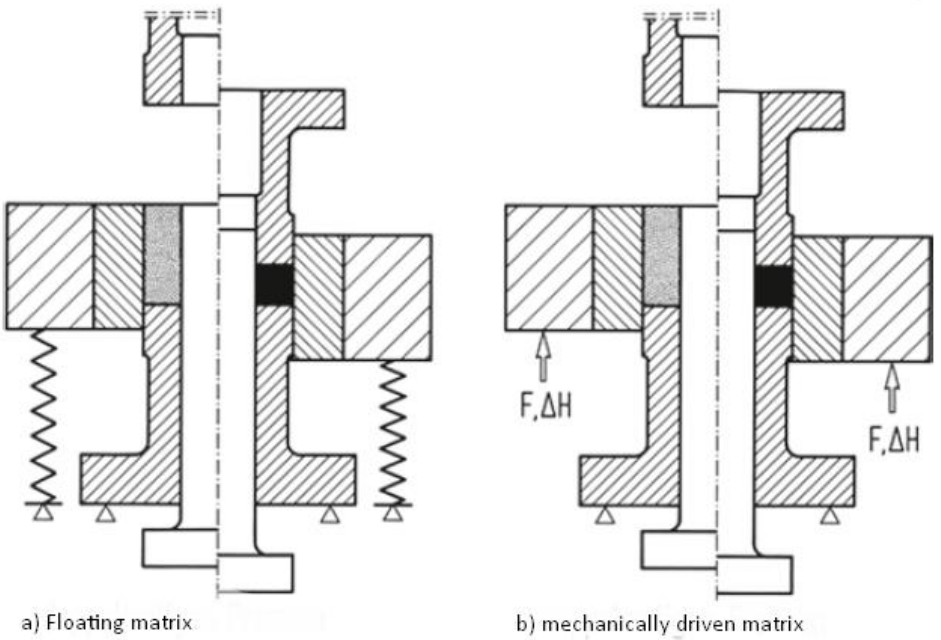

Figure 7:Double-sided uniaxial pressing configurations with a movable matrix and a fixed lower punch: a) floating matrix b) mechanically driven matrix, with the filled die before compaction on the left side of the symmetrical axis and the finished densification stroke on the right side [9]

3.2.1. Compaction cycle

The compaction cycle of a uniaxial die pressing process can be divided into three different stages, each of these is characterized by specific movements and positions of the tooling and poses specific technical problems.

1. Filling the die
2. Densification of the powder
3. Ejecting the compact from the die

At the beginning of the compaction cycle the empty die has to be filled with the prepared powdered material. This is usually achieved by some sort of filling device that moves over the die cavity and releases the material into the cavity through its own gravity, as depicted in Figure 8. Depending on the shape and size of the cavity, some are filled more easily than others. The unimpeded flow of the particles into the cavity is of the utmost importance during this step. The size of the individual particles should be considerably smaller than the smallest shapes of the cavity to avoid the formation of bridging. There can also be an occurrence of segregation during the powder flow, especially through narrow cross-sections. Depending on the particles sizes and their distribution and the shape and geometry of the cavity, significant differences in the particle bulk density distribution throughout the cavity can occur. This nonuniformity can then be further amplified during the compaction stage. The main technical challenge of this stage is therefore the reliable and reproducible filling of the cavity with an exact amount of material and the uniform distribution of this material throughout the entire cavity. The practical filling densities that are usually achievable prove to be far lower than the density under the condition of theoretical random packaging. This is caused by the fact that not all individual particles can reach their optimal position in the microstructure during the filling process. Interactions with the die walls also hinder the packing process, thus usually leading to lower densities close to the walling. [1] [6] [8] [10]

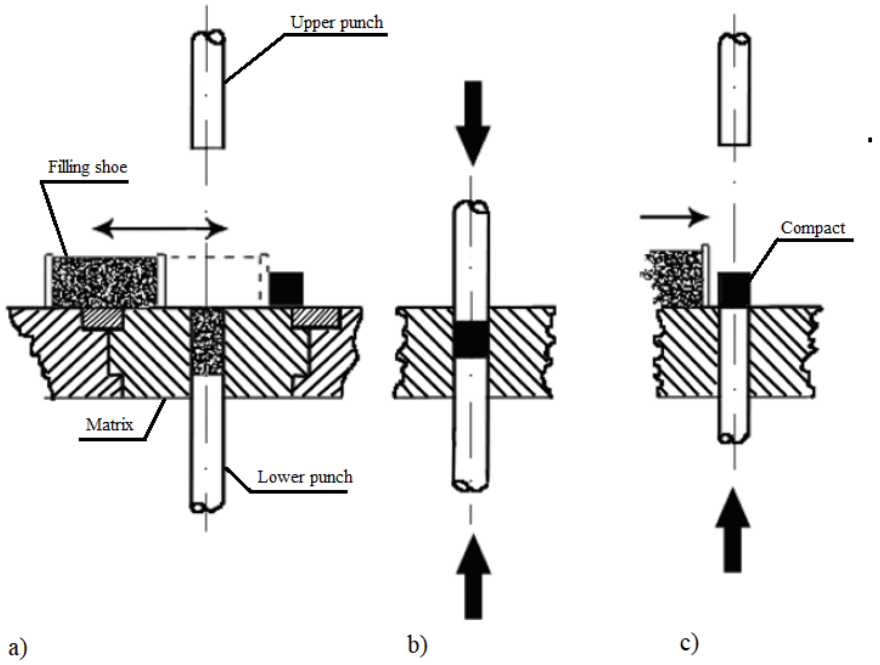

Figure 8: The three stages of the compaction cycle: a) filling b) densifying c) ejection [10]

The second stage of the compaction cycle the densification of the granular material into a compacted green part. The densification is primarily described by the relationship between the applied pressure and the resulting density of the compact, commonly expressed in a density-pressure plot, as depicted in Figure 9. This pressure usually equates to the applied forces of the compacting punches in relation to their cross sections. The state of stress and the distribution of stress in the compact are not taken into consideration by this relationship.

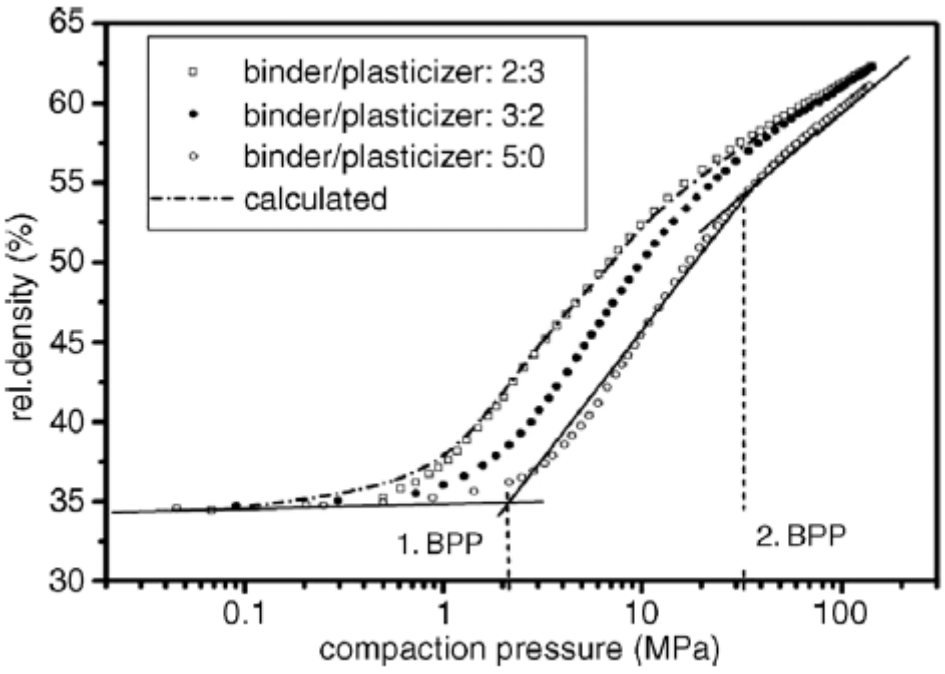

Figure 9: Pressure/density graph of alumina granulates with varying binder/plasticizer ratio with indication of both break point pressures [8]

In general, the densification of granular material involves the rearrangement and deformation of the individual granules. This rearrangement is influenced by the initial packing of the particles after the filling of the die, the particle size distribution and the hardness of the granules. Particles with high flowability and low intragranular friction usually lead to a more ideal packing structure with less flaws. The granule deformation is more influenced by the size distribution of the granule and the size of the primary particles that compose the granules and less by the actual size of the granules. Softer granules usually lead to higher green part densities than granules that are harder. [1] [8]

The pressure-density relationship usually is dividable into two or three different zones, that are interrupted by sharp breaks. When the densification begins, at first the granules are moved into the direction of the compaction and the initial increase in density is mainly caused by sliding and reorienting of the individual granules. Once the lower break point pressure, indicated "1. BPP" in Figure 9, is reached, the compaction pressure is starting to exceed the yield strength of the individual granules. During this stage of the densification, the deformation or fracture in the case of brittle granules, becomes the dominating influence on the relationship between the compaction pressure and the resulting density. The second break point pressure "2. BPP" marks the beginning of the degression of the pressure-density relationship and the intragranular compaction of the granules becomes the driving force behind further densification. Ideally, the intragranular voids are filled during this process and the green part is fully formed. However, these processes of densification do not occur exactly the same in each point of the particle microstructure. Because of the friction forces between the individual granules and the interaction between the die surface and the granules, as well as the different compression path that each granule takes, the resulting green compact is subject to point-to-point variation of the pressing density. Such a non-uniform density distribution, as exemplary depicted in Figure 10, is usually characterized by zones of higher density close to the compacting punch and zones of lower density in the section that is the farthest from the punches in axial direction. A variation in density also occurs in the direction lateral to the compaction direction. The occurrence of significant gradients in density is commonly counteracted through the introduction of ceramic additives that aim to reduce the friction forces during densification. [1] [8]

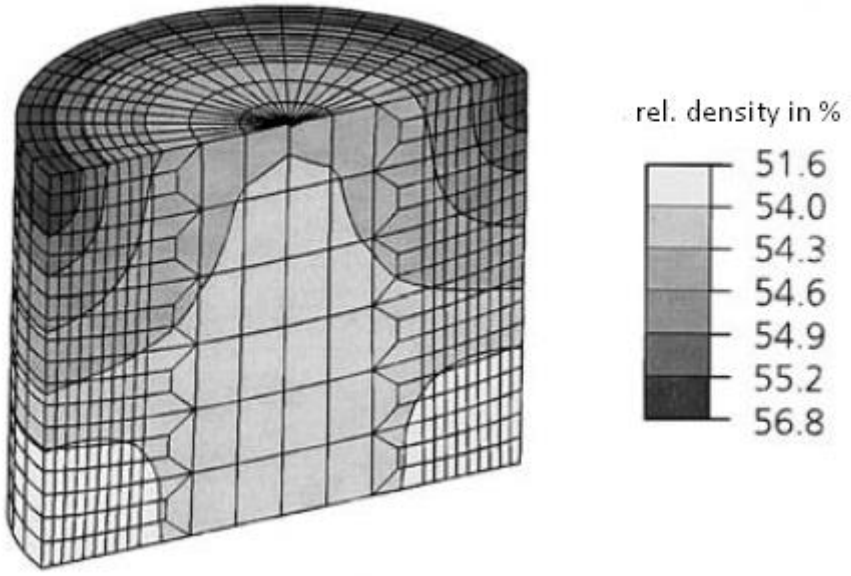

Figure 10: Density distribution in relative terms in the upper half of a dry pressed cylinder with a section view through the center in axial direction [1]

The third and last stage of the compaction cycle is the ejection of the finished green part from the cavity of the die. When the upper punch exerts its maximum pressure at the lower dead-point of the compaction, it starts to move upwards again. At this very moment the axial pressure is lifted from the green part and the elastic relaxation begins. Now the part is being ejected by either an upwards movement of the lower punch or a downwards movement of the matrix. The ejection pressure that is necessary to free the compact from the die is proportional with the height of the compact. The ejection pressure is varying in accordance to the travel distance of the ejecting punch or matrix and the movement of the green body, as depicted Figure 11. [10]

At the beginning of the ejection the pressure is increasing rapidly and quickly hits a peak point, due to the adhesive friction between the green part and the walling. This peak pressure can, in certain cases, exceed even the maximum compaction pressure that occurred during densification, which would lead to an additional densification of the green part or damage to the tooling. Once the adhesive friction is overcome, the ejection pressure reduces drastically and the sliding friction begins to define the ejection pressure. As the green part moves upwards and is partly ejected, the ejection pressure reduces further until it reaches zero, when the entire green part is ejected. [10]

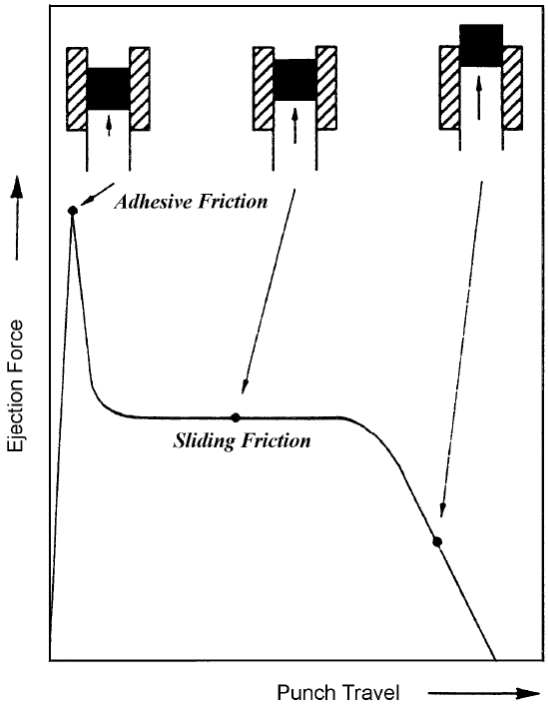

Figure 11: A schematic depiction of the relationship between the ejection pressure and the moving distance of the ejecting punch or matrix. [10]

As the compact exits the die, the protruding part of the body is suddenly freed from the compressive lateral strain as it crosses the contour of the cavity and therefore expands in a lateral direction. Because the rest of the green part that is still constraint by the cavity, a shearing stress starts to occur within the green part, that could ultimately lead to cracking. This risk could be reduced by tapering the upper rim of the cavity. The elastic expansion of the compact after it is ejected from the die is known as spring back and is influenced by the compaction pressure, the powder properties and additives as well as the shape of the compaction die. After the green part is finally completely ejected from the cavity it has to be removed from the press in order to start the next compaction cycle. In simple cases the filling shoe just pushes the green part way from the tooling as it moves over the cavity again and the part is collected by a rail or chute of some form. While components that are more fragile or have a delicate shape may be removed through some sort of handling or gripping device. [10]

3.3.Granulation of ceramic powders

The preparation of the raw material usually includes some form of granulation process to form press granulates by the controlled agglomeration of the primary particles. This allows for a better control of the particle properties like grain size and surface and the flowability of the powder. In addition, due to the fluctuating quality and properties of the raw material, particularly if sourced from natural occurring mineral deposits, the material is grinded down into a micron or even submicron powder to ensure homogeneity and consistency for the further handling and processing. Particles with such a low grain size exhibit usually very poor flowability and therefore warrant a controlled agglomeration process. Granulation methods can be subdivided into several different groups, depending on the main principle of action. Agitation methods use some form of mixing or tumbling to achieve particle bonding and the subsequent agglomeration between moist particles. Pressure methods use some form of extrusion or applied pressure to form particles into pellets. Spray techniques atomize particle suspensions into droplets, that are then dried, to achieve controlled agglomeration. Spray-drying is considered to be the most important granulation method for industrial processes and it was also used for the manufacturing of the ceramic granulates that were utilized over the course of this thesis. [8]

3.3.1. Spray-Drying

In most cases, ceramic powders undergo some variation of a suspension-based pre-processing step, such as wet grinding or mixing. Therefore, an agglomeration process as well as a drying process are necessary further down the line. A spray-drying granulation process is capable of handling both of these processing steps. A typical spray drying process, as shown in Figure 12, starts with the atomization of the liquid slurry. This suspension can be preconditioned for better performance during the spray-drying by adjusting the solid loading and adding various additives and is usually water based. The purpose of atomization is the formation of spherical droplets with the desired size and a very narrow distribution thereof. There are several different mechanisms that are commonly employed to achieve atomization. Centrifugal atomizers use rotating disks or wheels to disintegrate the slurry and to not rely on the pressurization of the slurry. Such atomizers can yield a very narrow droplet size distribution in the range of 15 - 250 µm. The droplet size output is mainly influenced by the

disk or wheel speed, the feeding rate and viscosity of the slurry as well as the surface tension and solid loading of the droplet. In pressure nozzle atomization, the liquid feed is forced through a nozzle orifice at very high pressures and disintegrates therefore into small droplets. Two-fluid nozzles operate at medium pressure for both the atomization gas and the suspension liquid and the ratio between the liquid and the gas is responsible for the achievable droplet size. [8]

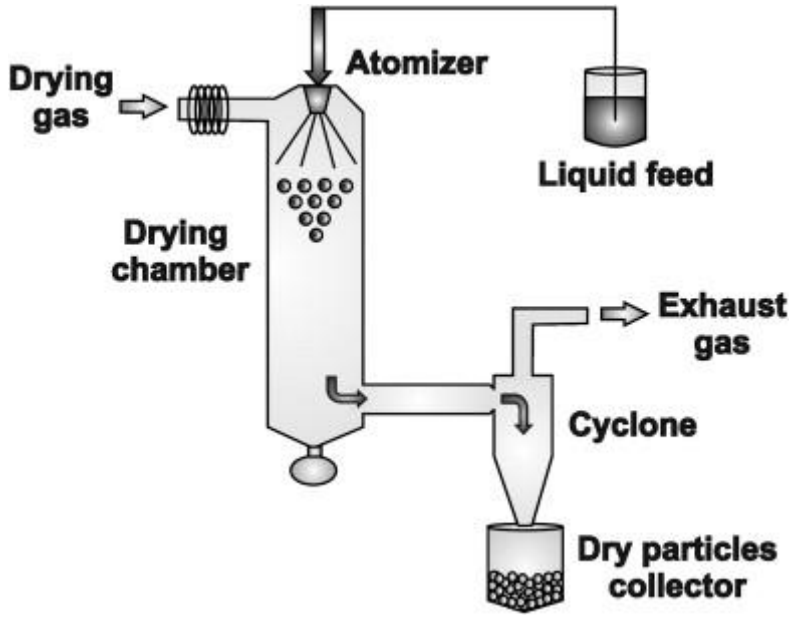

Figure 12: Schematic depiction of a typical spray-drying process [11]

At the end of the atomization the disintegrated droplets are injected into the drying chamber at the top and come into contact with the hot drying gas, usually air. The movement and interaction between the drying gas and the spray droplets can by categorized into three different conditions. A concurrent flow occurs, when the gas and the droplets flow in the same direction and is preferred for coarse and heat sensitive products. In the case of a countercurrent flow, the drying gas is streaming in the opposing direction of the falling droplets. This condition allows for a more efficient heat utilization but is restricted to materials that are non-heat-sensitive. Both these flow states can occur in a mixed-flow condition in a drying chamber, especially in chambers of large dimension of up to several meters. [8]

The drying process of the suspension droplets can be divided into two distinct stages. Within several seconds of contact with the drying gas, the droplet reaches an equilibrium with the surrounding gas, with no change in the moisture within the droplet. Then the drying begins and continues at a constant rate (stage 1), as shown in Figure 13. During this stage the droplet

starts to shrink but keeps a constant temperature. This remains up until the surface of the droplet can no longer be saturated with liquid. Once the critical point, marked “2” in Figure 13, is reached, the drying rate starts to diminish and the liquid-vapor interfaces starts to recede into the porous structure and subsequently increases the subsurface temperature. This continues until the vast majority of the liquid mass has evaporated and reaches a critical point when the primary particles establish surface contact and form a homogenous packing. [8] [12]

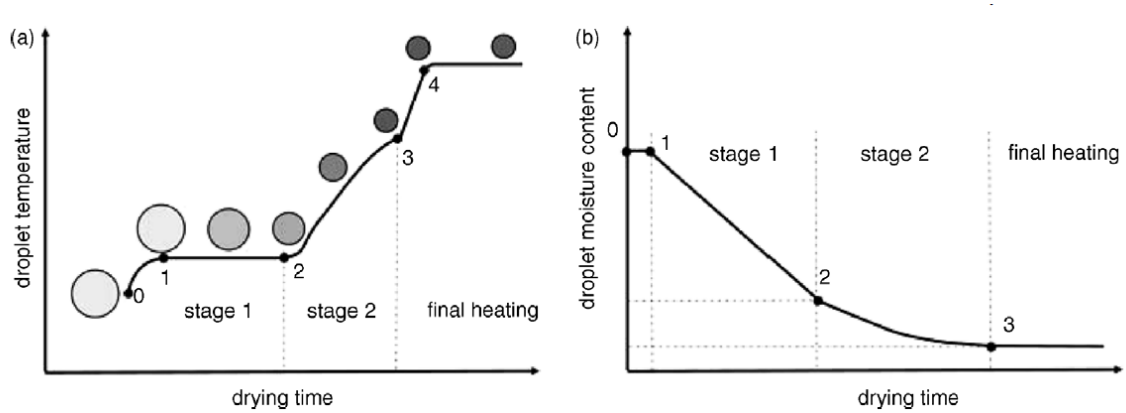

Figure 13:The droplet temperature (a) and the droplet moisture content (b) in relation to the drying time in a typical spray-drying process [8]

The final properties and characteristics of a spray-dried granulate depends on several parameters. Besides the actual drying process, the particles properties of the source powder, the solid loading of the suspension as well as the introduced additives play an important role during granulation. The ideal granule should be spherical in shape and homogenous in density throughout the entire volume. The formation of hollow granules can occur by using suspensions with a low solid loading or a too-rapid drying process. Furthermore, the amount of dispersant has to be limited as well, as enhanced particle mobility also leads to shell formation. The viscosity of the suspension is also of importance and has to be balanced appropriately. During atomization a low viscosity with the resulting shear thinning behavior is preferable, but a higher viscosity is required inside the drying droplet to ensure proper granulation. [8] [12]

4. Materials

4.1.Ceramic Granules

The ceramic granules that were used over the course of this thesis to produce the compacted disc-shaped green parts were manufactured via a proprietary spray drying process developed by *EPCOS* specifically for this product line. The main component of this granulate is the relaxor ferroelectric material lead magnesium niobate (PMN). This material and the additional ceramic auxiliaries used in the manufacturing process are outlined in the following chapter.

4.1.1. Lead Magnesium Niobate (PMN)

The central component of the ceramic granules is the prototypical relaxor ferroelectric material lead magnesium niobate ($MgNb_2O_9Pb_3$), abbr. PMN, which was first synthesized by Smolenskii and Agranovskaya in 1958 and has the common ABO_3 cubic perovskite structure in combination with a mixed B-site [13]. Relaxor ferroelectrics exhibit high electrostriction and are known for their frequency dependent dielectric response and their ability for local polarization at temperatures above their dielectric maximum, which is a unique property that normal ferroelectric materials do not display. In addition, lead magnesium niobate is characterized by its Curie point of -7°C and its very high dielectric constant of ~30000, which remains stable in the room temperature range. [4] [14]

The powder formulations utilized in this thesis consist of the main component lead magnesium niobate and either the custom blend “PTC” or the premanufactured ceramic auxiliary “Optapix”.

4.1.2. Additive blend “PTC”

This additive blend which will be referred to as “PTC” in this thesis is a custom formulation developed by *EPCOS* to improve the granule formation and compaction processes of lead magnesium niobate powder and consists of several additives and auxiliaries:

- Dolapix PC75: an organic deflocculating agent based on an synthetic polyelectrolyte [15]
- PEG 6000: a water soluble organic compound (polyethylene glycol) that is widely used as a lubricant and binder as well as a mould release agent in various compaction processes. [16]
- Methocel A4C: a water soluble methylcellulose derived from pine pulp that is widely used as thickener, emulsifier, binder and suspension aid. [17]
- Contraspum K1012: Commonly used as an effective antifoaming agent for ceramic bodies due to its surface activity (Alkylpolyalkyleneglycolether). [18]
- Mowilith DN 50: a vinyl acetate homopolymer dispersion with excellent shear stability properties that is mainly used in the preparation of adhesives. [19]

4.1.3. Additive blend "Optapix"

The ceramic auxiliary blend which will be referred to as "Optapix" in this thesis is the temporary binder with the designation "Optapix PAF2" produced by the company *Zschimmer & Schwarz*. It's a polyvinyl alcohol preparation with density of approx. 1,08 g/cm³ and a viscosity of ~4000 mPas, both at 20°C. Furthermore, this water-miscible yellowish liquid is characterized by a ph-value of ~5,5 and a maximum ignition residue after the binder burnout of 0,5% of the initial binder mass. [20]

This blend is widely used to increase the dry and green breaking strength of ceramic compacts, which is achieved by its creation of adhesive forces through a mechanism which increases the film formation between the particles of the raw material. In addition, due to its general slip compatibility this additive is exceedingly well suited for the manufacturing of spray-dried ceramic granules. Furthermore, it also contains a pressing aid, which is softening the individual granules and equalizes the applied pressure to minimize the remaining structures differences in the compacted green part. [20]

5. Analysing methods

This chapter outlines the various analysing methods and the measuring technologies that were employed over the course of this thesis to accurately characterize the properties of the used granular material as well as the manufactured ceramic bodies.

5.1. Particle size and particle shape analysis

The particle size distribution and the shape of the spray-granulated particle batches are key characteristics regarding to green part results and further process optimization. Therefore, a dynamic image analysis method was applied to identify cumulative and density particle size distributions and various shape metrics, as well as traditional microscopic imagery to gain additional insight into the particle shape of the various granule batches.

5.1.1. Particle Analyzer "CAMSIZER XT" by Retsch Technology

The particle analyzer designated "CAMSIZER XT" by *Retsch Technology* was utilized to accurately measure the particle size distributions of the various granule batches that were used over the course of this thesis. This device operates under the principle of the digital image analysis method, according to ISO 13322-2, by using a patented two-camera system that can accurately capture and measure thousands of individual particles from a wide measuring range (1 µm – 3 mm) in a matter of minutes. At first the powder sample is

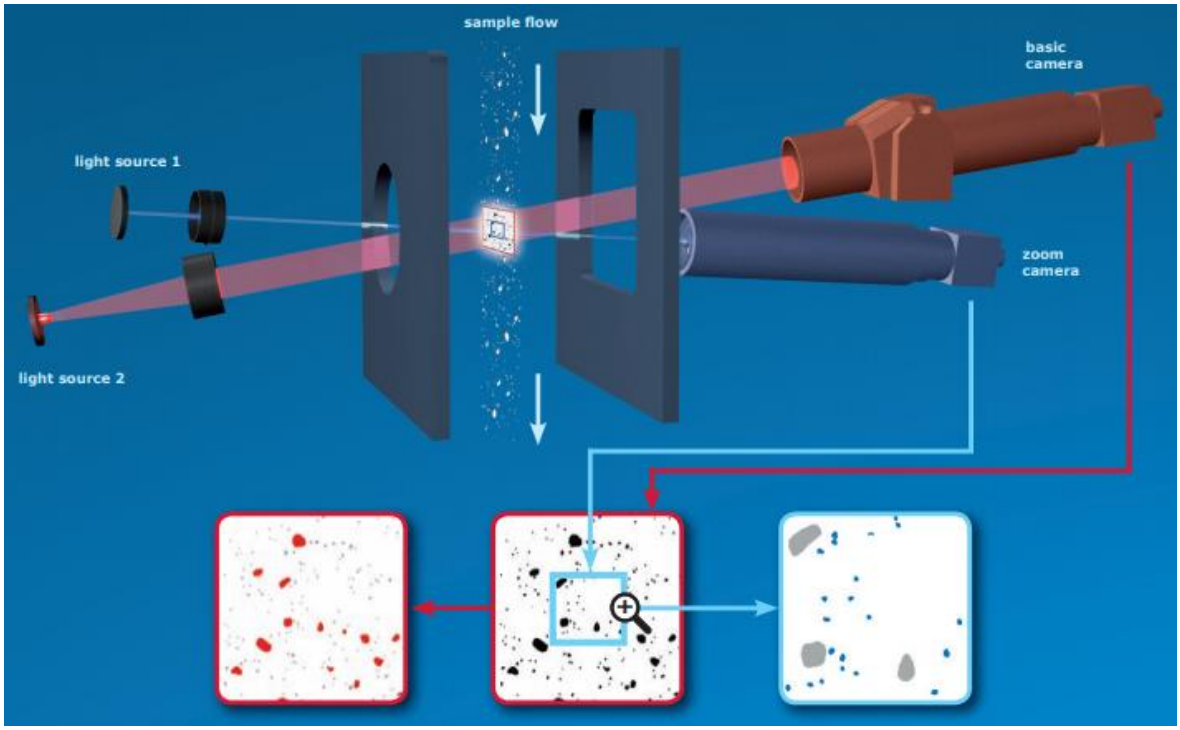

Figure 14: Depiction of the two-camera measurement principle of the CAMSIZER XT [21]

prepared and accelerated via air dispersion, wet dispersion or gravity dispersion. As depicted in Figure 14 the dispersed particles then pass in front of two pulsed LED light sources and cast a shadow which is captured by the basic camera, that is designed for a large field of view and larger particles, as well as the high-resolution zoom camera that captures the smaller particles in the micrometer range. The imagery of the projected shadows is then analyzed with the accompanying software, that automatically identifies and isolates individual particles and then measures and calculates various metrics of the projected particles, e.g. width, length and the diameter of the coextensive circle. [21]

The powder samples that were analyzed during this thesis were dispersed by pressured air at 20 kPa using the "X-Jet" module of the device, since the ceramic additives of the granules are highly soluble in water. The average duration of such a measurement was ~2 minutes with a framerate of 1:1, a gap width of 4,0 mm, a surface density of 0,5% and a default spherical particle shape. The number of individual particle projections that were captured and analyzed were in the range of 5.000.000 for the basic camera and 100.000 for the zoom camera for each measurement run.

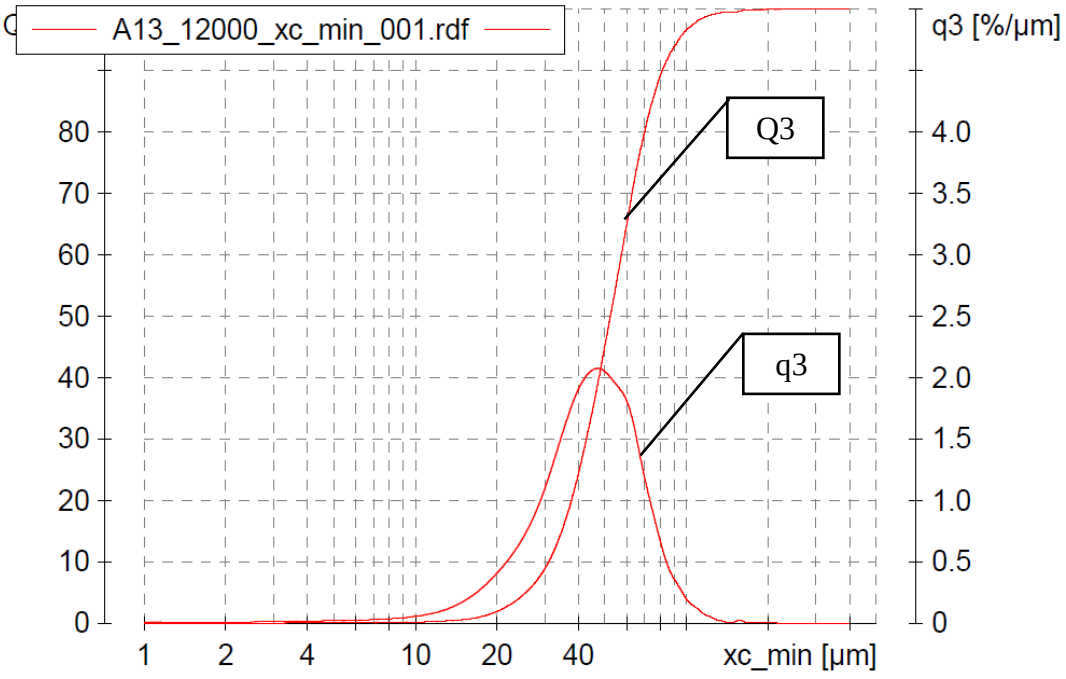

Figure 15: Cumulative (Q3) and density (q3) particle size distribution graph of the granule batch "A13"using the Camsizer XT

As can be seen in the sample analysis of Batch "A13" in Figure 15 the measurement software then calculates the particle size distributions (q3 and Q3) of the powder sample as well as important metrics that are further depicted in Table 1. The median diameter x_{50} for Batch

"A13" equals 52,4 µm. The cutoff point for the lowest decile of the particle population (x_{10}) is 31,0 µm, for the highest decile (x_{90}) this diameter is 81,4 µm.

Table 1: Measurement result parameters of a powder analysis using the Camsizer XT [21]

Metric	**Description**
X_{10}	Max. particle diameter of the lowest decile
X_{50}	Median particle diameter
X_{90}	Min. diameter of the highest decile
$SPHT_3$	Sphericity of particle projection
$Symm_3$	Symmetry
b/l_3	Aspect ratio

Furthermore, the measurement software calculates three additional parameters to characterize the particle shape. The Sphericity ($SPHT_3$) of the dispersed particle is calculated by using the circumference (P) and the measured area (A) of the particle projection. [21]

$$SPHT_3 = \frac{4\pi A}{P^2} \qquad (5\text{-}1)$$

The Symmetry ($Symm_3$) is calculated by using two distances (r_1 and r_2) that range from the center of the projected area to the borders in the measuring direction. [21]

$$Symm_3 = \frac{1}{2}\left(1 + min\left(\frac{r_1}{r_2}\right)\right) \qquad (5\text{-}2)$$

The Aspect Ratio (b/l_3) is calculated by using the particle width of the shortest chord ($x_{c\,min}$) and the longest Feret diameter ($x_{Fe\,max}$) of the measured set of a given particle projection. [21]

$$b/l_3 = \frac{x_{c\,min}}{x_{Fe\,max}} \qquad (5\text{-}3)$$

5.1.2. Light microscope “LEICA DM4000 M”

Further particle shape analysis was performed by using a common light microscope designated DM4000 M by Leica Microsystems to gain additional insight into the particle shape beyond the calculated metrics that result from an analysis with Camsizer XT. Also, possible unwanted particle agglomerations can be better examined by using this device, instead of the Camsizer XT, where pressured air is applied to the particles to properly disperse them. This process could also dissolve the particle agglomerations that occur during storage and handling. [22]

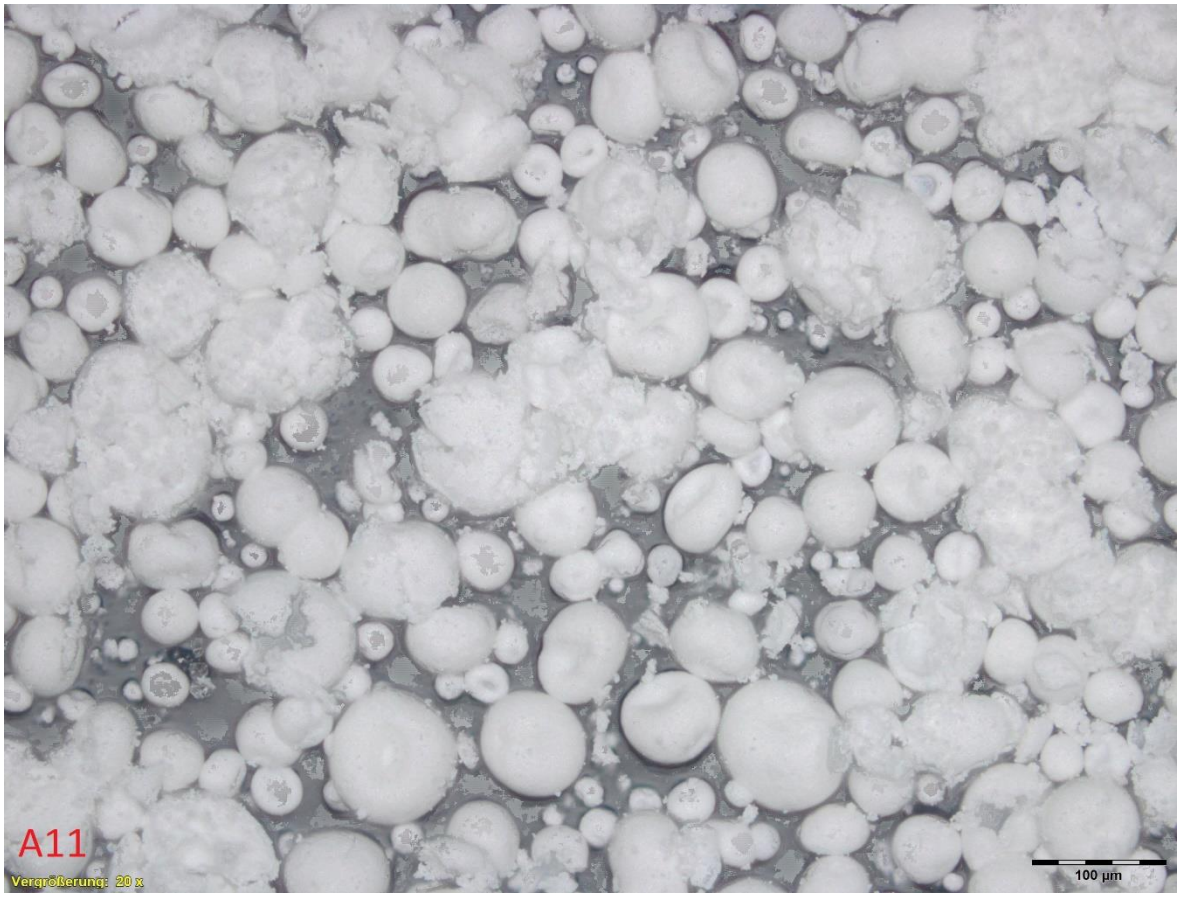

Figure 16: Image analysis of the granule batch "A11" using the Leica DM4000 M with a 20x magnification

Therefore, this shape analysis was performed by using a small amount of the undispersed granule batch. This sample was placed on the examining glass without a protective cover that could exert mechanical forces on the particles and thus destroy the agglomerated particles. After proper adjustment of the light source below the examining glass, several images were captured with magnifications ranging from 5-20x.

As can be seen in Figure 16, which shows an image analysis of granule batch “A11” at 20x magnification, most particles display the typical spherical shape with a one-sided indentation that results from spray-dried granulation processes. But, there are also unwanted bulged and agglomerated particles visible that could negatively impact the compaction process.

5.2. Rheology measurements

The rheology of granular materials is usually of great importance in the design and specification of hoppers and filling shoes. To accurately understand the flow properties of the granule batches used in this thesis, a shear cell adherent to the ASTM Standard D7891 and a flow cup compliant to DIN53211 / ASTM D1200 were used.

5.2.1. Freeman FT4 Powder Rheometer

The FT4 Powder Rheometer by Freeman Technology is a universal powder tester that includes a shear cell, a wall friction kit, and other equipment to characterize bulk properties, such as density, compressibility and permeability. The included shear cell was used to

Figure 17: Shear cell preparation setup on the left; shear test in progress on the right

quantify the particle shear properties and then calculate the flow function, which is a commonly used parameter to rank flowability. [23]

The shear cell setup, as depicted in Figure 17, consists of a segmented glass body with a diameter of 50 mm that is filled with a specified amount of the powder sample (~29 g in this case), to fill up the lower segment of the cylinder. Afterwards a mixing blade, that is proceeding downwards on a predefined path, homogenizes the sample to ensure reproducibility. This is followed by a gas permeable compression piston that applies a predefined pressure (9 kPa in this case) on the top of the sample to achieve the necessary

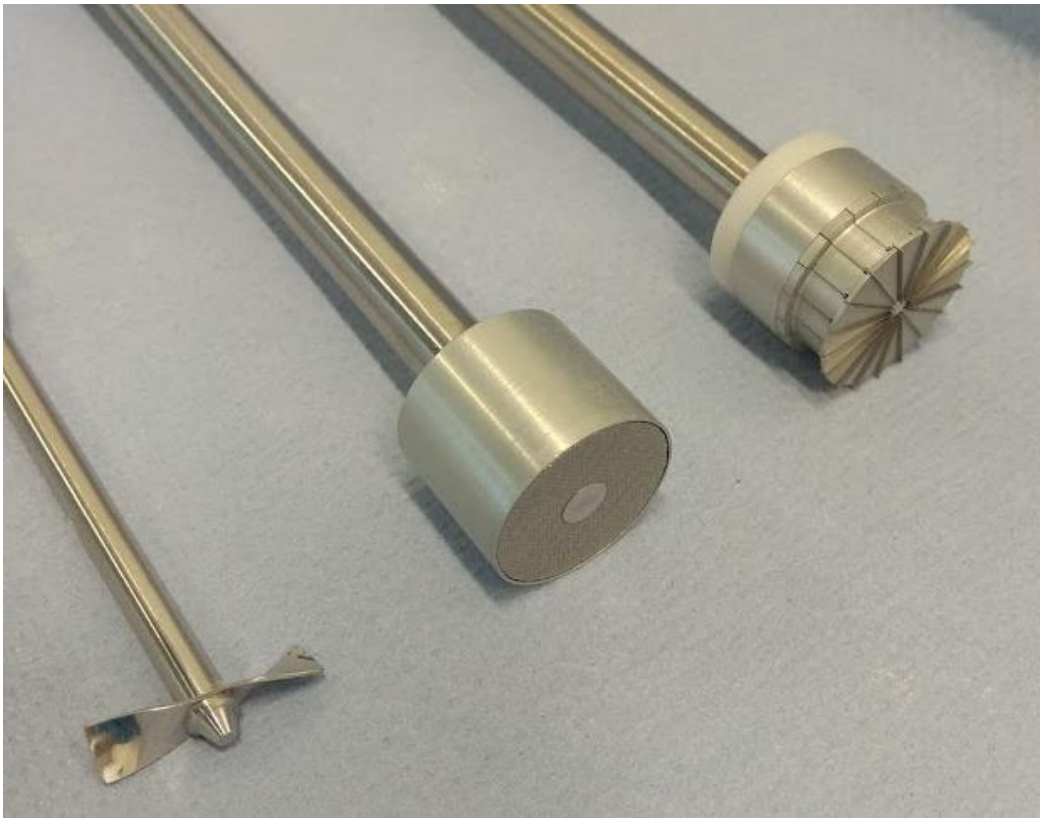

Figure 18: Shear cell equipment (left to right): mixing blade, precompression piston, shear piston

pre-compression for the following shear test. Now the upper segment of the sample cylinder is removed in a rotary motion to the side, which creates a smooth pre-compressed surface whereupon the shear piston applies a predefined sequence of shear and normal stress. This shear sequence starts with the exertion of a defined normal stress, and a subsequent simultaneous shear stress, that will be maintained until the particle flow reaches a state of equilibrium. This sequence will be repeated until the deviation of these states of equilibrium is under 1 percent. Now the imprinted normal stress will be reduced to this last configuration

and an increasing amount of shear stress will be introduced until the incipient failure point is reached. Afterwards the shear piston reduces the applied shear force by backwards rotation to zero and another sequence to find the flow equilibrium and maximum shear stress is started. Due to a reduction of the pre-compression the maximum measured shear stress will be reduced with each subsequent run. [23]

Because of the high degree of automation of the shear cell test runs, it's difficult to spot possible error sources, like the improper preparation of the powder sample. Therefore, each powder batch was analyzed three times in a consecutive manner to rule out operating errors and ensure reproducibility.

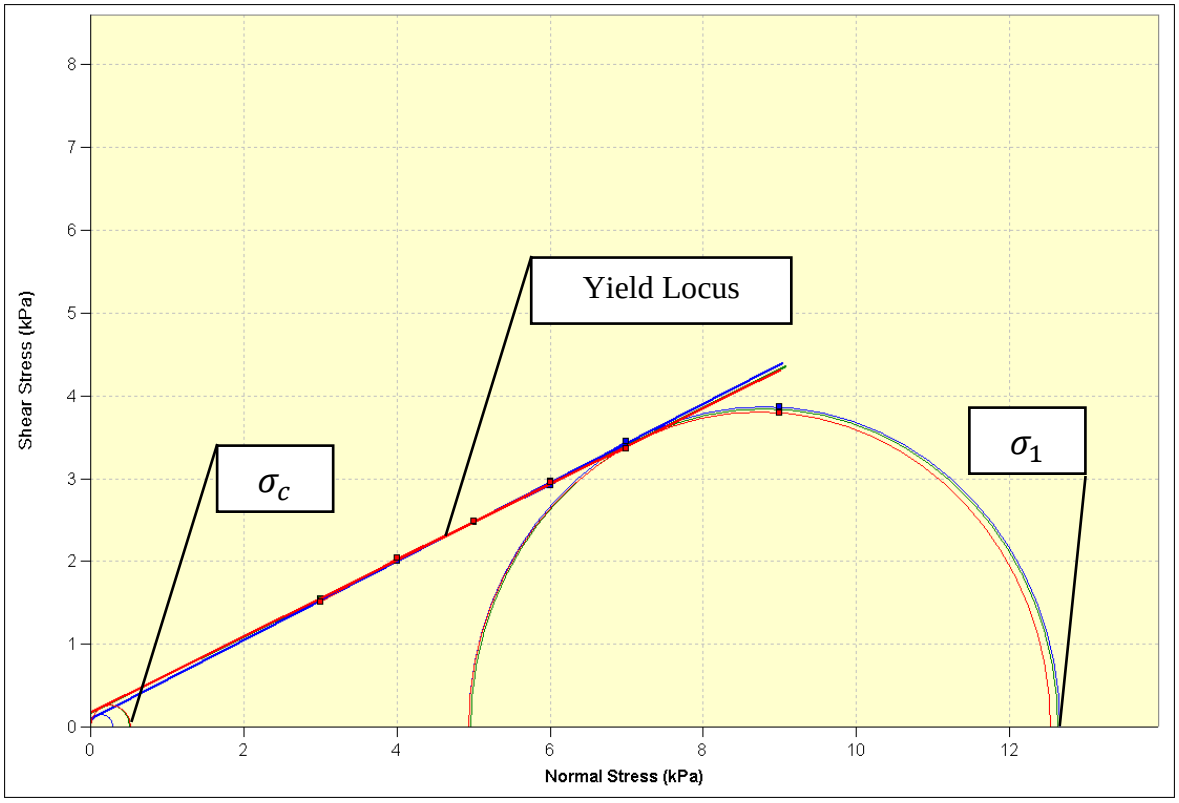

Figure 19: Mohr Circle results of two consecutive shear cell measurements (indicated red/blue)of the granule batch "A3" with the Freeman FT4 universal powder tester

With the results of the shear cell analysis the accompanying software of the Freeman FT4 produces the Mohr Circle graph, as depicted in Figure 19, which shows the powders yield locus, which is a parameter to determine the angle of internal friction, cohesion and the resulting overall strength under compressive load for a given powder sample. The extension of the yield locus fit in the graph shows that when the value of the normal stress reaches zero, the value of the shear stress is also very close to zero, which indicates a weak internal cohesion and excellent flowability of the powder. This conclusion is further supported by

the calculation of the Flow Function ff_c which equals in the case of granule batch "A3" to 29,97 out of a three-run average which is classified as "Free-Flowing". [24]

$$ff_c = \frac{\sigma_1}{\sigma_c} \qquad (5\text{-}4)$$

The Major Principal Stress σ_1 is defined as the greater of the two values at which the larger Mohr Circle intercepts the x-axis (Normal Stress = 0), the unconfined Yield Strength σ_c is defined as the greater of the two values at which the smaller Mohr Circle intercepts the x-axis. The interpretations of the Flow Function are listed in Table 2 regarding the flowability of the sampled granule batches. [24]

Table 2: Interpretation of the Flow Function results regarding powder flowability [24]

Flow Function value	**Flowability**
$ff_c < 1$	Not flowing
$1 < ff_c < 2$	Very cohesive
$2 < ff_c < 4$	Cohesive
$4 < ff_c < 10$	Easy-flowing
$ff_c > 10$	Free-flowing

5.2.2. Flow cup viscometer measurements

The viscosity of a fluid or powder is the representation of the internal resistance to deformation it musters against externally applied stresses and is therefore an important measure to accurately judge the flow behavior of a given powder sample. A flow cup is a simple device that has been widely used to determine the viscosity of powders and fluids by measuring the deceleration time. The flow cup setup that was used over the course of this thesis, as depicted in Figure 20, consists of a flow cup designated SIMEX 4 which is made of anodized aluminum according to the DIN 53211 standard with a defined filling volume of 100 ml ±1 ml and an outflow nozzle diameter of 4 mm ± 0,02 mm. The nozzle is made of stainless steel and the surface facing the fluid sample is polished. This cup is specified for a viscosity range of about 100 – 500 cSt (mm²/s) which equals to deceleration times of about 20 – 100 seconds. [25]

To measure the deceleration time, at first the flow cup is placed on a ring mount with a catching container, that rests on weighing scale (type "Viper SW 15 SM"), underneath. Then

Figure 20: Flow cup viscometer measurement setup

the nozzle is sealed and the powder is slowly filled into the flow cup. After the flow cup is filled, a sharp blade is used to draw the upper surface of the powder sample smooth and align it with the flow cups peripheral edge to ensure a reproducible sample volume. Now the nozzle is opened and the time measurement begins. The powder sample starts to form a continuous stream through the nozzle. The first tear-off of this continuous stream represents the end of the deceleration time and the time measurement will be stopped. After the whole powder sample rests in the catching container, the weight can be measured and with the defined volume of the flow cup, the bulk density can be calculated. With the accompanying nomogram, the kinematic viscosity can be derived from the experimental deceleration time and can be converted to the dynamic viscosity by using the determined bulk density of the powder sample.

The flow cup experiments that were conducted over the course of thesis were carried out by the same operator to ensure comparable results. In the case of granule batch “A11”, three test runs, each one on a different day, were executed to check accuracy and reproducibility

of the measurement setup and procedure. The results, which are shown in Table 3, indicate that the flow cup is capable to reliably characterize the powder samples that were used over the course of this thesis.

Table 3: Experimental results of the repeated flow cup measurements of granule batch "A11"

Test Run	Weight [mg]	Bulk Density [g/cm³]	Deceleration Time [s]	kin. Viscosity mm²/s	dyn. Viscosity [mPas]
1	184,1	1,84	47	194,1	357,3
2	183,2	1,83	47	194,1	355,6
3	186,8	1,87	46	189,6	354,3

5.3. Powder compaction and green part properties

The main drawback of dry compaction processes is the non-uniform density distribution throughout the compact. The interaction between the individual particles as well as the interaction of these particles with the walls of the encapsulating die negatively impacts the pressure diffusion during compaction, thus creating variations in density.

Figure 21: The PTC-03DT universal powder tester by KZK Powder Tech Corp.

To accurately quantify the wall friction and powder compactibility, the PTC-03DT Powder testing center, manufactured by the *KZK Powder Tech Corp*, was applied to analyze the granule batches that were used over the course of this thesis. This device provides the geometry independent test results necessary to design dry powder compaction processes in a controlled and automated manner. The device can apply a maximum force of 98,1 kN and a maximum temperature of 300 °C on the pressing test die and produces cylindrical compacts with a height ranging from 2 – 16 mm. The testing procedure consist of three sub-tests, that focus on the powder properties, the compaction and ejection properties as well as the green part properties. [26]

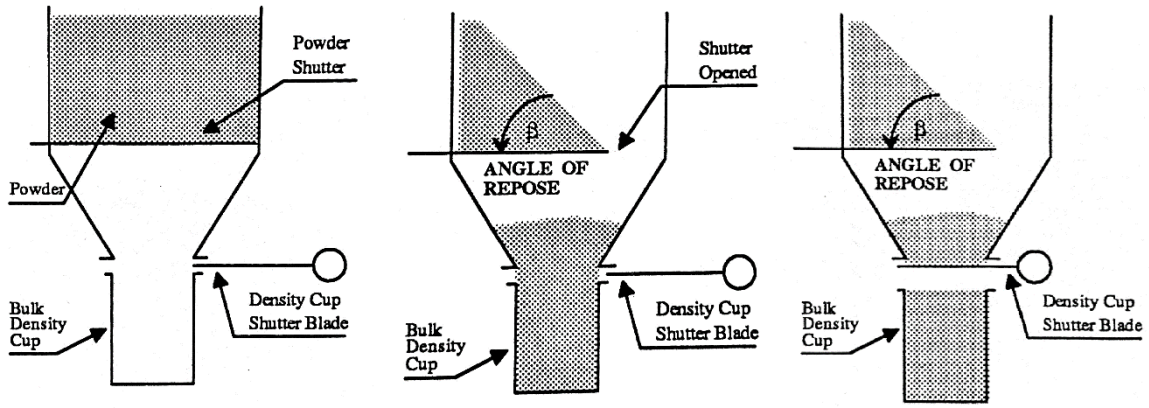

Figure 22: Powder tester sample preparation (left), angle of repose measurement (middle), bulk density setup (right).[26]

The first sub-test quantifies the properties of the powder sample by measuring the angle of repose (β), the bulk density and the tap density. At first the powder tester, as depicted in Figure 22, is filled with about 20 cm³ of the powder sample with a closed powder shutter and an open density cup shutter blade. Then the powder shutter is opened and the sample starts to fill the bulk density cup. After the powder flow stops, the angle of repose (β) can be measured. Afterwards the density cup shutter blade is closed and the over-filled density cup is dismounted and weighed. Now the bulk density (ρ_b) of the powder sample can be calculated. The tap density (ρ_{tp}) is defined as the density of a lose powder that is subjected to a prescribed amount of tappings. To conduct this test, the filled density cup is mounted back into the powder tester and the density cup shutter blade is opened again. The tapping actuator then vibrates the powder tester in a pre-defined manner and when done, the density cup shutter blade is closed and the density cup is removed and weighed again. [26]

The second sub-test characterizes the powder compaction and ejection characteristics by compacting up to 4 powder samples into green bodies and ejecting them from the test die set. This whole procedure is recorded by the internal force and distance sensors. To start the procedure, a portion of the powder sample with a pre-calculated weight is prepared. The bottom punch ("Pressing punch" in Figure 23) is then lowered into the starting position and the powder sample is filled into the cavity at the position "Die Insert". The top punch is then lowered and locked into the "Die insert" position and the compaction process is started. During compaction, the force and distance is continually logged. After the compaction is finished the top punch is unlocked and the ejection process is started. During this process, the ejection pressure (punch force per cross section area) is logged as well as the travel distance. The ejected green bodies are weighed and the height and diameter is measured with a micrometer screw to quantify the elastic relaxation (e_a). The two relevant parameters that can be extracted from this sub-test are the compatibility and slide coefficient. This sub-test was conducted with a 12,7 mm diameter test die, a fixed compact length of 10 mm, a maximum pressure hold time of 5 seconds, a desired compact density that equals 60 % of the theoretical material density, no heating and two green compacts were produced. [26]

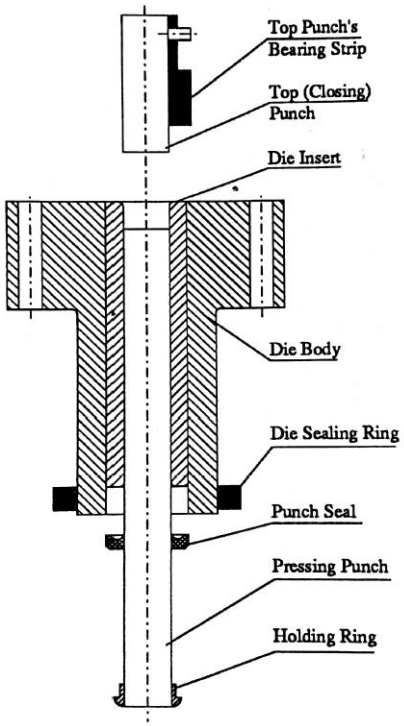

Figure 23: The cold pressing test die set of the PTC-03DT powder tester: [26]

The third sub-test routine analzyes the strength and cohesiveness of the green compacts that were produced in the second sub-test. This is achieved by crushing the first green compact in axial direction and the second one in radial direction. For this, the green compacts get

placed into a axial or radial crushing fixture, as depicted in Figure 24, and are then placed between the top and bottom punch of the test die set. The press then start to increase the compacton force, until the force sensors detect a sharp turning point with a decline in the forwarded force. This indicates plastic deformation of the green compact and the procedure is stopped. With this data the axial (w_{sa}) and radial green strength as well as the cohesiveness of the green compact can be calculated. Afterwards the top punch is withdrawn and the fixture is removed and the crushed green compact can be inspected. [26]

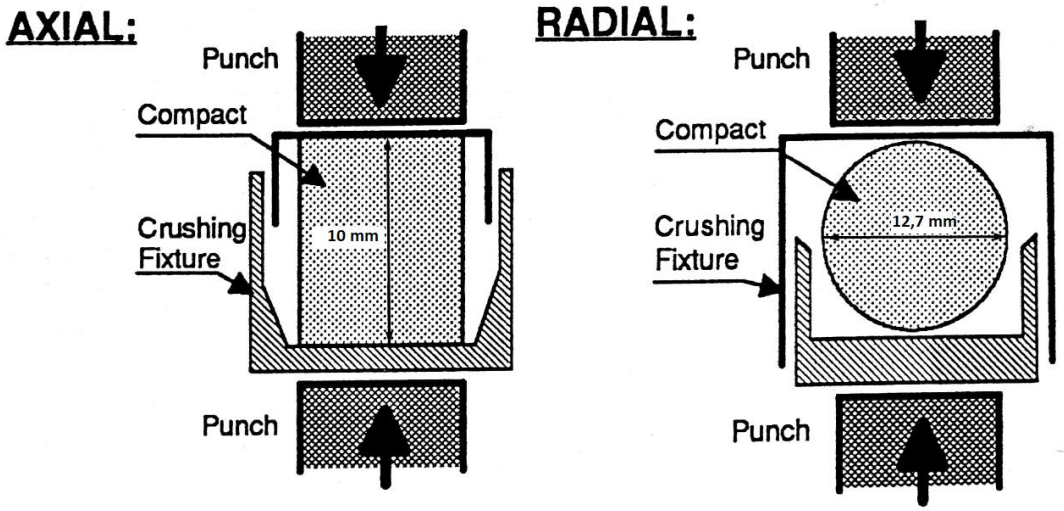

Figure 24: Schematic depiction of the axial and radial green compact crushing setup

After the whole test routine is finished, the software then calculates a large of number of different parameters, that characterize the powders dry compaction behavior. A few selected parameters, that have been the focus of the PTC-03DT Powder tester results over the course of this thesis are detailed in Table 4 below.

Table 4: Main parameters of the PTC-03DT measuring results [26]

Symbol	Parameter	Unit
β	Angle of repose	[°]
p_{nc}	Net isostatic pressure for the test compact	[MPa]
e_a	Green compact radial expansion	[-]
w_{sa}	Axial strength of the test compact	[MPa]
C	Cohesiveness of the green compact	[-]

The Angle of Repose (β) represents the actual ability of a powder sample to uniformly fill the cavity of a die. An angle of β = 0 equals ideal flowability (liquids) and an angle of β = 90 represents no flow (solids). To ensure a high powder flowability the angle of repose should be below 40° and ideally around 30°. [26]

The net isostatic pressure for the test compact (p_{nc}) represents the pressure that is required in isostatic compaction, with no friction between the die walls and the powder, to reach the specified density of the compacted green part. For compaction processes in rigid dies, this pressure value is equal to the local pressure at the position in the green compact where the local density is equal to the average compact density of the entire green part. This means in effect, the net isostatic pressure for the test compact (p_{nc}) equals the absolute minimum compaction pressure needed for a desired green part density. [26]

The green compact radial expansion (e_a) is the ratio between the radial (perpendicular to the compaction direction) dimension of the ejected compact to the corresponding dimension of the green part under full load. These dimensions are typically measured in the mid height of the compact. This expansion ratio is a function of time, therefore it is measured immediately after the press ejected the green compact from the test die set. [26]

The axial strength of the test compact (w_{sa}) represents the maximum axial crushing pressure that is registered during the third sub-test. This is the strength that is responsible for holding the compacted green part together during the ejection from the die. [26]

The cohesiveness of the green compact equals the ratio between the axial green strength of the test compact (C) and the maximum friction pressure (p_{fm}) that occurs between the die walls and the green compact. This friction pressure (p_{fm}) is calculated using the maximum pressure on the pressing punch (p_c) and the closing punch (p_d) as well as the height (h) and diameter (d) of the green compact. [26]

$$C = \frac{w_{sa}}{p_{fm}} \quad , \quad p_{fm} = \frac{p_c - p_d}{\pi * d * h} \qquad (5\text{-}5)$$

5.4. Geometric green part measurements

Height and diameter of the compacted green parts, that are produced during the experimental manufacturing runs, are important metrics in order to judge the quality of the compaction process and the impact that different powder properties and operating conditions have on the green part results. The height of the manufactured green parts was measured using a common dial gauge and the inner and outer diameter was derived from an automatic optical inspection system.

5.4.1. Height measurements – Dial gauge

The height of the compacted parts was measured using a digimatic indicator type "ID-H0530" manufactured by Mitutoyo which offers a high accuracy due to its resolution of 0,5 µm and a measuring force smaller than 2,0 Newtons. As depicted in Figure 25 the device is mounted on a comparator stand that offers rigid positioning and a flat surface to clamp the green parts. [27]

Figure 25: Height measurement setup using a dial gauge and comparator stand with a clamped green part

The height of the manufactured green parts was measured on four different spots on the same side to get a more accurate average. Since the surface of the compacted disks was not perfectly flat, the variation in height could be analyzed in addition. A schematic depiction of the four measuring points is depicted in Figure 26. The four points are each in a 90° relation

to the previous and next one and have a margin of about ~3 mm to the outer rim of the disk. In the main series of experiments, the orientation of the green parts in respect to the ejection trajectory from the die could not be marked or backtracked due to the high volume and fast pacing of the press. Therefore, the alignment of the four measuring points is starting from a random direction followed by 90° turns clockwise. But in smaller scale pre-experiments the orientation of the compacted green parts was marked, hence it was possible to adhere to the front-back/left-right alignment of the four measuring points.

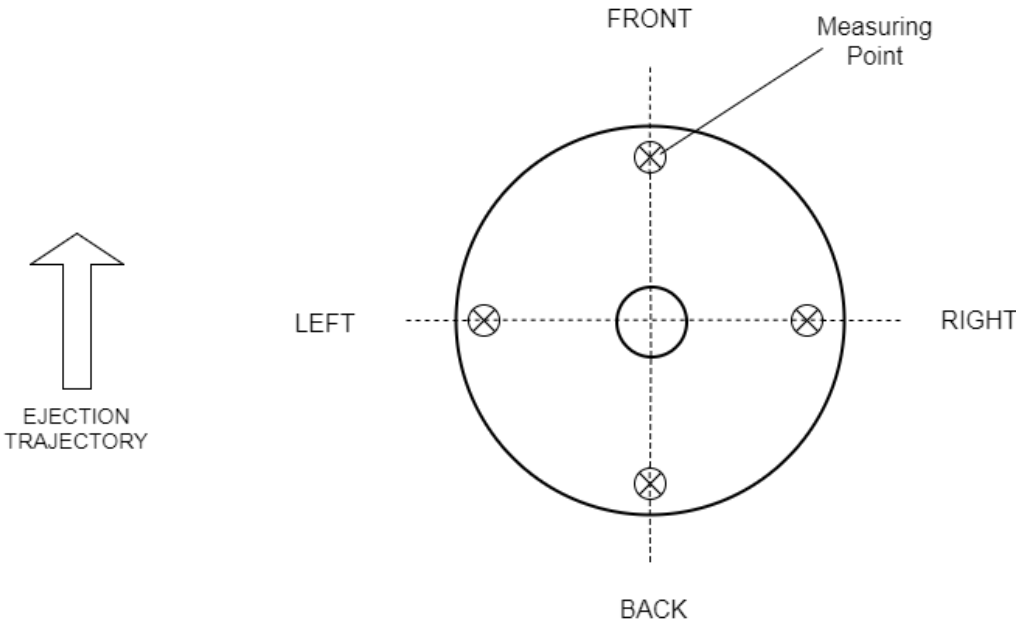

Figure 26: Schematic depiction of the four measuring points and the respective orientation definition of the green part

To ensure accurate measurement of the disk height, the dial gauge was tared after a maximum of ten measured green parts and the compacted discs of each experimental series were measured in a consecutive manner in a timeframe below 24 hours.

5.4.2. Diameter measurements – Automatic Optical Inspection

The inner and outer diameters of the green parts were measured by using an automatic optical inspection system, custom-built by *TCM/ISWAT,* that is placed on top of the conveyor belt, that transports the green compacts away from the ejection rail. As depicted in Figure 27, the lens and camera system is placed right behind the alignment funnel, that ensures proper positioning for the moving green parts. A direct angle ring light, which is placed under the lower side of the optical lens, provides shadow-free illumination of the green parts with a high degree of uniformity.

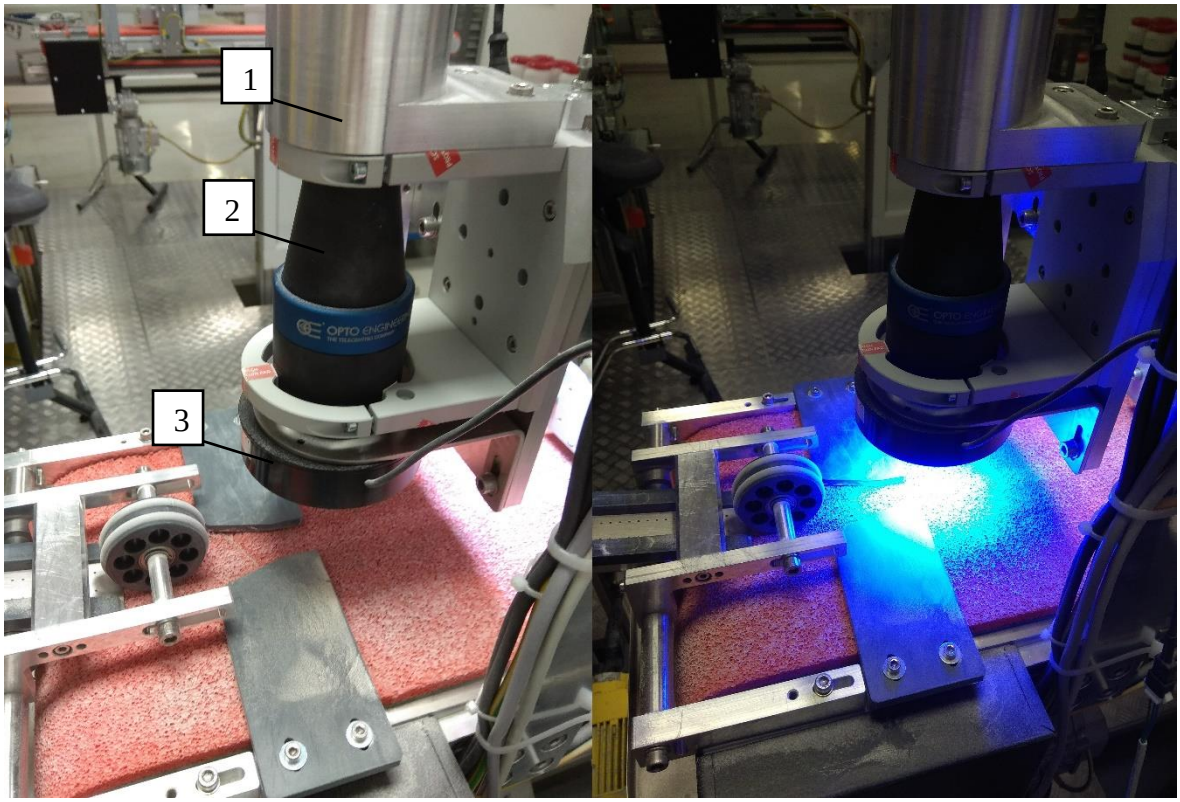

Figure 27: Automatic optical measurement system without illumination (left) and with active illumination (right)

The industrial camera (1) used in this setup is a type “DMK 23GM021” by *Imaging Source* with a 1/3 inch Aptina CMOS Sensor (*Micron* MT9M021), a resolution of up to 1280x960 (1,2 MP) and a maximum frame rate of 115 fps. Furthermore, it offers a sensitivity of 0,015 lx and a dynamic range of 8/12 bit. [28] The tele centric lens (2) attached to the camera system is a type “TC13036” by Opto Engineering and offers a magnification of 0,133 for 1/3” image detectors. It is designed for an object field of view of 36 x 27 mm and a working distance of 102,5 mm. Furthermore, it offers an effective f-number of 8, a typical telecentricity smaller than 0,04 degrees and a typical distortion smaller than 0,03 %. [29]

The direct angle ring light (3), type “FLDR i90B” manufactured by *Falcon Illumination*, consists of 196 LEDs that transmit on the 470 nm wavelength with a maximum illumination diameter of 87 mm and a working range of 5 – 100 mm. [30]

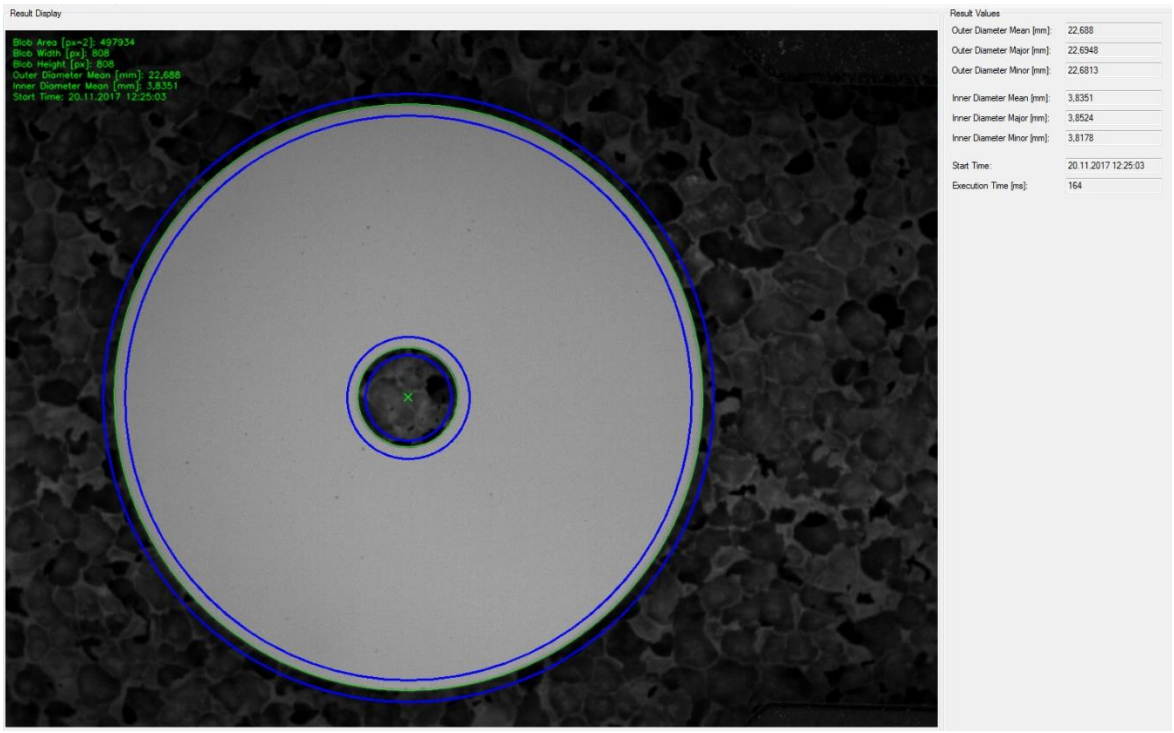

Figure 28: Image caption of the geometric analysis using the automatic optical inspection system

As the green parts are traversing below the optical measurement system, their top side is continually captured by the analysis software. The boundary layers, as depicted in Figure 28, are colored in blue and are mapped onto the image to delimit the search area for the circle outline, wherein the software tries to fit an ideal circle on the contour, both for the inner and outer diameter of the ceramic disc. The dimensions of this ideal circle are then calculated and saved internally. This whole measurement is repeated at least six times for each green part, as it traverses along the conveyor belt beneath the optical system. The average inner and outer diameters are then saved into a file and additional parameters like the maximum and minimum diameter that is captured from each ceramic disk, as well as the standard deviations of the data set are also calculated. Should the measurement system not produce at least six full measurements of the green part, the measurement values are discarded and the part is skipped. Due to this circumstance, the green parts of the experimental manufacturing runs are remeasured manually approx. 24 -48 hours after the initial compaction, so a running order can be established with no skipped parts. With the exception, that if a green part is automatically skipped three times in a row by the automatic optical

inspection system, the green part gets ejected from the manual re-measurement and is not part of the experimental data set anymore. This is because of the fact that manual handling of the green part like the stacking of the parts in the storage tray or the placing on the conveyor belt has a consistent influence on the green parts outer diameter and is probably caused by deburring effects on the outer contour. This loss in the outer diameter, as shown in Figure 29, has been detected by repeated manual measurement of a chosen stack of identical green parts in a short succession where each unique part was measured within an interval of approx. 120 seconds. The average loss of dimension for the outer diameter per measuring repetition equaled to approx. 1,6 µm, which stacks up with each repeating measurement. This change in dimension is not insignificant as the average standard deviation for an individual green part regarding the outer diameter is approx. 2 µm.

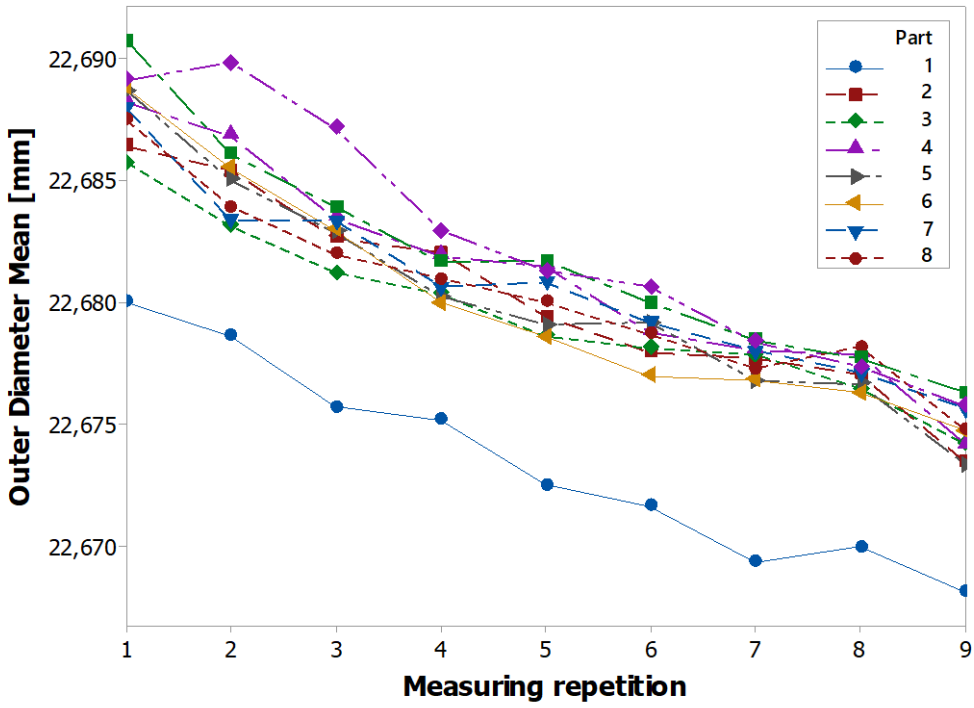

Figure 29: Change of the outer diameter of the green parts due to the repeated measurement with the automatic optical inspection system

5.5. Weight measurements

To accurately measure the weight of the compacted green parts a micro scale type "MSA225S-100-DI" by Sartorius, with a draft shield chamber, was used. The scale achieves a repeatability of smaller than ±0,015 mg with objects below 60 mg and a linearity smaller than ±0,1 mg. In combination with a fast average response time of 6 seconds, automatic leveling and a readability of 0,01 mg this scale was chosen for the weight measurement of the compacted green parts, that weigh approximately 2800 mg. [31] To compensate for off-center load the green parts were placed on an aluminum tray, as depicted in Figure 30. Furthermore, the weighing was always conducted with a closed chamber and the scale was tared after measuring a maximum of ten green parts and re-calibrated daily to ensure accurate weight data. The discs from each experimental series were measured in a consecutive manner in a time frame below 24 hours.

Figure 30: Green part weight measurement setup

5.6. Powder humidity measurement

The powder humidity was measured using a halogen moisture analyzer type "HG53" manufactured by Mettler Toledo. Halogen drying is based on the principle of thermogravimetry, whereby the moisture content is determined by measuring the weight loss of the powder sample during exposure to high intensity halogen light over a set time.
The powder samples that were analyzed over the course of this thesis were exposed to a temperature of 105 °C over a time of 5 minutes.

5.7. Loss on ignition measurement

A loss on ignition measurement was conducted with all the used granule batches to verify their organic mass fraction. The ceramic additives and auxiliaries that were used over the course of this thesis are of organic nature and have a far lower ignition temperature than lead magnesium niobate. By burning out these organic compounds and measuring the weight differences, the binder mass fraction can be determined and verified.

To begin with the measurement procedure, at first the porcelain crucible is pre-heated at 1000 °C for about two hours to achieve a reproducible weight constancy. After the crucible has cooled to room temperature, the weight is measured and it is stored in a desiccator with silica gel to prevent the intake of moisture. After that, a weighed portion of the powder sample is prepared (5,5 ± 0,5 mg) and placed into the crucible. The filled crucible is then weighed and once the annealing furnace has stabilized at 800 °C the crucible is mounted inside. After 60 minutes, the crucible is removed and is weighed again.

The net-weights are then calculated by subtracting the weight of the empty crucible from the weight values of the filled crucible before (m_b) and after (m_a) the annealing process. Then the loss on ignition in percent of total mass (GV) is calculated as follows:

$$GV\ [-] = \frac{m_b - m_a}{m_b} \qquad (5\text{-}6)$$

Since the humidity content of the powder samples was generally very low (0,1 – 0,2 %) the distortion due to the water content in the powder sample was neglected.

6. Experimental setup and procedure

The green part compaction experiments were carried out by using a hydraulic press with a one-sided die compaction and floating matrix setup as depicted in Figure 31. The granules are inserted via a custom-built funnel and filling shoe setup (1) into the pressing tool (2). After the compaction, the green parts are ejected onto an air rail (3), that floats the green parts onto the conveyor belt (4) with the integrated optical inspection system (5).

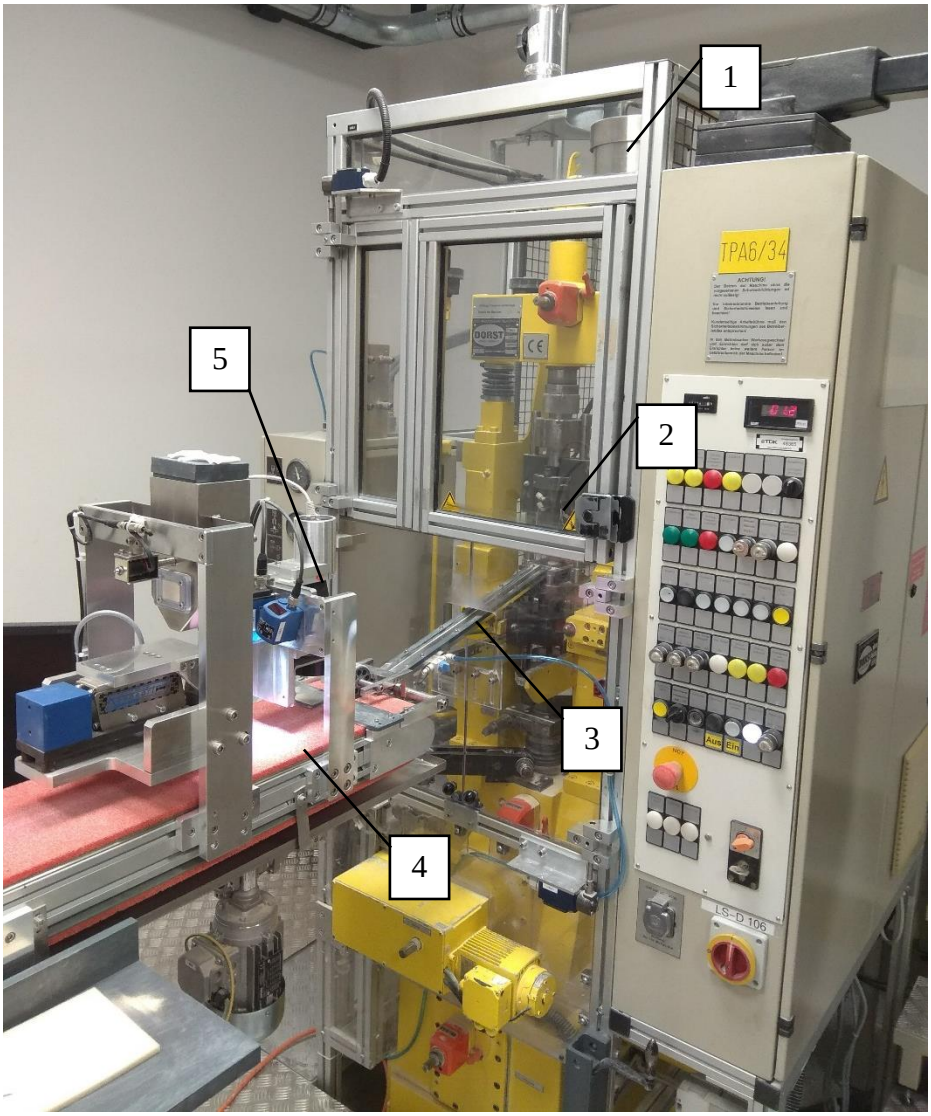

Figure 31: Experimental setup for the green part compaction process

The hydraulic press is a model “TPA-6” with a “PQC-2E” control unit, both manufactured by *Dorst Technologies*, which is capable of uni-axial die compaction with a pressure of up to 6 tons and a pace of up to 70 strokes per minute. The custom-built pressing tool, as depicted in Figure 32, is characterized by a fixed bottom punch (1), a mechanically driven matrix (2) and a movable needle (3) in the center axis. The filling shoe rests on the movable

matrix and moves in a linear motion from the back to the front over the cavity that is formed by the matrix and the bottom punch and thereby fills it with granules. Afterwards the upper punch (4) moves downwards and applies a pre-defined amount of force over a set distance, which is logged by the control unit for each individual stroke. During this process, the matrix is lowered in a corresponding manner to compensate for the granule compression. When the upper punch has cleared the cavity, the mechanically driven matrix lowers to the point where to upper surface of the matrix and bottom punch align to effectively extract the compacted green part. Then the filling shoe moves forward from its backward position and pushes the green part onto the air-rail. After the ejection, the matrix is elevated again to form the necessary height of the cavity and the described cycle starts over.

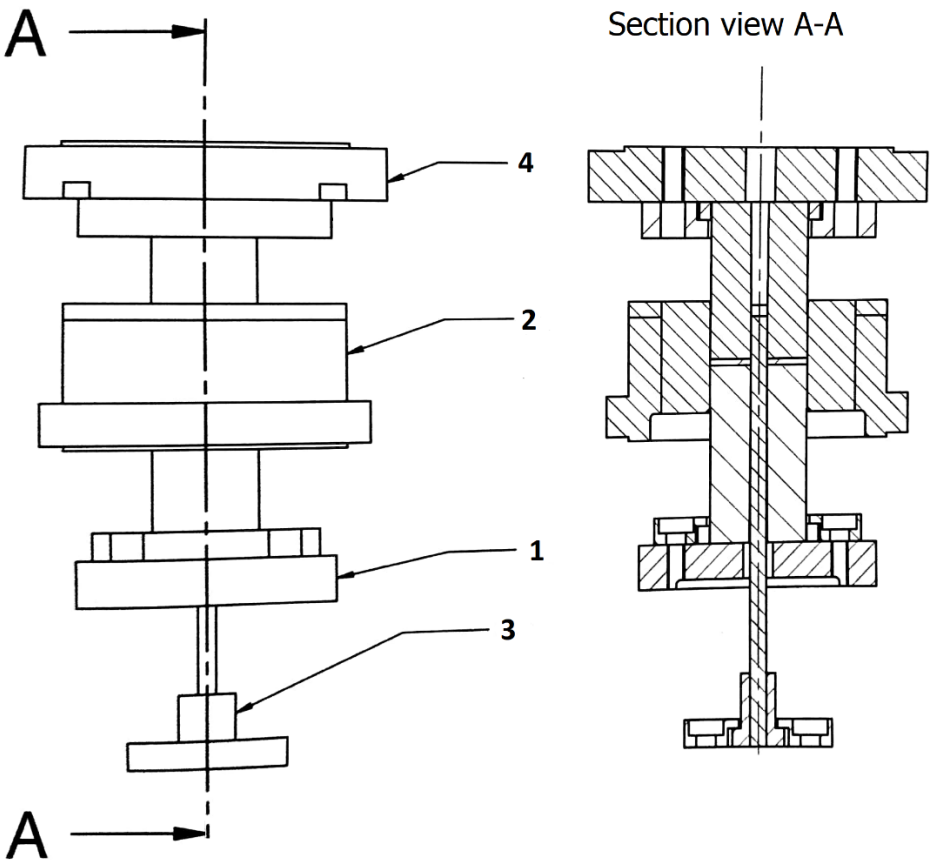

Figure 32: Technical drawing of the pressing tool consisting of the upper (1) and lower punch (4), the movable needle (3), as well as the matrix (2) with section view A-A [5]

Two different hopper designs were used for the experimental runs over the course of this thesis. The first hopper design, which will be referred to as type “H42”, is characterized by its cylindrical and conical shape with a 42-degree angle in respect to its center axis. The second hopper, which will be referred to as type “H20”, is also manufactured in the typical cylindrical and conical shape with a 20-degree tapering, a base diameter of 200 mm and a total height of 381 mm. Both are manufactured with stainless steel and are connected to a manual valve at the end of the funnel, with an inner diameter of 22 mm, as depicted in Figure 33. This shutoff is then further connected to the filling shoe tube (PVC type 22/3 22/28 by *REHAU*). The hopper is mounted with sideway bearings on the cylindrical surface to allow for a rotary movement that equalizes the strain on the tube that is caused by the movement of the filling shoe.

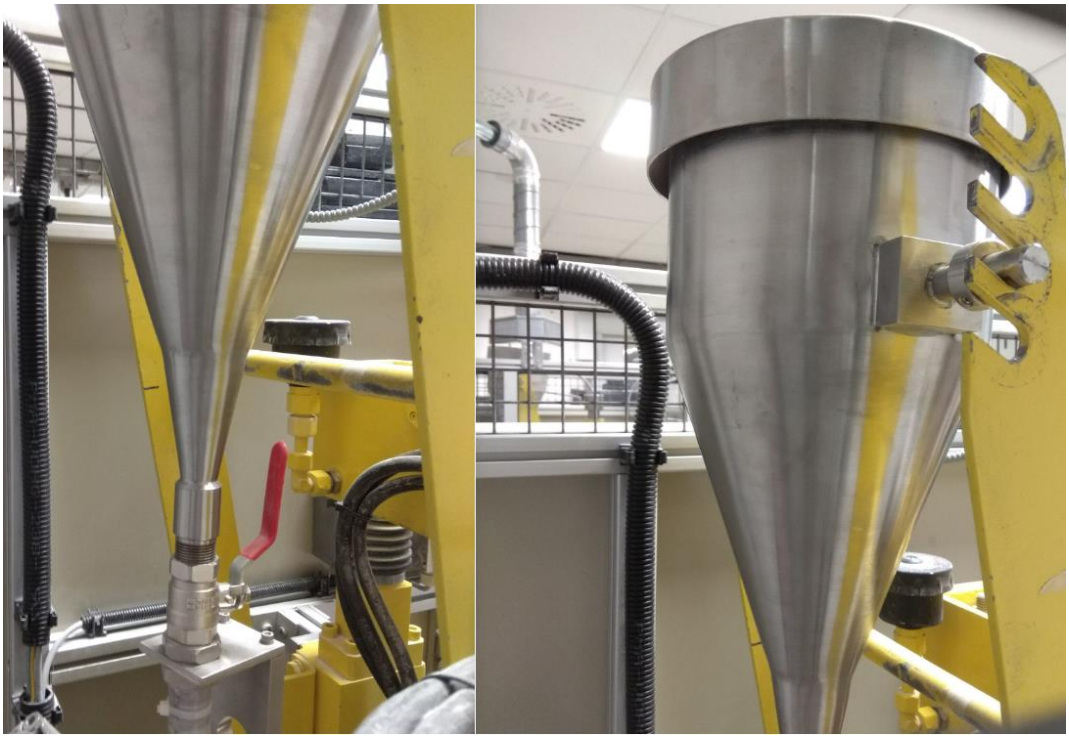

Figure 33: Funnel valve connection on the left, funnel bearing setup on the right

Since the uniform insertion of the granules into the cavity of the pressing tool is of the utmost importance for the green part compaction results, two different custom-built filling shoes, as depicted in Figure 34, were used for the experiments that were conducted over the course of this thesis. The first filling shoe, designated “F30” is characterized by its 30° angle at which the insertion tube is angled in respect to the gliding surface and the tight dimensions of the opening groove. The second filling shoe, which can be considered as a further development, is characterized by its steeper insertion angle of 45° and a much wider opening groove of the sliding block. The filling shoe is mounted to a pneumatic cylinder, as depicted in Figure 35,

that applies movement in forwards and backwards direction and force in a downwards direction, in order to achieve the necessary pressure between the sliding block and the pressing matrix during the granule insertion process.

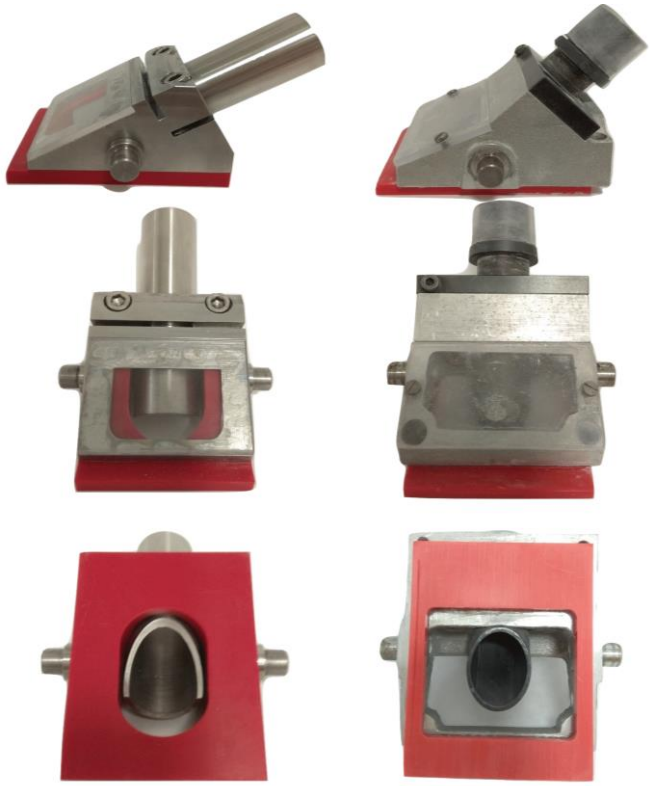

Figure 34: Various views of the filling shoe type F30 in the left column and type F45 in the right column

Figure 35: Filling shoe mount and actuation setup

For some experiments a modified version of the filling shoe “F45” was used. A conventional metal screen with a 2 mm mesh width was implemented directly beneath the filling pipe into the gliding block, as depicted in Figure 36. The mesh was angled at 45° in relation to the sliding direction. The relatively wide mesh was chosen in order to minimize the inhibition on the flow of the granules, while still providing some sort of mechanical barrier to the granules. The reasoning behind this implementation was, that the mesh would act as some sort of mechanical barrier and disrupt the flow patterns of the downwards particle stream and possible size segregation as well as dampening the downwards pressure of the filling tube and funnel. This should lead to a more consistent die filling, independent of the filling level in the funnel. This modified filling shoe is designated “F45_Mesh_Inlay” as it is further mentioned in this thesis.

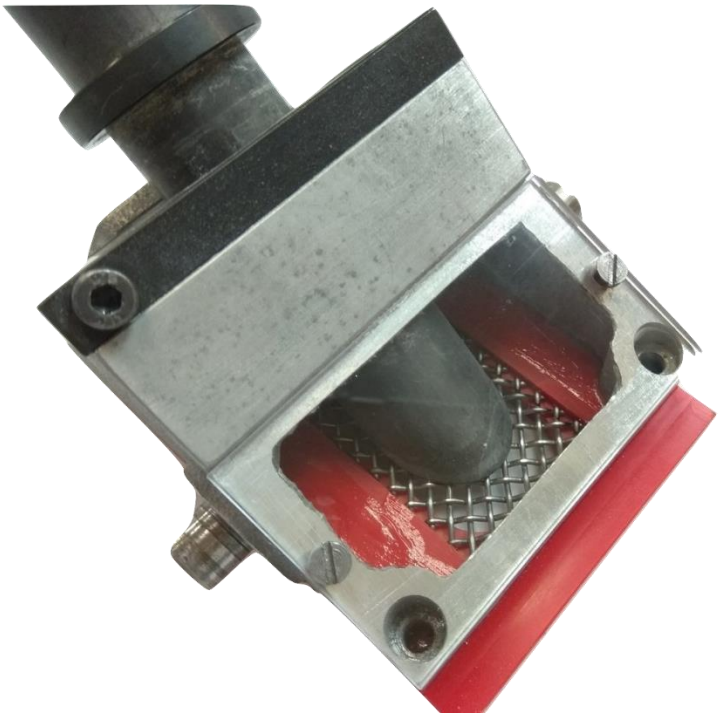

Figure 36: Modified version of the filling shoe "F45" with a 2 mm metal screen directly beneath the filling pipe

6.1.1. Used granule batches

To accurately evaluate the impact of varying particle properties on the compaction process and the resulting green parts, several different granule batches have been used for the experimental runs over the course of this thesis. Most of them have been directly sourced from the ongoing mass-manufacturing process at *EPCOS*, while others were prepared for experimental use only. The material formula and the granulation process were the same in all cases as well as the mass fraction of the added binder blend (3%) and there has been no doping. The standard rotation speed of the spray drying process was 12000 rpm. A portion of the granule batch A11 was dry sieved with a mesh width size of 200 µm to sort out or break up unwanted particle agglomerations. Small portions of the granule batch A13 were spray dried at various disk atomizer speeds ranging from 5000 to 15000 rpm. One sample of the unaltered batch "A13" had its fine material removed with a recirculating air separator with an analytical separation limit of 21 µm and a total mass removal of 5 %. Powder batch "A16" was initially sieved directly after granulation, a portion was split off and sieved again prior to pressing.

Table 5: List of used granule batches

Granule Batch	Binder	Description
A03	Optapix	default mass-manufacturing batch
A07	Optapix	default mass- manufacturing batch
A08	PTC	default mass- manufacturing batch
A11	PTC	default mass- manufacturing batch
A11_S	PTC	Sieved with mesh width size 200 µm after spray-drying
A13_5000	PTC	Rotary disk atomizer speed: 5000 rpm
A13_10000	PTC	Rotary disk atomizer speed: 10000 rpm
A13_12000	PTC	Rotary disk atomizer speed: 12000 rpm, default mass-manufacturing batch
A13_12000_coarse	PTC	Rotary disk atomizer speed: 12000 rpm, fine material removed, analytical separation limit = 21 µm
A13_15000	PTC	Rotary disk atomizer speed: 15000 rpm
A16	PTC	default mass- manufacturing batch, sieved with mesh width size of 200 µm after spray-drying
A16_S	PTC	sieved with mesh width size of 200 µm after spray-drying and prior to pressing

A selection of granule properties is displayed for the granule samples that were used over the course of this thesis in Table 6 below.

Table 6: Overview of the used granule batches with selected particle property parameters

Granule Batch	x_{50} [µm]	moisture content [-]	ignition loss [-]	deceleration time [s]	Cohesive ness [-]	Axial green strength [MPa]	Angle of repose (°)	flow function [-]
A03	46,4	0,0034	0,0337	56	3,32	17,5	40	30,0
A07	43,8	0,002	0,0305	51	2,20	10,2	37	21,0
A08	46,3	0,0011	0,0315	42	1,86	6,9	35,5	20,5
A11	53,1	0,00145	0,0312	48	1,68	6,2	31	79,5
A11_S	50,1	0,0012	0,0293	46	1,93	6,6	34	-
A13_05000	74,6	0,0014	0,0296	53	1,91	5,5	30	-
A13_10000	54,7	0,0015	0,0294	55	1,92	5,7	31	-
A13_12000	52,3	0,001	0,0293	50	1,71	5,8	31,5	-
A13_12000_coarse	53,8	0,0008	0,0288	50	1,84	6,2	31	-
A13_15000	45,2	0,0015	0,0293	52	1,91	6,1	34	-
A16	55,7	0,0008	0,0291	56	1,52	5,2	29	-
A16_S	54,5	0,0007	0,0289	56	1,75	5,6	32	-

6.2. Execution of Experiments

As mentioned in the theoretical background of this thesis, various process parameters had to be considered in the experimental series. This includes the flowability and compactibility of the different granule batches as well as the equipment and tooling that is used for the uniaxial die compaction and the operating conditions of the compaction process itself. Therefore, various experiments have been planned and conducted with the goal to isolate one or more process parameters for the uni-axial die compaction.

Table 7: Overview of the conducted experiments

Trial	Granule Batch	Hopper	Filling shoe	Strokes [1/min]	Binder
1	A03	H42	F30	15	Optapix
2	A07	H42	F30	15	Optapix
3	A08	H42	F30	15	PTC
4	A11	H42	F30	15	PTC
5	A03	H20	F45	15	Optapix
6	A03	H20	F45	20	Optapix
7	A11_S	H20	F45	15	PTC
8	A11_S	H20	F45	20	PTC
9	A11	H20	F45	15	PTC
10	A13_12000	H20	F45	15	PTC
11	A13_5000	H20	F45	15	PTC
12	A13_10000	H20	F45	15	PTC
13	A13_15000	H20	F45	15	PTC
14	A16	H20	F45	15	PTC
15	A16	H20	F45	15*	PTC
16	A16	H20	F45_Mesh_Inlay	15	PTC
17	A16_S	H20	F45	15	PTC
18	A13_12000_coarse	H20	F45	15	PTC

*) with force control enabled

At the start of every experiment the pressing tool, the filling shoe and the hopper were cleaned of any particle residue. The sliding block of the dismounted filling show was inspected for compressed particle residue and the sliding surface was grinded down when necessary. After the cleaning procedure was finished, the hopper with closed valve was filled with approx. 5,5 kg of the selected granule batch to ensure that the downwards pressure from the hopper into the filling tube and shoe was comparable between the different experiments. Now the hopper valve is opened and the granules flow into the filling tube and shoe. The desired machine stroke pace is entered into the control unit and after the air-rail and conveyor belt is switched on, the compaction cycle is started. The first 50 to 100 compacted green parts are used to dial in the different parameters of the hydraulic press to achieve green parts with the desired specification of 2775 mg in weight, 1,5 mm in height and a resulting green

density of 4,65 g/cm³. The stroke distance and the initial position of the upper punch, as well as the needle position have to be optimized. This has to be balanced in conjunction with the applied compaction force to achieve the desired geometric specification while still keeping the compaction pressure low. The height of the cavity can be adjusted by moving the matrix to control the amount of material that is injected during the die filling. This parameter has to be counterbalanced by the distance the upper punch moves downwards and the resulting pressure during compaction to achieve the target height and density. The weight and height of the green part are measured on the spot and once the ideal parameters have been found, up to 50 parts will be pressed to warm up the hydraulic press to see if the green part results are stable. Once the compaction pressure and green part results are holding closely to the target values, the press will then be stopped and the logging module is reset, configured and started. The green parts used for parametrization are discarded. Now the automatic optical inspection (AOI) system is started and the experimental production run begins. Approximately 550 green parts are produced without the change of any operating parameters, force control or any other interference in the compaction process. The inner and outer diameter of the green parts are measured and saved by the automatic optical system. After the green parts have traversed through the measuring area, they are picked up carefully while using latex gloves and stacked into matching trays in chronological order. Since the data logger of the hydraulic press can only display 500 data points of the force progression at one time, which is captured photographically, the force timeline for the parts after the 500^{th} part cannot be retraced. After the desired amount of green parts is produced the compaction cycle is stopped. Now the hopper valve is closed and the remaining granules in the filling shoe and tube as well as the hopper are cleaned out.

All experimental production runs that have been conducted over the course of this thesis have been carried out by the same machine operator in a climatic room, where the granule batches were stored as well.

At a later time, the compacted green parts are manually run through the automatic optical inspection system again, to establish a running order of measured parts with a full data set regarding the inner and outer diameter. This is necessary because the AOI does not always produce a full data set for each individual green part that passes through the camera's field of view. A more detailed description of this circumstance can be found in chapter 5.4.2. Furthermore, with this second measurement series the expansion of the green parts can also

be examined. Afterwards the green parts height and weight is measured in running order as well, as outlined in chapter 5.4.1 and 5.5. Consequently, the green part density for each individual part can then be calculated and the time progression of the measuring values can also be tracked.

6.3.Channel Wheel Separator

To accurately determine the influence that submicron and single-digit micron particles have on the compaction of the ceramic discs, a circulating air separator was used to split up granule samples into two fractions. The device used was a *Hosokawa Alpine* A100 MZR classifier with high dispersing capabilities that is commonly used as an analytical classifier for micron sized powders and can separate several kilograms of powder per hour. The setup of this device is pictured in Figure 37. The spinning channel wheel (1) separates the powder sample into two different fractions, the fine material and the coarse material. This channel wheel is driven by a high voltage tree-phase electric motor (2) that allows for the adjustment of the rotational speed. The initial powder sample (3) is fed into the channel wheel in an axial direction by the means of a worm drive that is connected to flexible shaft that is powered by an auxiliary electric motor (4).

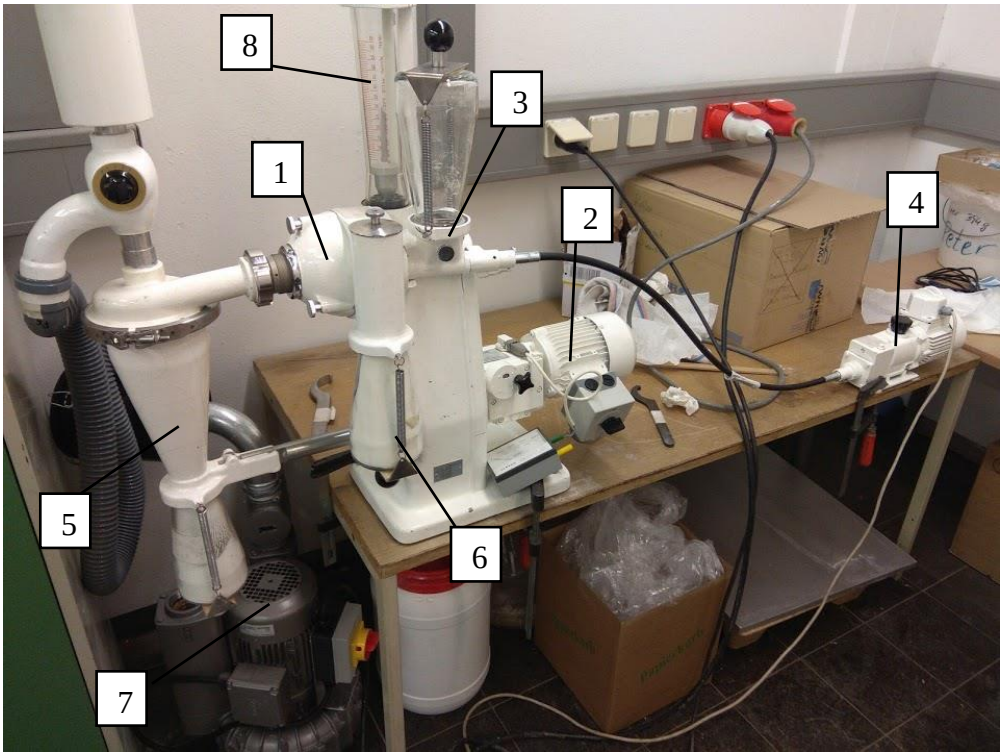

Figure 37: Setup of the Hosokawa Alpine A100 MZR channel wheel separator

The channel wheel then separates the powder sample into two fractions, with a relatively sharp separating limit. The finer material overcomes the rotational pull that is caused by the spinning channel wheel and moves in axial direction into the cyclone (5) and is ideally completely removed from the air stream and collected in the sample glass beneath. However, the heavier particles are accelerated outwards in a radial direction and are collected by the sample glass next to the channel wheel (6). The necessary volume stream is generated by vacuum through an exhaust fan (7) with an additional filter to capture the residue particles. The volume flow that applies to the channel well chamber is displayed at the air flow meter that directly channels into chamber. The airflow ($\dot{V}_k$)in combination with the rotational speed (n_k) of the channel wheel are the two operating parameters that govern the separation limit and the selectivity of the separation and for ideal separation these to parameters should correlate with each other according to the following formula. [32]

$$\dot{V}_k = 55 - \frac{n_k}{1000} \left[\frac{Nm^3}{h}\right] ; \; n_k \, [rpm] \qquad (6\text{-}1)$$

In the case of the granule batch "A13" the aim was to remove as much particles of the size range below 10 µm to examine the influence of the particles close to submicron size on the compacted green parts. To find the ideal operating condition for the air separator several small-scale experiments have been conducted to determine the separation limit for each combination of airflow and rotational speed. Hereby the analytical separation limit was calculated by using the cumulative size distribution of the feed material (Q_A) and the mass fraction of the coarse material (g) to determine the analytical separation limit (x_A) according to the following relationship. [32]

$$Q_A\left(x_A\right) = f; \;\; and \;\; f = 1 - g \qquad (6\text{-}2)$$

The mass fraction of the fine material (f) was not directly used for this calculation, as the separation in the cyclone does not collect 100% of the particles that are funneled through and therefore the fine sample cannot be viewed as representative of the fine fraction. Through this course of action, a volume flow of 52,5 Nm³/h and a rotational speed of 2500 rpm was chosen for the separation of approx. 12,6 kg of the granule batch "A13", which resulted in the removal of approx. 5% of the initial powder sample in the form of the fine fraction.

Afterwards, the separation limit was calculated again by using the particle size distribution the feed material, the coarse (Q_g) and fine (Q_f) material as well as the different mass fraction by using the method of miscounting. This method exploits the circumstance that the areas of miscount for the fine and coarse fraction have the same size, when they are cut off by their analytical separation limit and the mathematical relationship between these areas is listed in the following. [32]

$$g * Q_g(x_A) = f * (1 - Q_f(x_A)) \qquad (6\text{-}3)$$

In this case, an analytical separation limit of 21,2 µm was calculated. The particle size density distribution of the initial feed material and the fine and coarse fraction are shown in Figure 38.

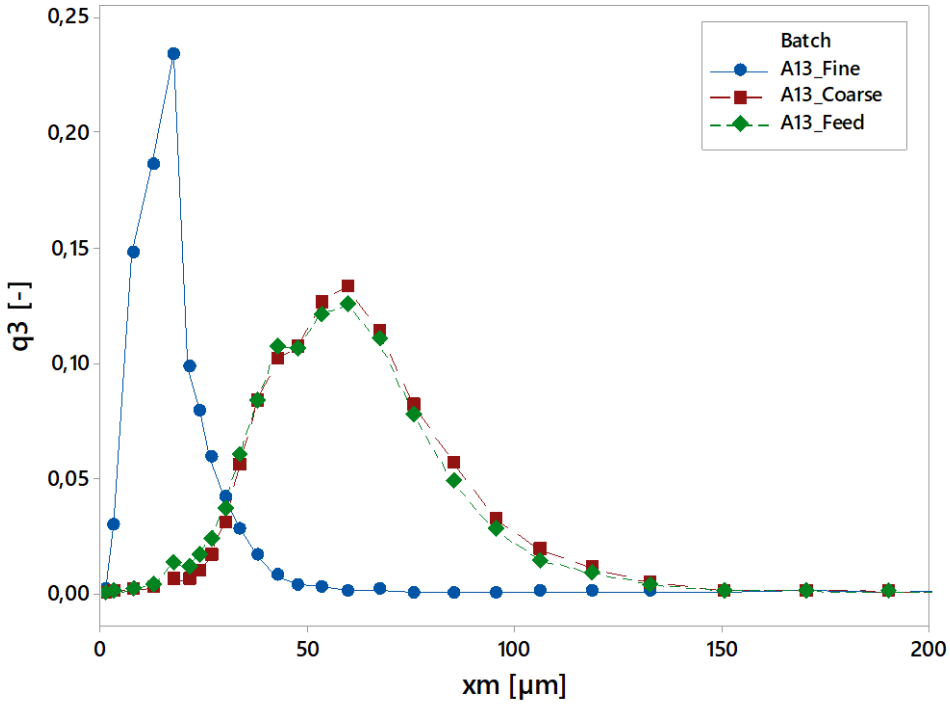

Figure 38: Particle size density distributions (q3) of the powder sample "A13" that was separated through a channel wheel separator, with the initial feed sample and the fine and coarse fractions

7. Results and discussion

This chapter outlines the impact of different process parameters regarding the operating conditions of the press, the properties of the used ceramic material and the die insertion equipment and their respective impact on the weight and geometry of the manufactured green parts. All experimental manufacturing runs have been carried out as described in chapter 6 and the varying process parameters are described in the respective subchapters. The default machine settings were 15 parts per minute with disabled force control. For all statistical analysis a significance level of $\alpha = 0,05$ was upheld.

7.1. Comparison of the binder formulations

The selection of the binder is of critical importance and can influence various parameters of the pressing powder and the subsequent processing of such a material. Some of these include the granule plasticity and strength, the die friction and spring back as well as the spray drying behavior. [33]

To accurately evaluate the impact of the two different binder systems that were currently and previously employed in the mass-manufacturing runs, several experiments were conducted. As outlined in 4.1, there are two distinct binder mixtures, the first one designated "Optapix" which consists solely of the prefabricated ceramic additive "Optapix PAF2" by *Zschimmer & Schwarz* and the second being an in-house formulation of *EPCOS* designated "PTC". For each binder mixture two different powder batches were chosen, and they were all manufactured using the same in-house process at *EPCOS* with an overall binder content of 0,03 in terms of mass. Granule batches "A03" and "A07" contain the "Optapix" binder and the batches "A08" and "A11" contain the "PTC" binder system. In all cases the stroke pace of the compaction cycle equated to 15 strokes per minute and the Hopper "H42" in combination with the Filling shoe "F30" with disabled force control were used.

The first noticeable differences between the two binder systems are the differences between the final weight of the green parts. Both "Optapix" batches have deviated quite far from the initial target weight of 2775 mg, as shown in Figure 40, while the "PTC" batches seem to hold the part weight throughout the experimental manufacturing run. The same general trend seems, as depicted in Figure 39, to be true for the green parts height as well (target of 1,5

mm). The powder batch “A03” displays a significantly (~ 4x) wider variance in both weight and height in comparison to the three other batches that are grouped together very closely.

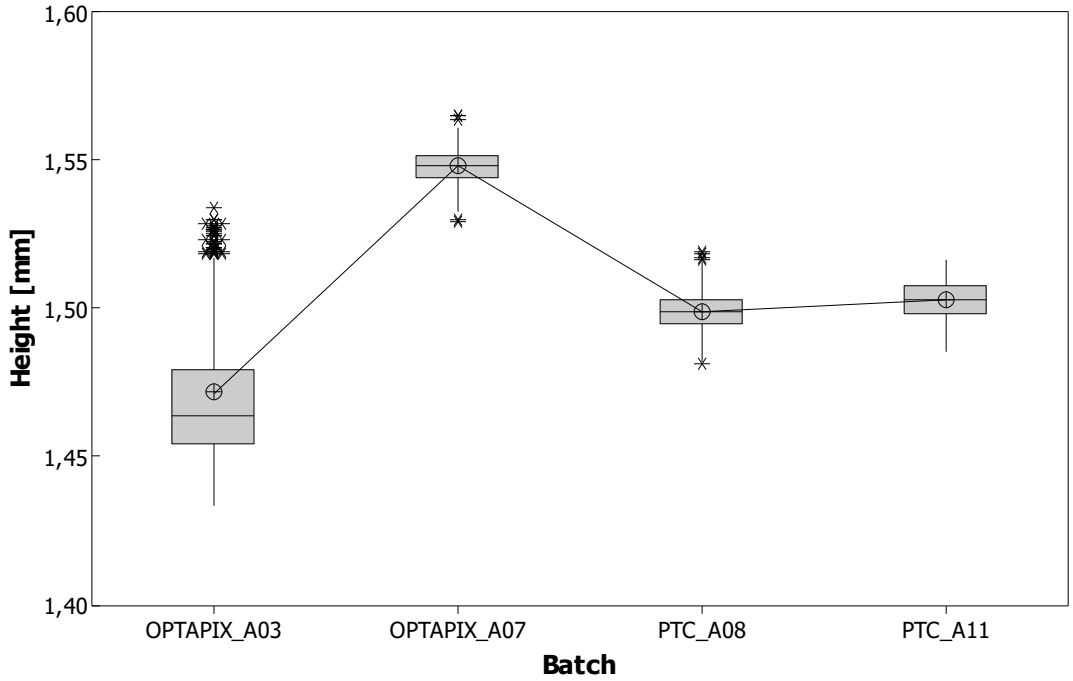

Figure 39: Green part height results of the two different binder systems "PTC" and "Optapix"

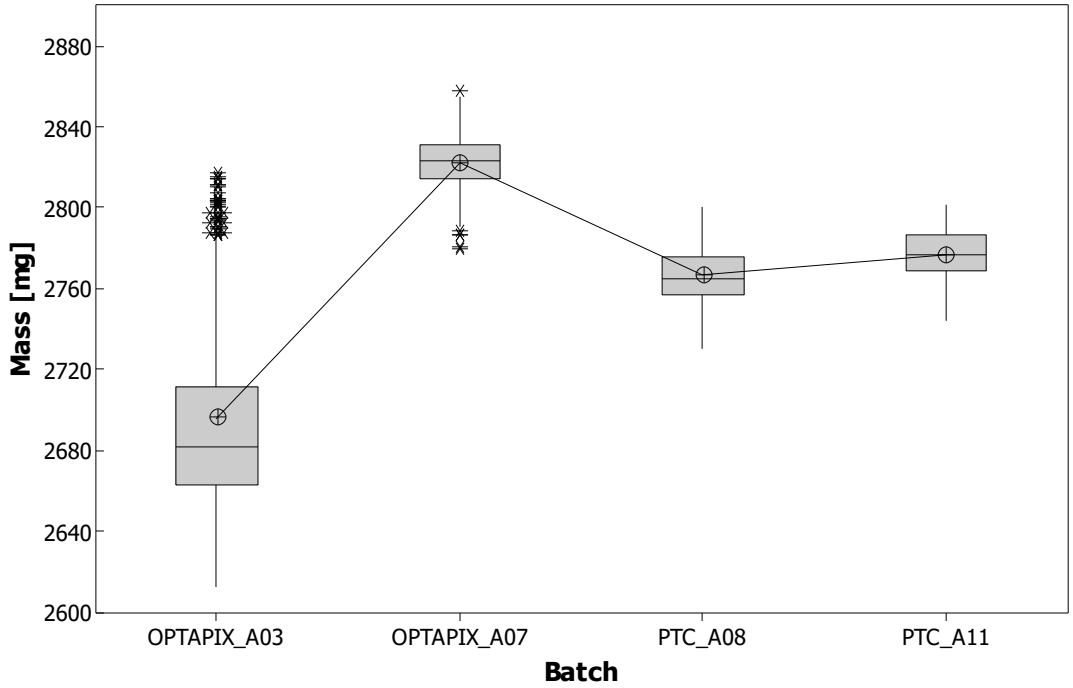

Figure 40:Green part weight results of the two different binder systems "PTC" and "Optapix"

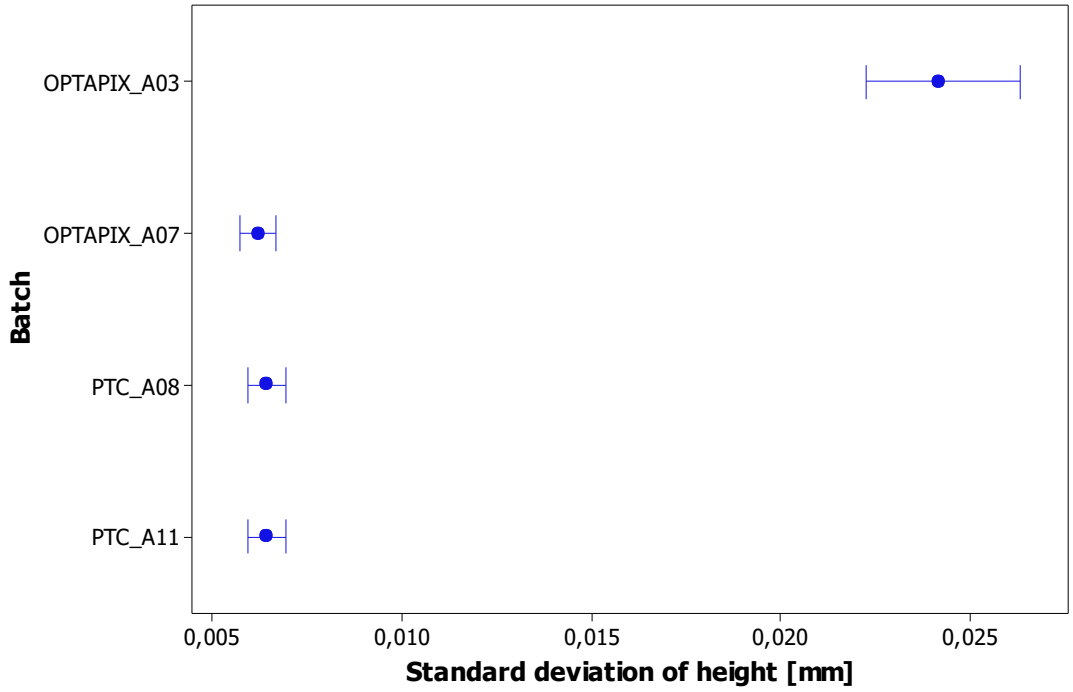

Figure 41: Standard deviations of height and their respective 95% Bonferroni-Intervals of granule batches with the binder systems "PTC" and "Optapix"

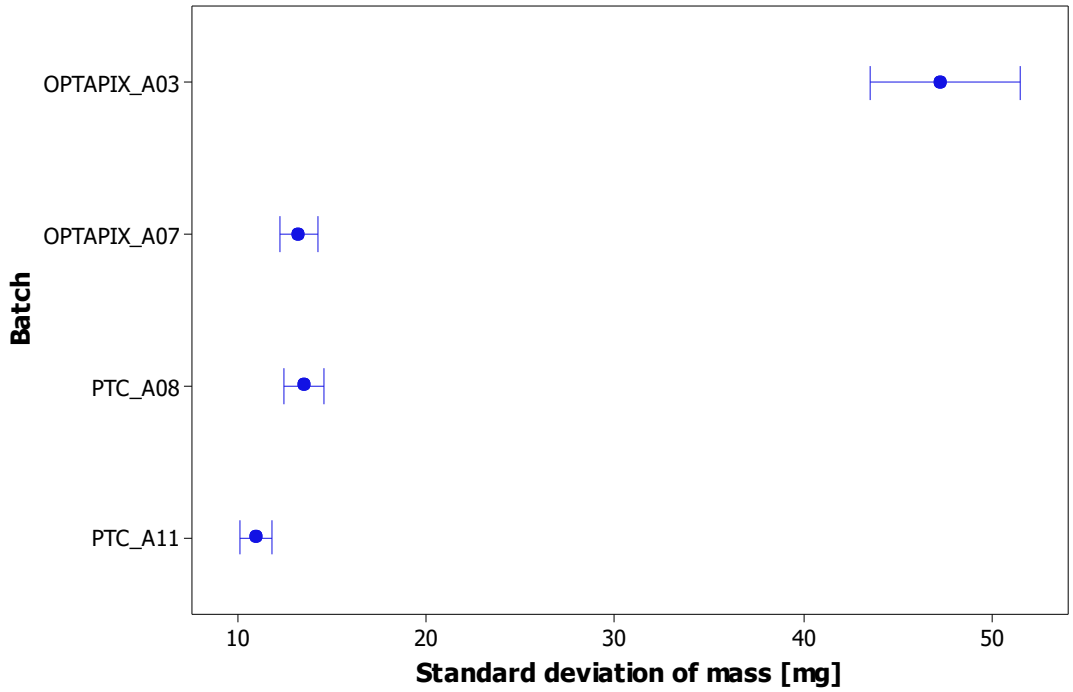

Figure 42: Standard deviations of mass and their respective 95% Bonferroni-Intervals of granule batches with the binder systems "PTC" and "Optapix"

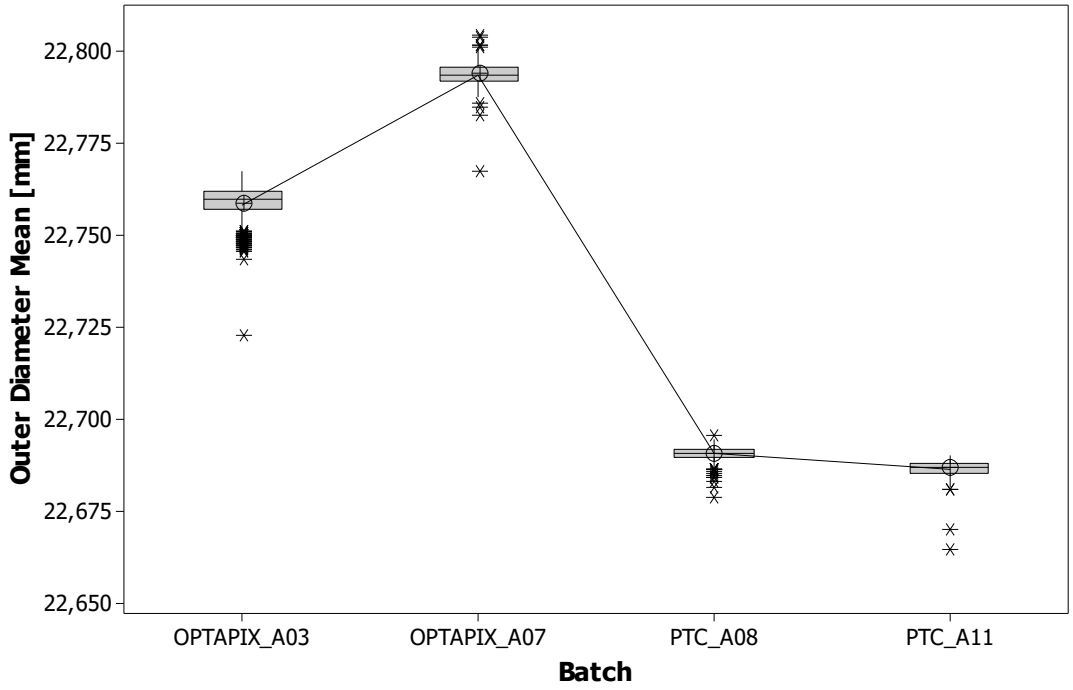

Figure 43: Outer diameter of the green part for various powder batches with the binder systems "PTC" and "Optapix"

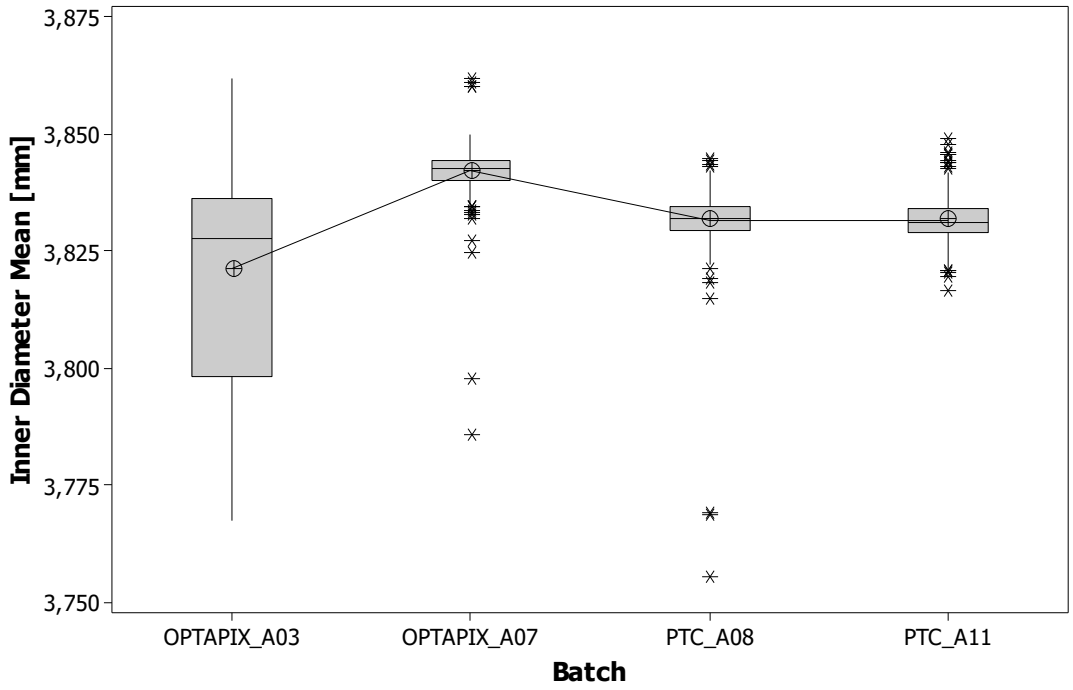

Figure 44: Inner diameter of the green part for various powder batches with the binder systems "PTC" and "Optapix"

A comparison of the standard deviations of the weight and height of the measured green parts, as well as a testing them for equal variances provides valuable insight in the stability of the green part results throughout the entire production run. The respective standard deviations of weight and height and their 95% Bonferroni confidence intervals are shown in Figure 41 and Figure 42. With exception to the powder batch “A03” the confidence intervals of the other powder batches are again closely grouped and no clear conclusion can be drawn. An examination of the outer diameter, as depicted in Figure 43 however shows a clear distinction between the two binder systems. In the case of the “PTC” batches a mean of approx. 22,68 mm has been measured, while in the case of “Optapix” batches there is a significantly wider outer diameter occurring, but the standard deviations are closely grouped together. In the case of the inner diameter, as shown in Figure 44, powder batch “A03” shows a significantly higher variance again.

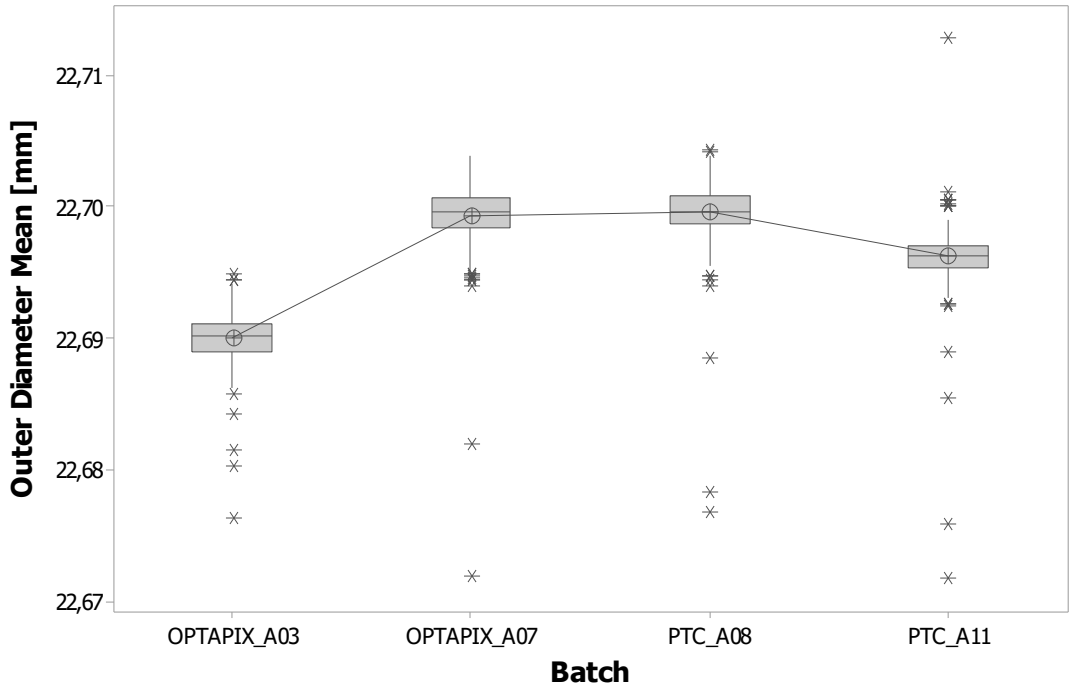

Figure 45: Outer diameter of the green parts measured directly after ejection with comparison of the binder systems "PTC" and "Optapix"

The diameter data that is shown in Figure 43 and Figure 44 was captured during the manual re-measurement that occurred 24 – 48 hours after the initial pressing. By comparing the outer diameter data from the initial measuring right after ejection, as depicted in Figure 45, it shows that the diameters of all four different batches are closely together in the range of 22,69 - 22,70 mm. This leads to the conclusion that there is significant change in the outer

diameter of the green parts compacted with “Optapix” that is not caused by the initial spring back during the compaction cycle, but occurs on a larger timeframe over the course of several days while the green bodies are stored until further processing. The inner diameter of the green parts does not seem to be impacted in the same way. The fact that this phenomenon does not occur with green parts that are manufactured with the binder system “PTC” implies the causation with the ceramic additive “Optapix”.

Conclusively there is a clear distinction between the two different binder systems that have been tested experimentally. Powder batch “A03” seems to be a bit of an outlier regarding the weight and height results of the green bodies. But both powder batches with the “Optapix” binder show a significant change in the green part outer diameter over the course of several days in storage, which could introduce additional problems further down the processing.

7.2. Influence of the compaction cycle time

An increase in the stroke pace of the hydraulic pressing machine is desirable because of the economic realities of mass manufacturing. The increase of output over the course of a given timeframe, e.g. a typical work shift, results in a more efficient use of the employed resources and offers therefore a clear competitive advantage. The impact of such an increase of the cycle time on the compacted green parts was examined in an experimental comparison. Two distinctly different powder batches, one with the binder “PTC” (A11_S) and other with the binder “Optapix” (A03) have been chosen and both have been tested with machine stroke rates of 15 and 20 parts per minute. The hopper type “H20” and the filling shoe “F45” have been used with disabled force control. It should be noted that the powder batch “A11_S” has been sieved after granulation with a conventional sieve with a mesh width of 200 µm with no relevant residue.

In the case of powder batch “A03” there is a clear improvement because of the increased stroke rate of 20/min regarding the green part results in both weight and height, as shown in Figure 46 and Figure 47, even though the absolute values of both drifted away from the targets. This increase in the average weight of mass of approx. 62 mg could be explained by an improvement in the flowability and die filling caused by the speedier motion of the filling

shoe and the lower resting time in between fillings that could cause the buildup of internal resistances in the filling tube and chamber of the filling shoe.

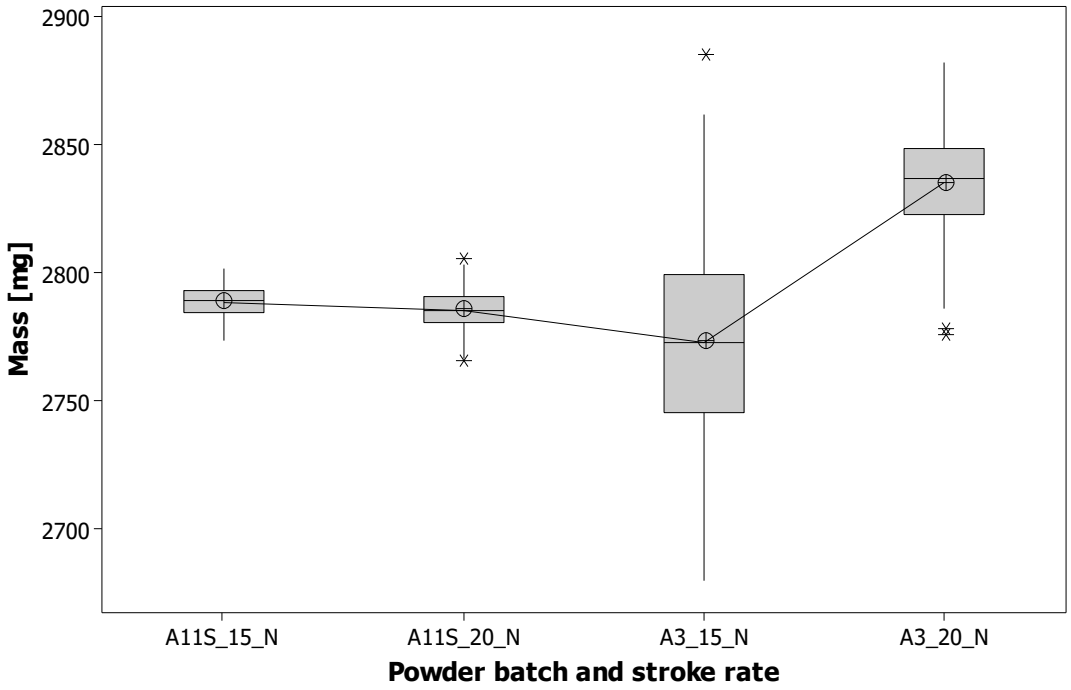

Figure 46: Green part weight data of the powder batches A03 and A11S in relation to the employed stroke rates of 15 and 20 parts per minute

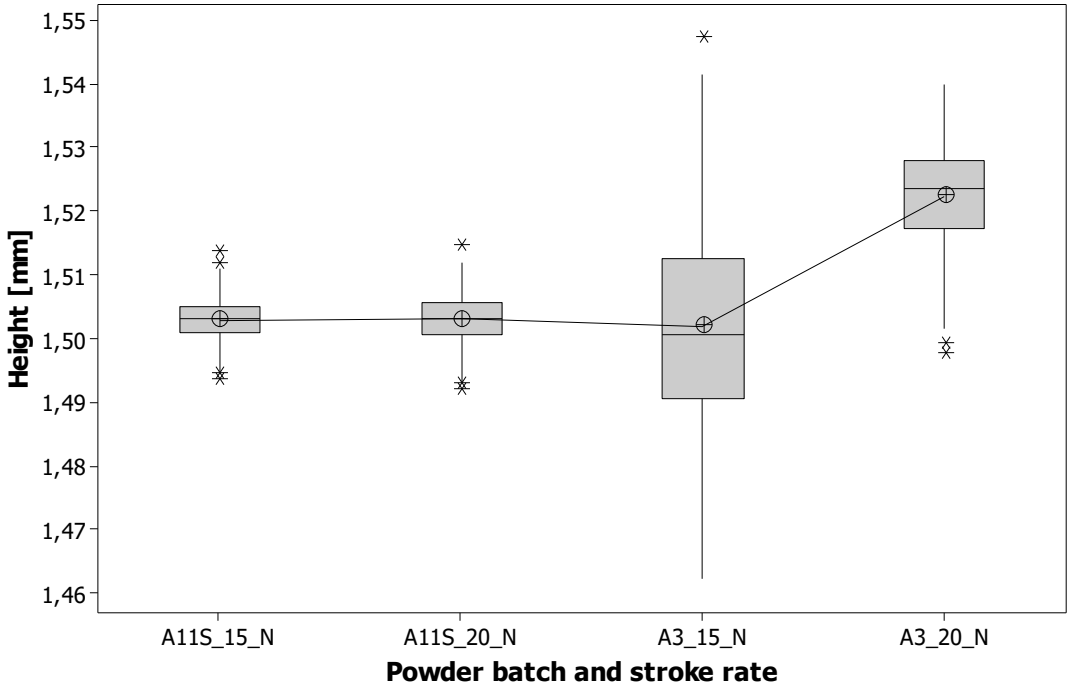

Figure 47: Green part height data of the powder batches A03 and A11S in relation to the employed stroke rates of 15 and 20 parts per minute

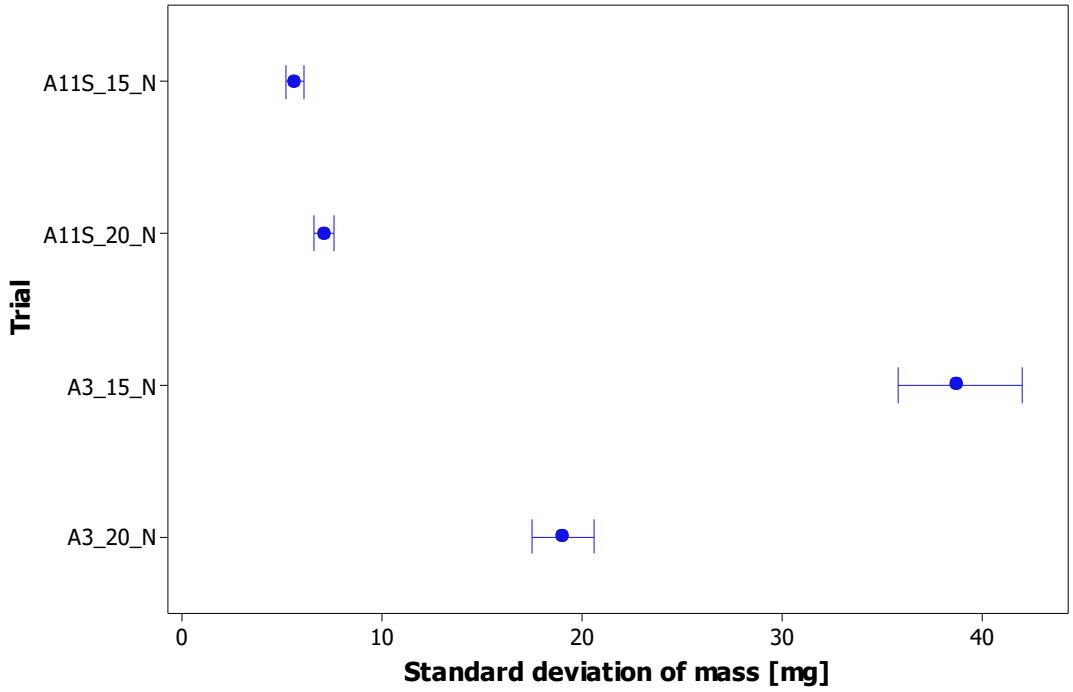

Figure 48: Standard deviations of mass of the green part and their respective 95% Bonferroni confidence intervals in relation to the stroke rate

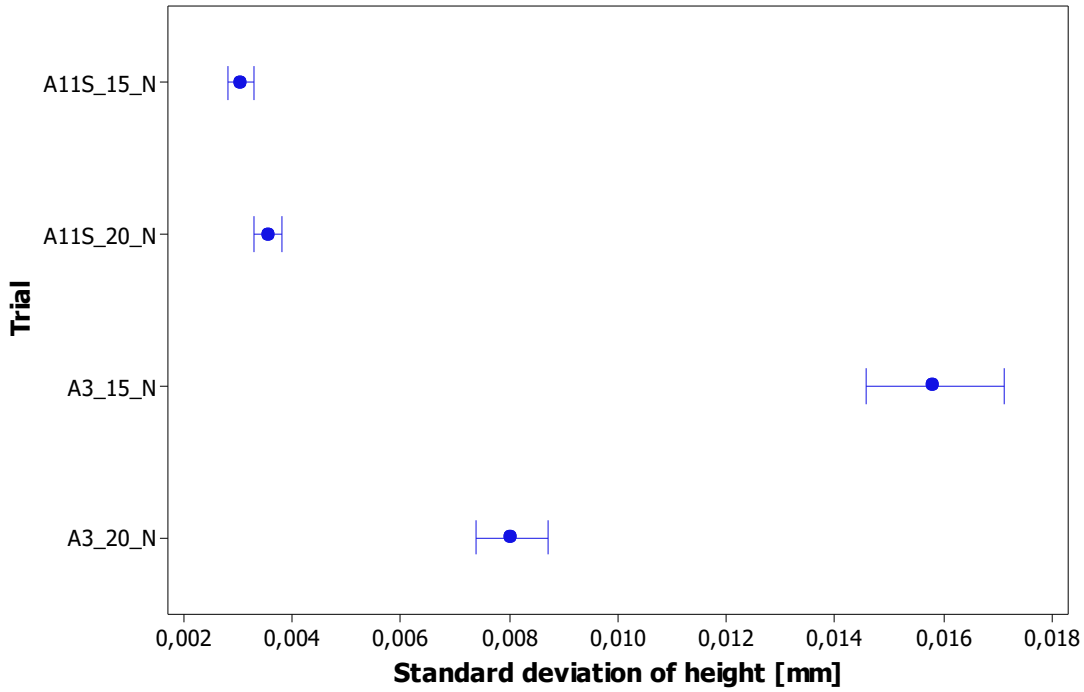

Figure 49: Standard deviations of height of the green part and their respective 95% Bonferroni confidence intervals in relation to the stroke rate

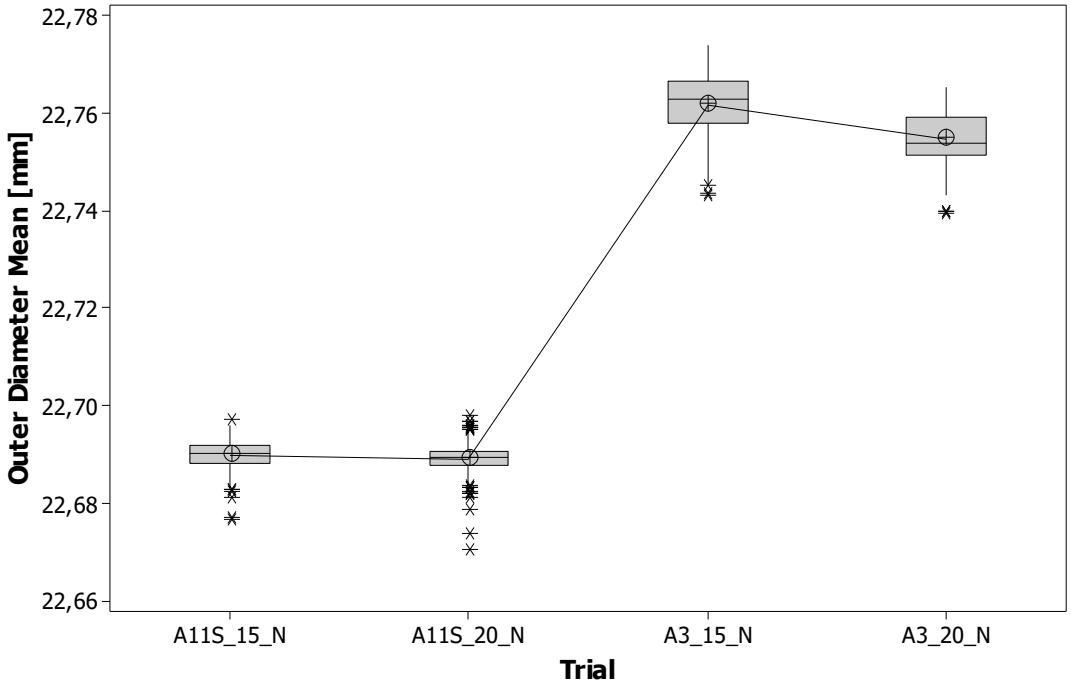

Figure 50: Green part outer diameter data of the powder batches A03 and A11S in relation to the employed stroke rates of 15 and 20 parts per minute

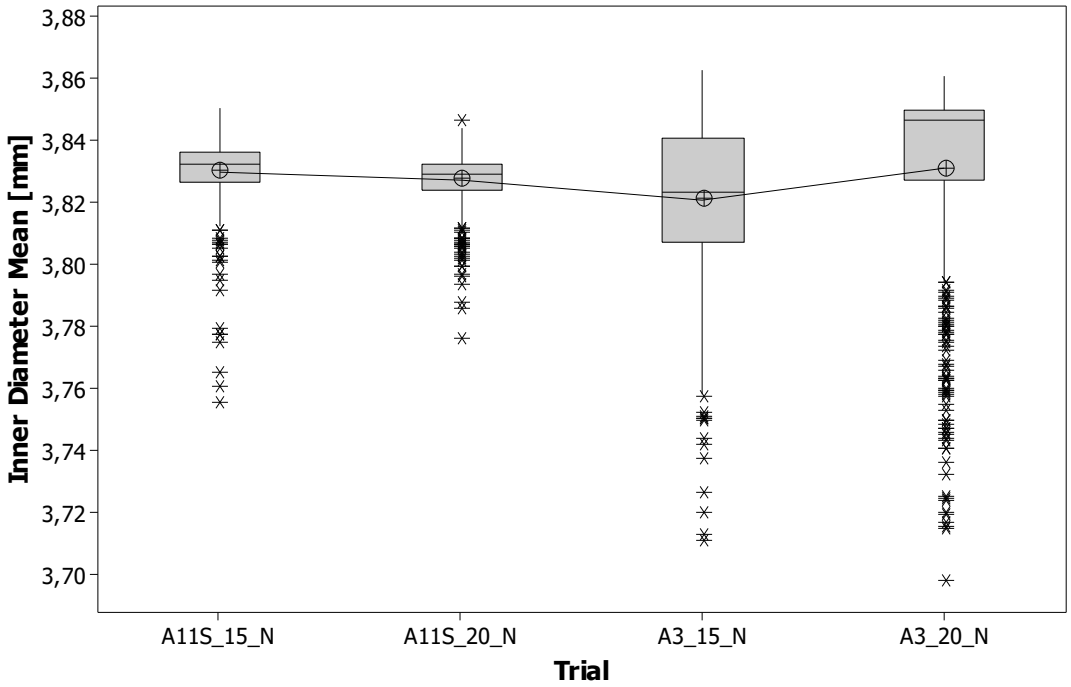

Figure 51: Green part inner diameter data of the powder batches A03 and A11S in relation to the employed stroke rates of 15 and 20 parts per minute

This conclusion is further supported by the statistically significant difference of the standard deviations, as shown in Figure 48 and Figure 49, which shows that the standard deviation and the respective confidence interval is approx. halved by increasing the machine stroke pace from 15 to 20 parts per minute. The data regarding the outer and inner diameter, as depicted in Figure 50 and Figure 51 shows no noticeable differences in regard to powder batch “A03”, but it should be added that the standard deviation tightened from 0,0062 to 0,0049 mm in regard to the outer diameter and widened from 0,025 to 0,032 mm in regard to the inner diameter. Both of these results achieve the threshold for statistical significance.

In the case of powder batch “A11_S” the differences caused by the increased stroke rate are not as clearly pronounced as with powder batch “A03”. It should be mentioned that powder batch “A11_S” already shows a significantly lower part-to-part variation level in terms of mass and weight as well as the diameters of the green bodies. There are no mentionable differences in the achieved absolutes values through the increased stroke rate. But there is a small, but statistically significant widening of the standard deviation for both the mass and the height of the green bodies as well as tightening of the standard deviation of the inner diameter. It could be speculated that a further increase in the stroke rate would further pronounce these differences but due to the mechanical limitations of the compaction cycle controlling mechanism an increase would not have been possible without extensive adjustment to the machinery.

7.3. Variation of the particle size distribution

The grain size and the distribution thereof in a given powdered material is very important throughout the entire compaction cycle. From the flowability of the powder to the establishment of the packing structure in the die and the formation of binding forces during densification, the grain size and distribution are one of the key metrics to accurately assess and improve the performance of a uniaxial die pressing process. [33] Therefore several granule samples with distinctly different grain size distributions where sourced and

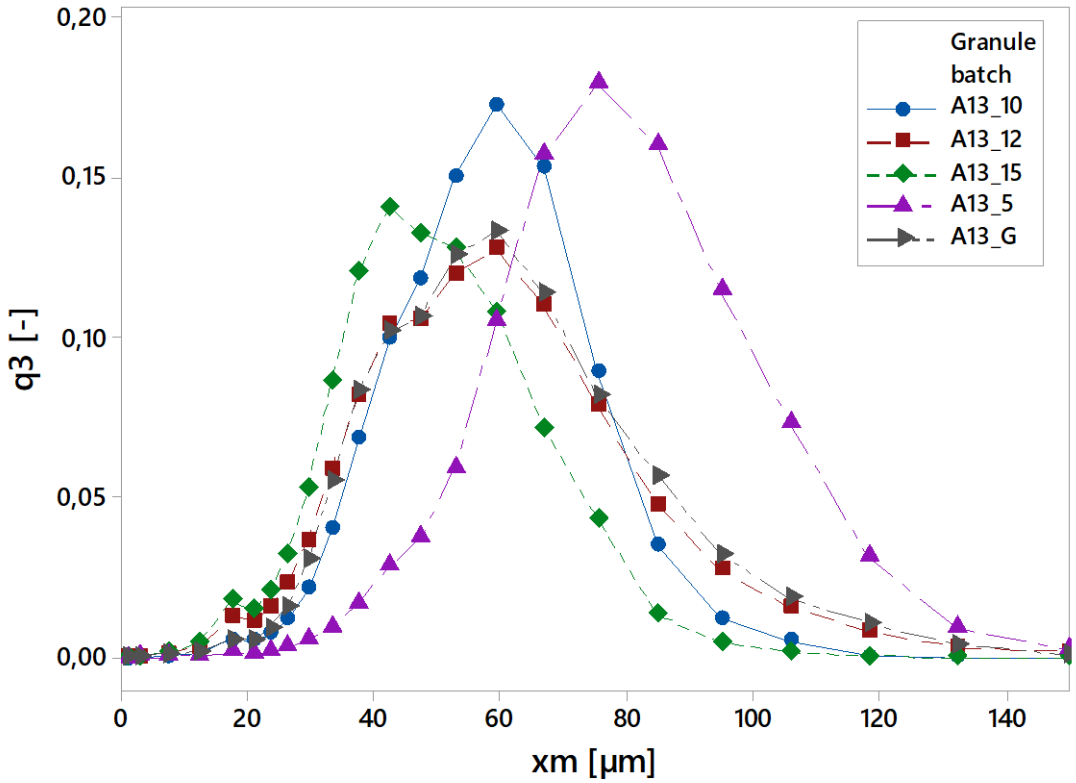

Figure 52: Particle size density distribution (q3) of the different "A13" samples with disk atomizer speeds of 5000 , 10000, 12000 and 15000 rpm as well as one sample with removed fine material

in one case the fine material was separated from an unaltered granule batch with a recirculating air separator. In all cases the EPOCS internal granule batch of “A13” was sourced as the basis for the experimental runs for this comparison. Four different samples with varying disk atomizer speeds during spray-drying, ranging from 5000 – 15000 rpm, were prepared. The fifth sample was an unaltered “A13” with a disk atomizer speed of 12000 rpm were the fine material was removed using a recirculating air separator with an analytical separation limit of approx. 21 µm, resulting in the removal of 5% of the total mass. The disk atomizer speed has proven to be an effective intervention regarding the grain size distribution, as shown in Figure 52. Higher speeds equate to a finer distribution (15000 rpm), whereas lower speeds shift the distribution into a coarser state, in comparison to the default

12000 rpm. All experimental runs were conducted with a machine stroke rate of 15 parts per minute, the hopper “H20” and the filling shoe “F45” with disabled force control. Further particle data for the “A13” samples is listed in chapter 6.1.1 as well as in the appendix.

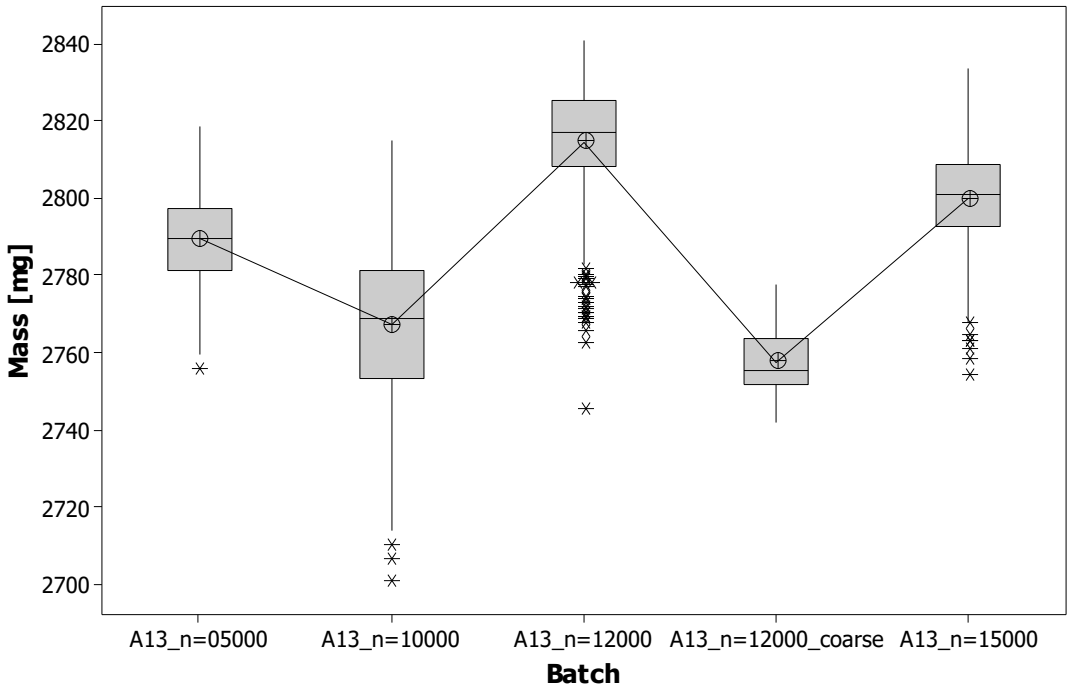

Figure 53: Green part weight data of the powder batches A13 with varying disk atomizer speed of 5000, 1000, 12000 and 15000 rpm as well as a batch with fine material removed (A13_n=12000_coarse)

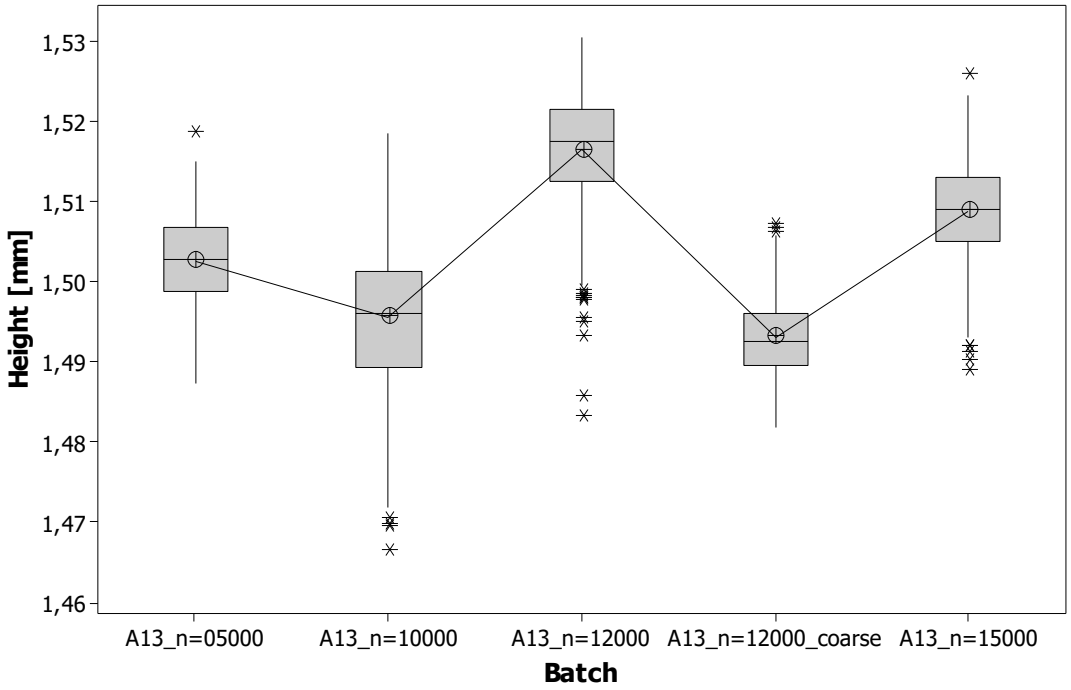

Figure 54: Green part height data of the powder batches A13 with varying disk atomizer speed of 5000, 1000, 12000 and 15000 rpm as well as a batch with fine material removed (A13_n=12000_coarse)

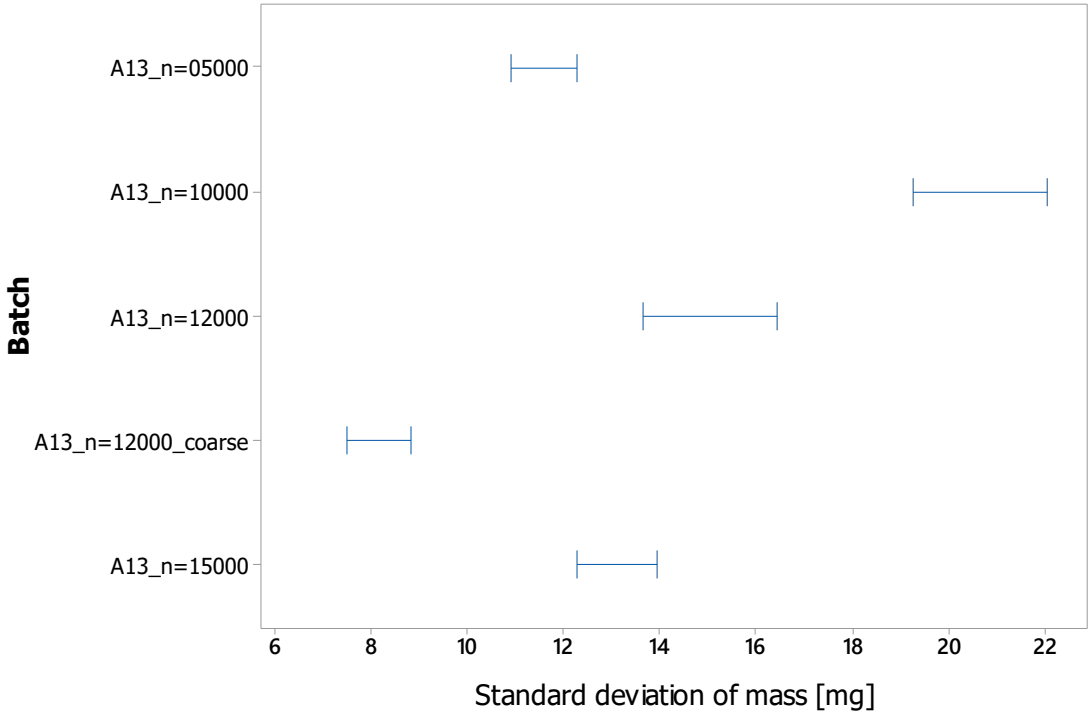

Figure 55: Green part standard deviation data of mass data with their respective 95% Bonferroni Intervals for the powder batches A13 with varying disk atomizer speed of 5000, 10000, 12000 and 15000 rpm as well as a batch with fine material removed (A13_n=12000_coarse)

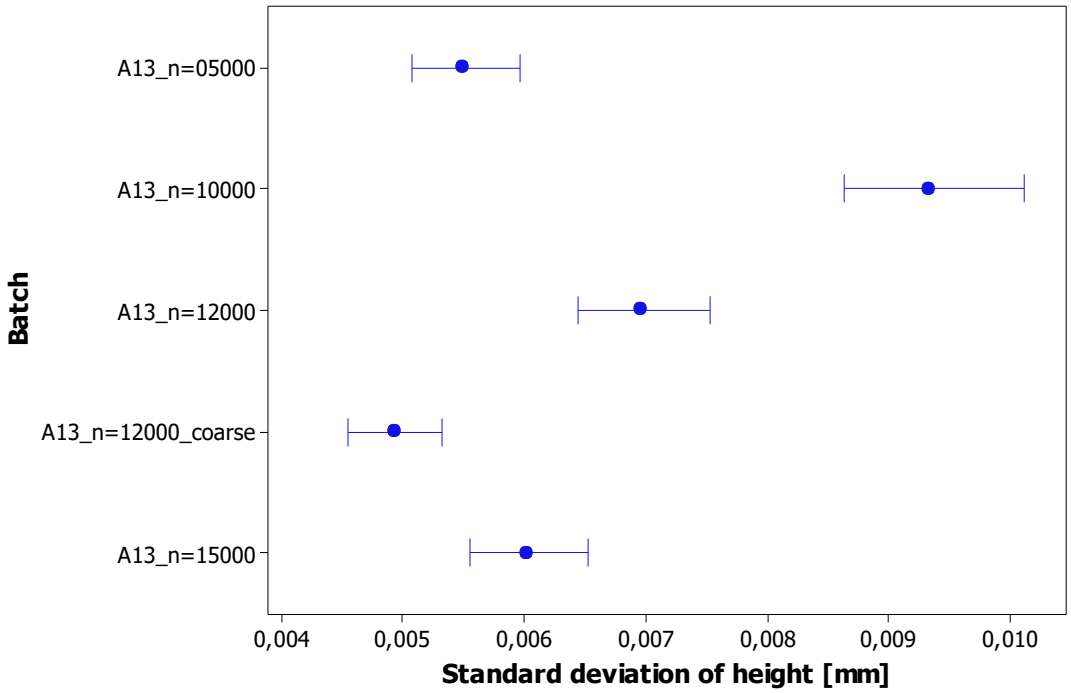

Figure 56: Green part standard deviation data of height data with their respective 95% Bonferroni Intervals for the powder batches A13 with varying disk atomizer speed of 5000, 10000, 12000 and 15000 rpm as well as a batch with fine material removed (A13_n=12000_coarse)

The results of these experiments show that the absolute values of the green parts regarding their weight and height show that some batches, in particular the batch with the default 12000 rpm have drifted away from their targets of 2775 mg and 1,5 mm. As shown in Figure 53 and Figure 54. The default batch with 12000 rpm shows a weight mean of approx. 2814 mg and an average height of 1,516 mm. The confidence intervals for the standard deviations regarding weight and height are shown in Figure 55 and Figure 56.The most notable result from the disk atomizer trials was the granule batch with a disk atomizer speed of 5000 rpm. It shows in both cases, weight and height, a statistically significant improvement of the standard deviation, from 14,97 mg to 11,55 mg and from 0,00695 mm to 0,00548 mm. This is in contrast to the intermediary granule batch with a disk atomizer speed of 10000 rpm. This powder performs in both cases significantly worse than the granular batch with the default 12000 rpm. In addition, the granular batch with 15000 rpm appears to have a slight edge against the default 12000 rpm in terms of the standard deviation of weight and height, but these results do not reach the threshold for statistical significance. Regarding the inner and outer diameter, as shown in Figure 57 and Figure 58, there are no notable results of statistical significance.

To examine the possible negative influence of submicron and single digit micron particles in the granule batches, one of the unaltered samples of batch "A13" with the default disk atomizer speed of 12000 rpm had its fine material removed with a multi-component recirculating air separator. With a volume flow of 52,5 m^3/h and a wheel speed of 2500 rpm an analytical separation limit of 21,2 µm was achieved and resulted in the removal of approx. 5% of the total mass of the original granule batch. This coarse granule batch (A13_n=12000_coarse) has then been used for an experimental production run with the same parameters as the other granule batches with varying disk atomizer speeds. The results of the measured parts are listed in the same graphs already discussed in chapter 7.3. In terms of weight and height, the coarse granule batch performed significantly better than the original unaltered granule batch with the same disk atomizer speed (12000 rpm). The standard deviations tightened from 14,97 to 8,14 mg in weight and 0,00695 mm to 0,00490 mm in height. It also achieved a lower standard deviation in terms of weight in comparison to the already superior granule batch with 5000 rpm. Additionally, this coarse batch was the only one of the four altered batches that achieved a lower standard deviation for the inner and outer diameter in comparison to the original one with a disk atomizer speed of 12000 rpm.

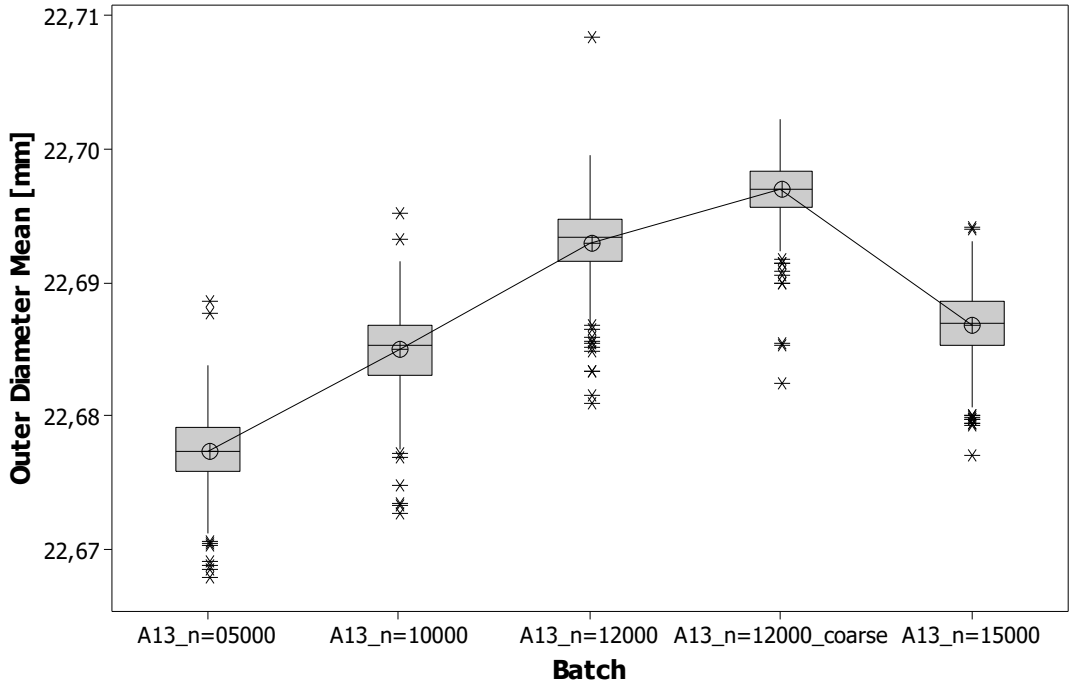

Figure 57: Green part outer diameter data of the powder batches A13 with varying disk atomizer speed of 5000, 1000, 12000 and 15000 rpm as well as a batch with fine material removed (A13_n=12000_coarse)

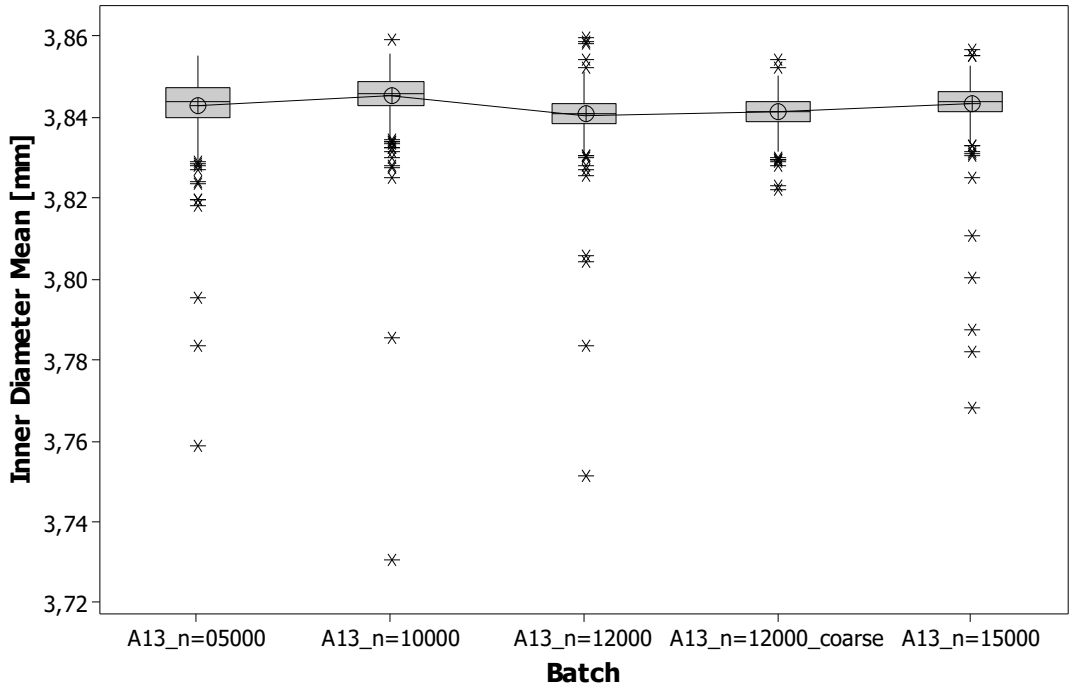

Figure 58: Green part inner diameter data of the powder batches A13 with varying disk atomizer speed of 5000, 1000, 12000 and 15000 rpm as well as a batch with fine material removed (A13_n=12000_coarse)

7.4. Sieving of the granule batches

To properly identify the occurrence and possible impact of unwanted particle agglomerations during storage and handling in between the spray-drying process and pressing, several experimental comparisons were conducted. Two different granule batches were chosen and prepared with a conventional mesh screen with a mesh width of 200 µm. This screen size was chosen large enough to not filter out any granules, as approx. 99 % of the particle population of both batches were smaller than 200 µm and therefore no residual content after sieving was noticed. In the first case, two samples granule batch "A11" were prepared, one was the original unaltered granule batch from mass manufacturing, further designated as "A11", that was not sieved after granulation or prior to pressing. The second sample of the granule batch "A11" was sieved approx. two weeks before pressing, further designated as "A11_S". The second experimental series used the granule batch "A16", which was also split into two different samples. The first sample, further designated as "A16" was the original unaltered batch from the mass manufacturing run, but in this case, was sieved directly after the spray-drying process before it went into storage and was pressed approx. 8 weeks later. Part of this sample, further designated as "A16_S", was then split off and was sieved again approx. 4 days before pressing.

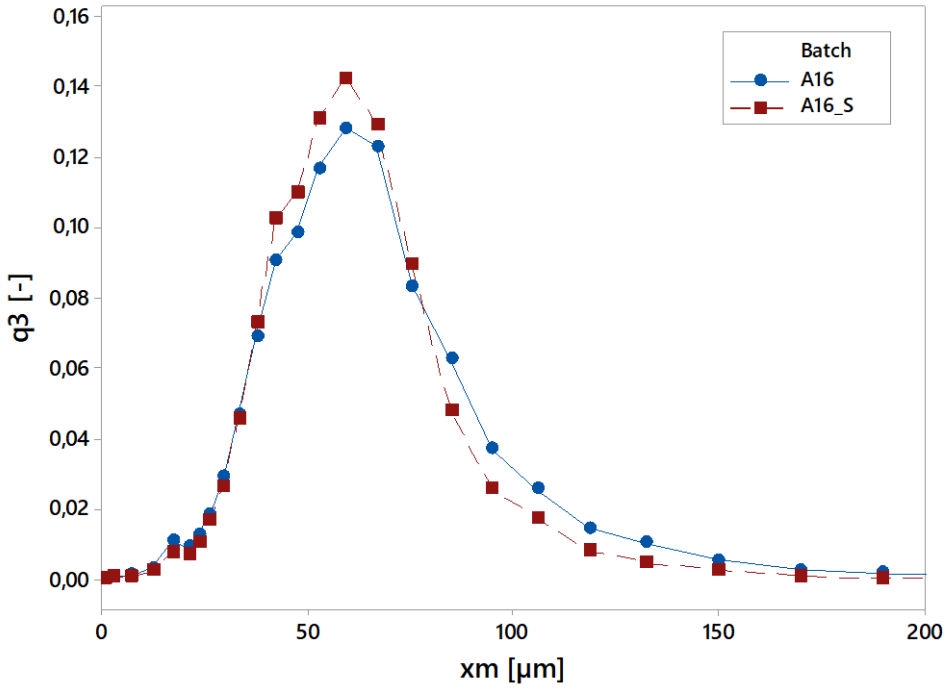

Figure 59: Particle size density distribution of the granule batch A16, directly sieved after granulation and A16_S, which was sieved again prior to pressing (200 µm mesh width)

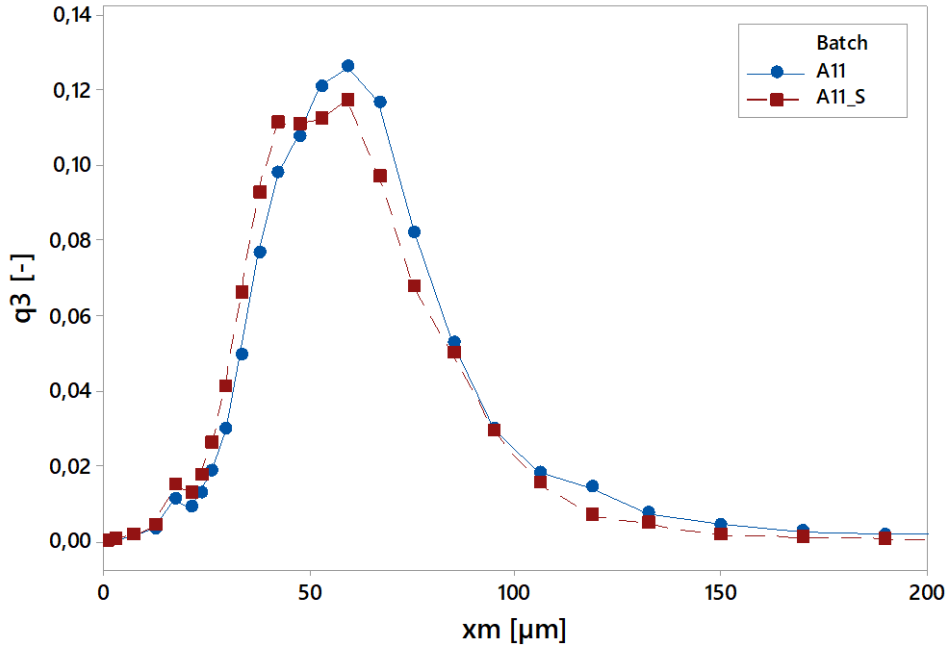

Figure 60: Particle size density distribution of the granule batch A11 and A11_S, which was sieved prior to pressing (200 µm screen opening width)

The particle size analysis shows that for both granule batches, additional sieving shifts the particle size distribution into a finer state, albeit the effects are very minimal. In the case of the granule samples "A16" and "A16_S" the parameter $x_{50,}$ the median particle diameter, shifts from 55,7 to 54,5 µm and in the case of "A11" and "A11_S" from 53,1 to 50,1 µm. Additional particle size and shape analysis using a light microscope has not yielded any mentionable insight.

In the case of the granule batches A11 and A11_S, the sieving prior to pressing has yielded in a significant tightening of the standard deviation, as depicted in Figure 63 and Figure 64, both in terms of height and weight of the green parts. The standard deviation of mass has lowered from 13,5 mg to 5,5 mg and the standard deviation of the height has reduced from 0,00598 mm to 0,00301 mm. This is one of the most significant results from all the experimental runs that were conducted over the course of this thesis. The absolute values of both mass and height, as depicted in Figure 61 and Figure 62 for both trials show no noticeable differences, despite the stark difference in variance. The data for the inner and outer diameter is shown in Figure 65 and Figure 66 and shows no clear difference between the batches "A11" and "A11_S", with the exception of the standard deviation of the outer diameter which has been reduced from 0,0032 mm to 0,0027 mm.

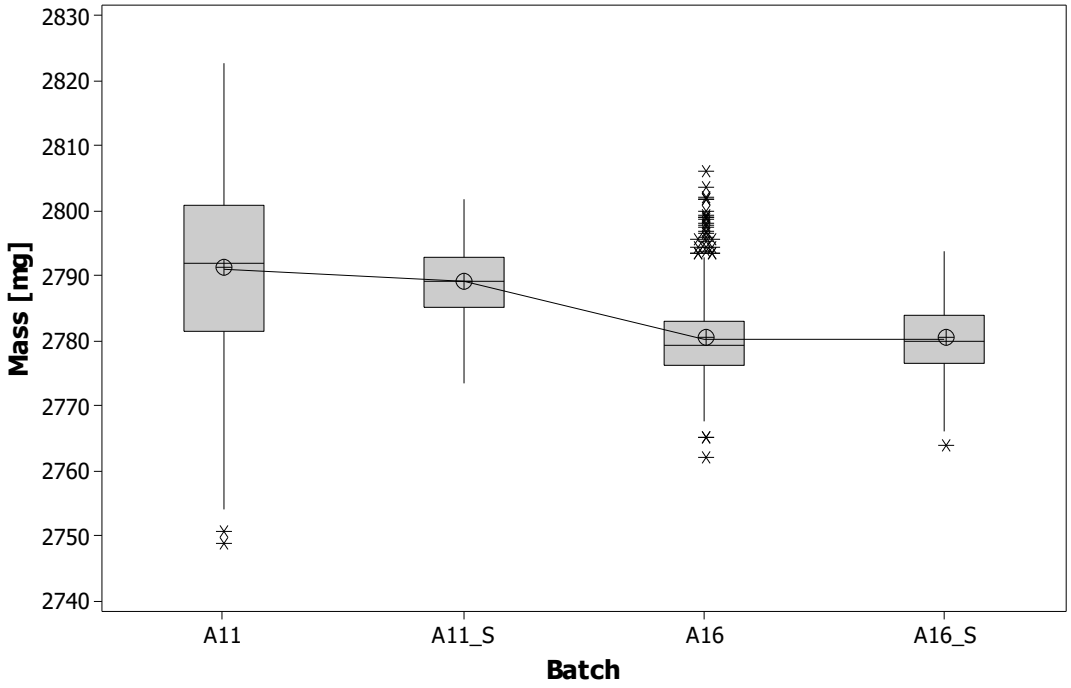

Figure 61: Green part weight data of the powder batches A11, unsieved or sieved prior to pressing and A16, one sieved after granulation and the other sieved again prior to pressing

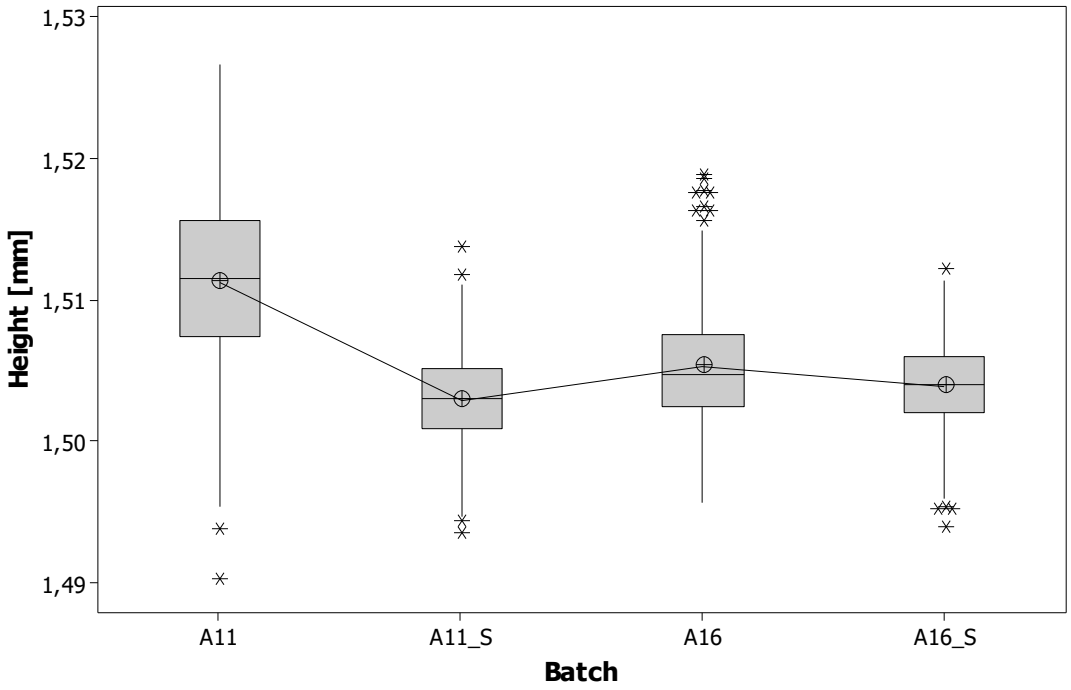

Figure 62: Green part height data of the powder batches A11, unsieved or sieved prior to pressing and A16, one sieved after granulation and the other sieved again prior to pressing

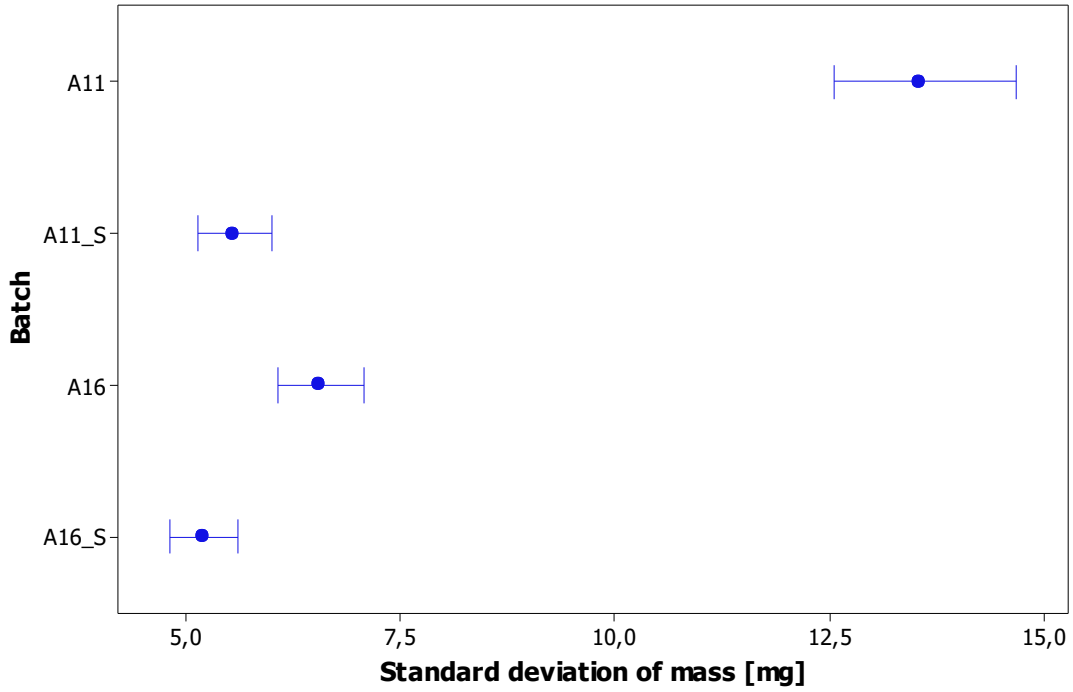

Figure 63: Standard deviation of weight data with their respective 95% confidence intervals of the powder batches A11, unsieved or sieved prior to pressing and A16, one sieved after granulation and the other sieved again prior to pressing

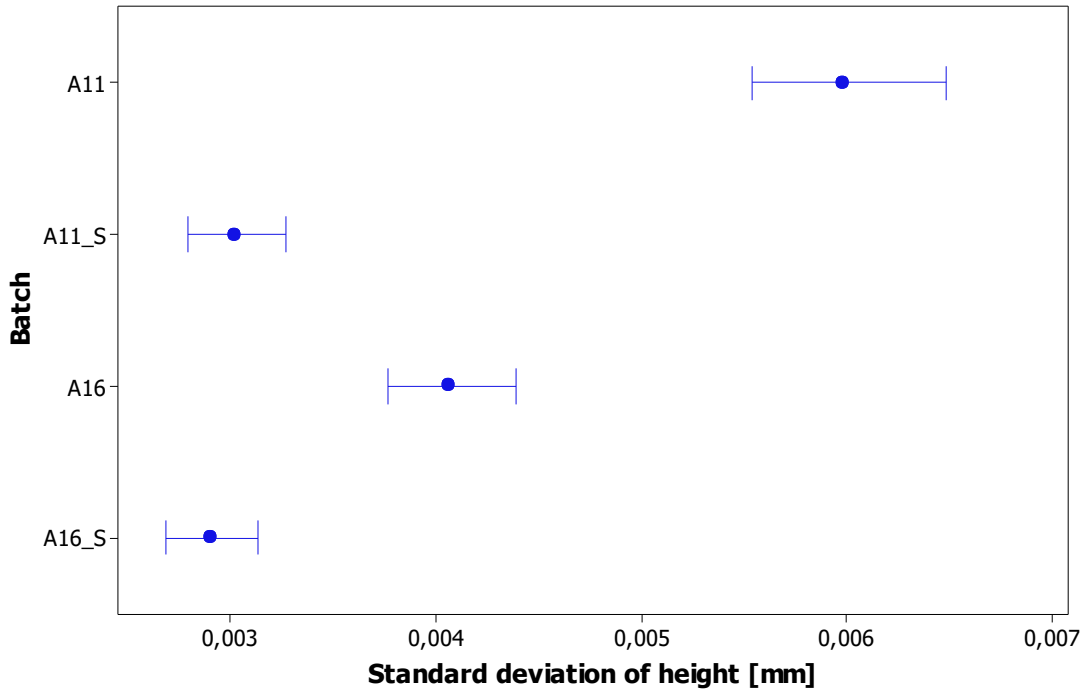

Figure 64: Standard deviation of height data with their respective 95% confidence intervals of the powder batches A11, unsieved or sieved prior to pressing and A16, one sieved after granulation and the other sieved again prior to pressing

In the case of granule batch “A16” and “A16_S” the absolute values of the weight and height and the green parts are closely grouped together, and the standard deviation of both weight and height has been reduced by sieving the granule batch again prior to sieving. The standard deviation of weight has been reduced from 6,52 mg to 5,17 and the standard deviation of height from 0,00405 mm to 0,00289 mm. The experimental data regarding the inner and outer diameter has not yielded any meaningful insight.

Both these experimental series have shown that sieving after granulation and prior to pressing result in both cases in an improved consistency of the green part pressing. In the case of granule batch “A11” which has not been sieved after granulation, the green part results could be improved in terms of weight and height by sieving the powder in a relatively short time frame before pressing. In the case of granule batch “A16” the same conclusion can be made, even though the powder was sieved directly after the spray-drying process. The initial speculation of unwanted particle agglomeration could unfortunately not be corroborated, since particle analysis of the size and shape of the granules did not provide further evidence.

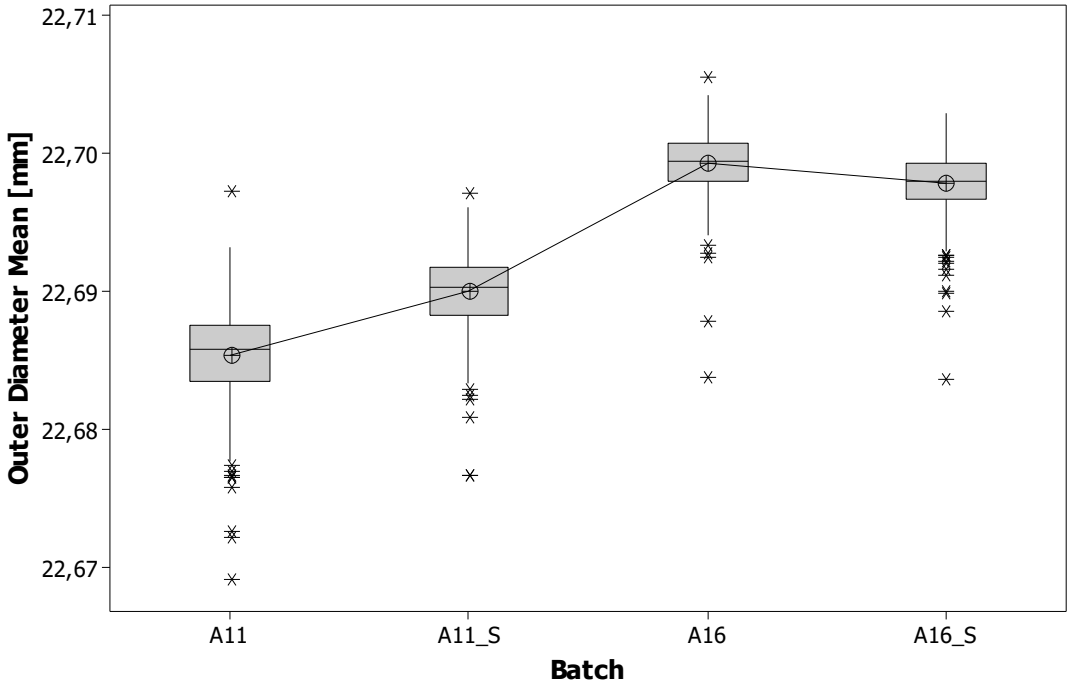

Figure 65: Green part outer diameter data of the powder batches A11, unsieved or sieved prior to pressing and A16, one sieved after granulation and the other sieved again prior to pressing

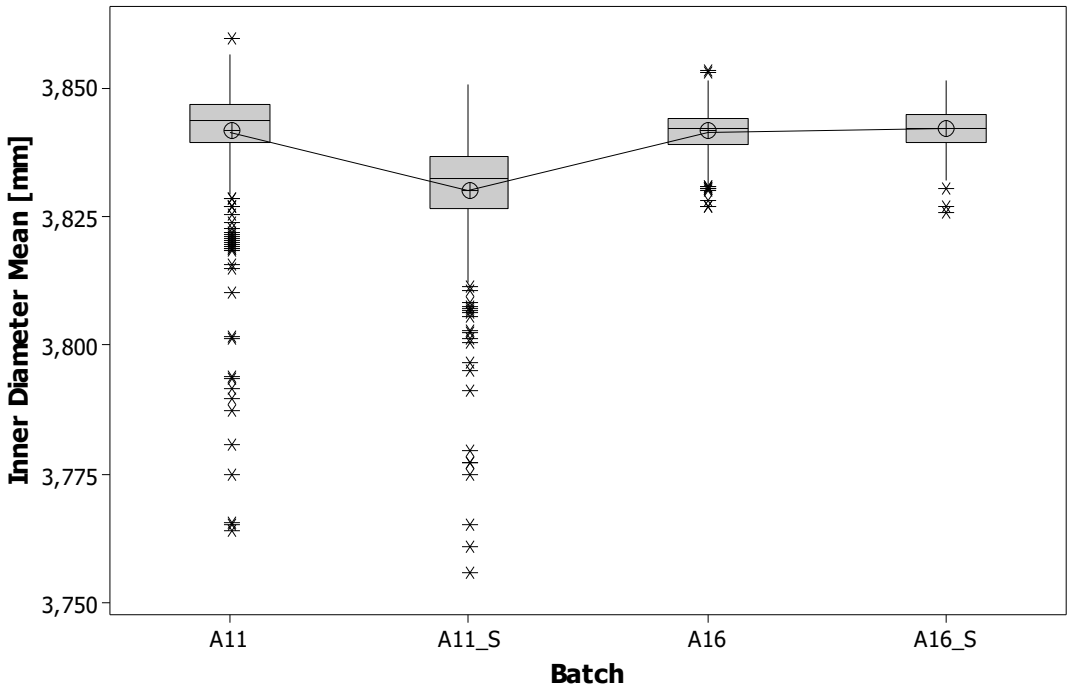

s

Figure 66: Green part inner diameter data of the powder batches A11, unsieved or sieved prior to pressing and A16, one sieved after granulation and the other sieved again prior to pressing

7.5. Influence of die filling equipment on the green parts

The filling process is of the utmost importance for the entire compaction cycle and the final properties of the green parts. Once the particles are placed into the cavity, the microstructure of the compact is more or less fixed. One way to avoid size segregation and inhomogeneities as well as point-to-point and part-to-part variation of fill density is to optimize the die filling and feeding equipment. [33]

Two accurately assess the impact of the filling shoe and the feeding funnel, two different filling equipment setups were chosen. Both were developed internally at *EPCOS* and both were tested with two different granule batches, A03 and A11, under the same circumstances to isolate the influence of the filling shoe and the funnel. The filling setup, further designated ”OLD”, consisted of the filling shoe “F30” with the characteristic 30 ° filing tube angle in respect to the matrix surface and the Hopper “H42” with a tapering angle of 42°. The filling setup, further designated as “NEW” consisted of the filling shoe “F45” and the hopper “H20”.

In the case of powder batch “A03” the usage of the filling setup “NEW” had a positive impact on the green part results in terms of weight and height. As depicted in Figure 67 and Figure 68 the absolute values have held very close to the targets of 2775 mg and 1,5 mm in comparison to the drift that occurred when using the “OLD” filling equipment. This also translates into significantly tighter standard deviation of both weight and height, as depicted in Figure 69 and Figure 70. The standard deviation of weight has reduced from 47,22 mg to 38,72 mg and the standard deviation of height has reduced from 0,024 mm to 0,016 mm. In terms of inner and outer diameter, as depicted in Figure 71 and Figure 72 there were no notable differences regarding batch “A03”. In the case of powder batch “A11” the introduction of the “NEW” filling equipment did not result in such a significant positive result. The absolute values of both weight and height have been held close to the targets by both filling setups, however the standard deviation of weight has widened from 10,8 mg to 13,5mg by using the “NEW” filling equipment. Additionally, the standard deviations of both the inner and outer diameter have also increased by using the “NEW” filling equipment. For the outer diameter the standard deviation widened from 2,1 to 3,2 µm and for the inner diameter from 4,4 to 11,5 µm. These results have shown that there is some sort of interaction between the different filling shoe setups and their respective changes in geometry with the

green part results, but no general trend was noticeable. This leads to the conclusion that changes to the filling shoe setup should only be considered if the desired properties of the granule batches have been established, since varying particle properties lead to drastically different results.

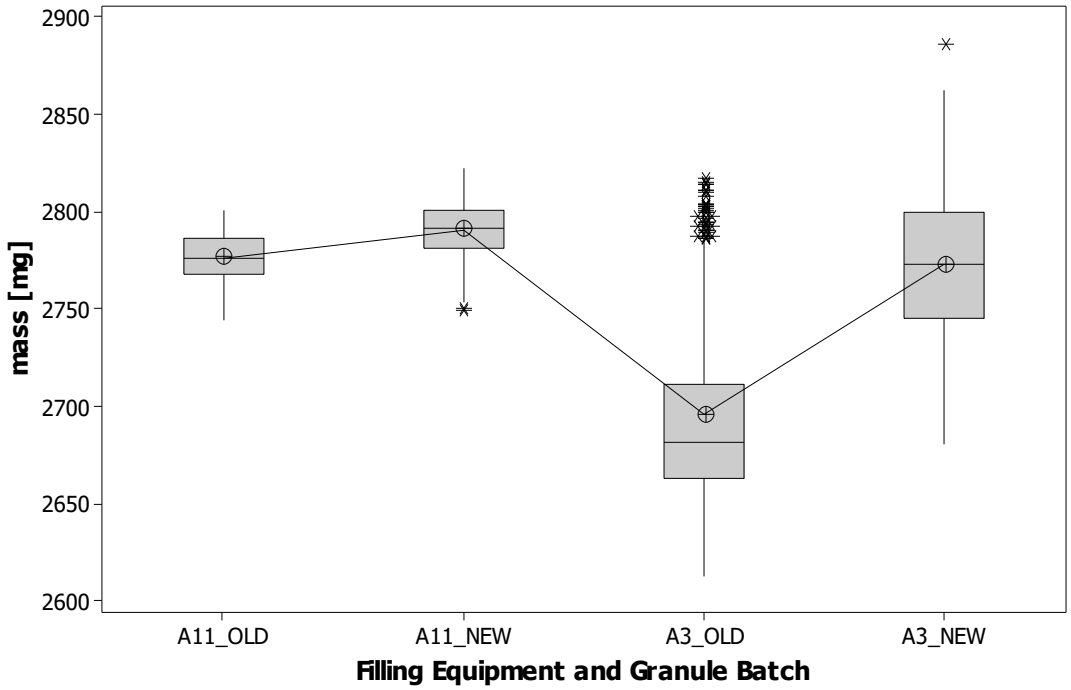

Figure 67: Green part weight data of the powder batches A11 and A03 with different filling equipment (Old vs. New)

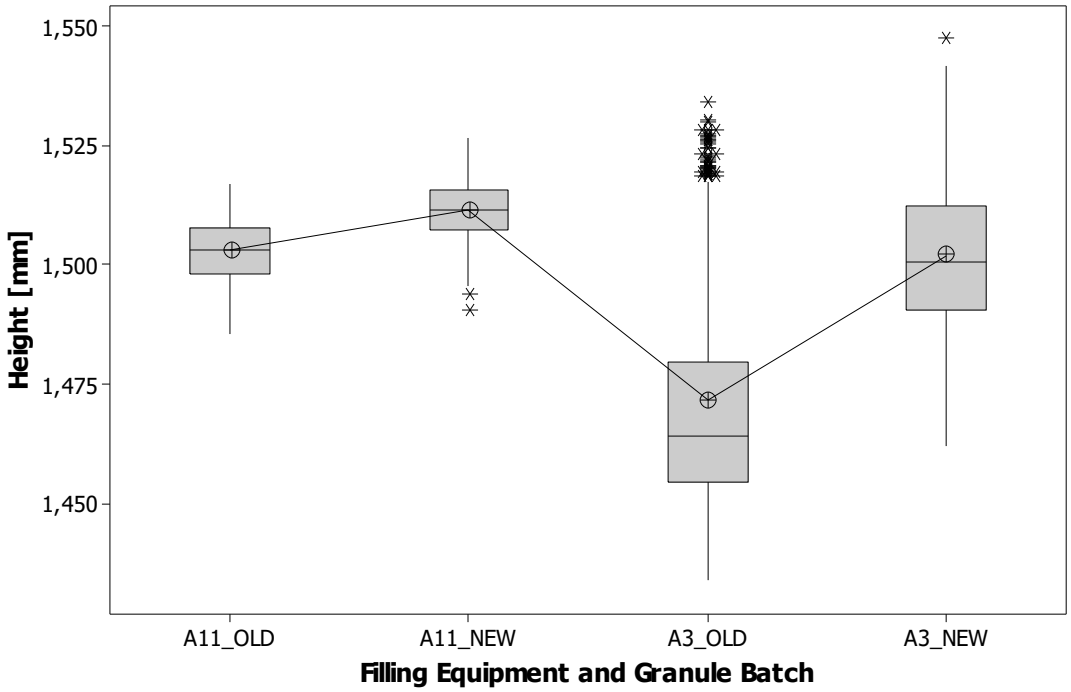

Figure 68: Green part height data of the powder batches A11 and A03 with different filling equipment (Old vs. New)

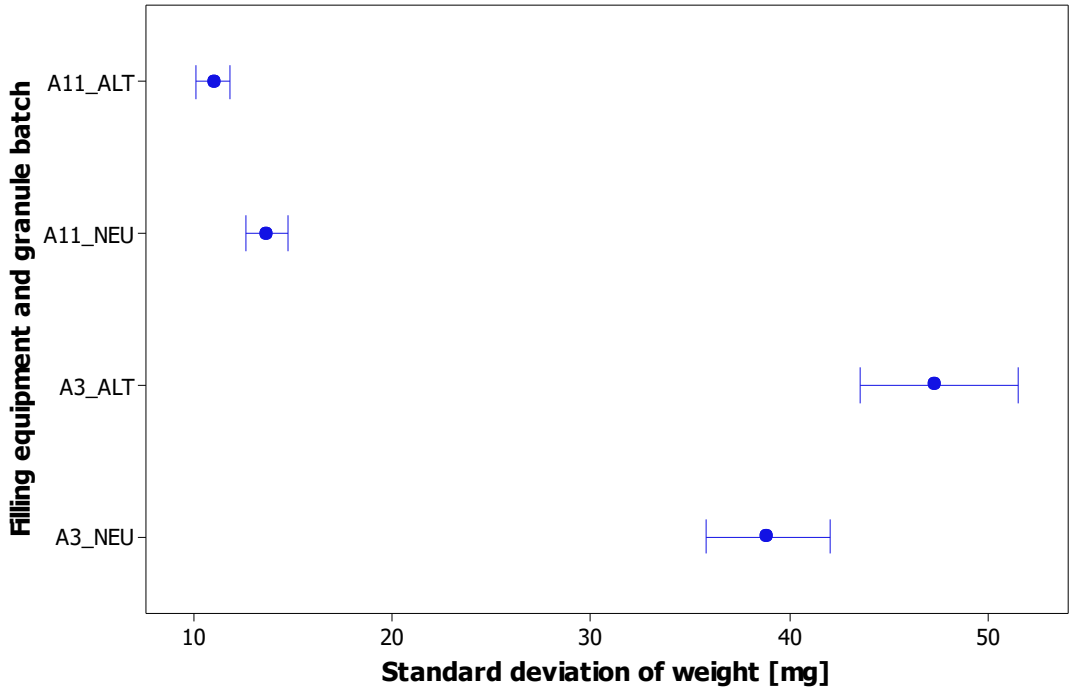

Figure 69: Standard deviation of weight data and their respective 95 % confidence intervals for the powder batches A11 and A03 with different filling equipment (Old vs. New)

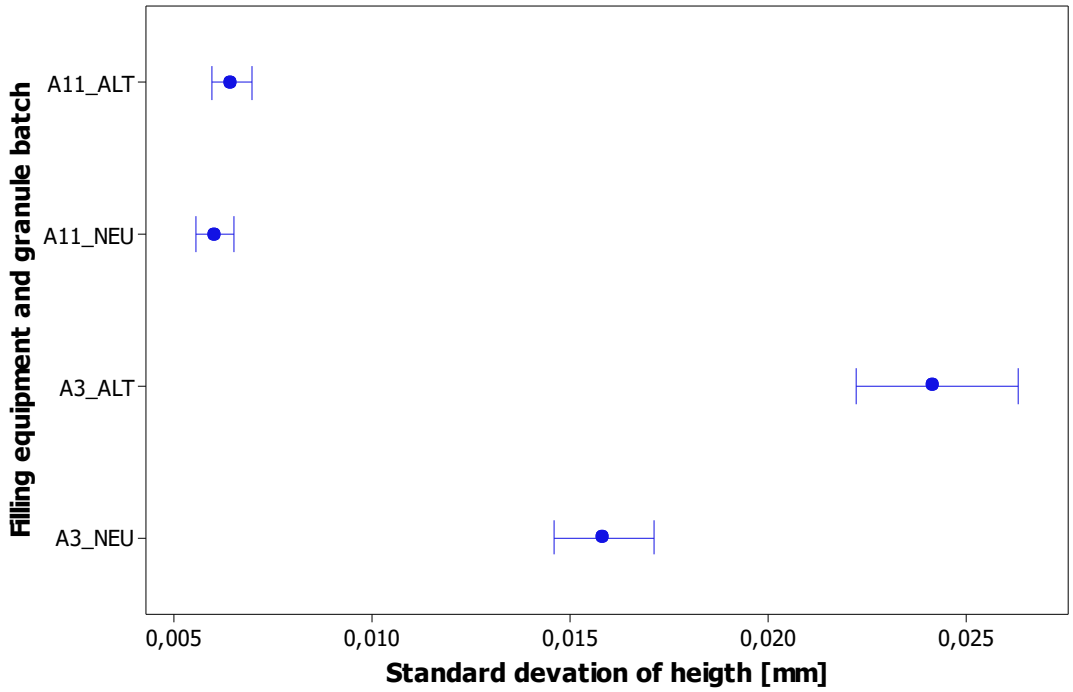

Figure 70: Standard deviation of height data and their respective 95 % confidence intervals for the powder batches A11 and A03 with different filling equipment (Old vs. New)

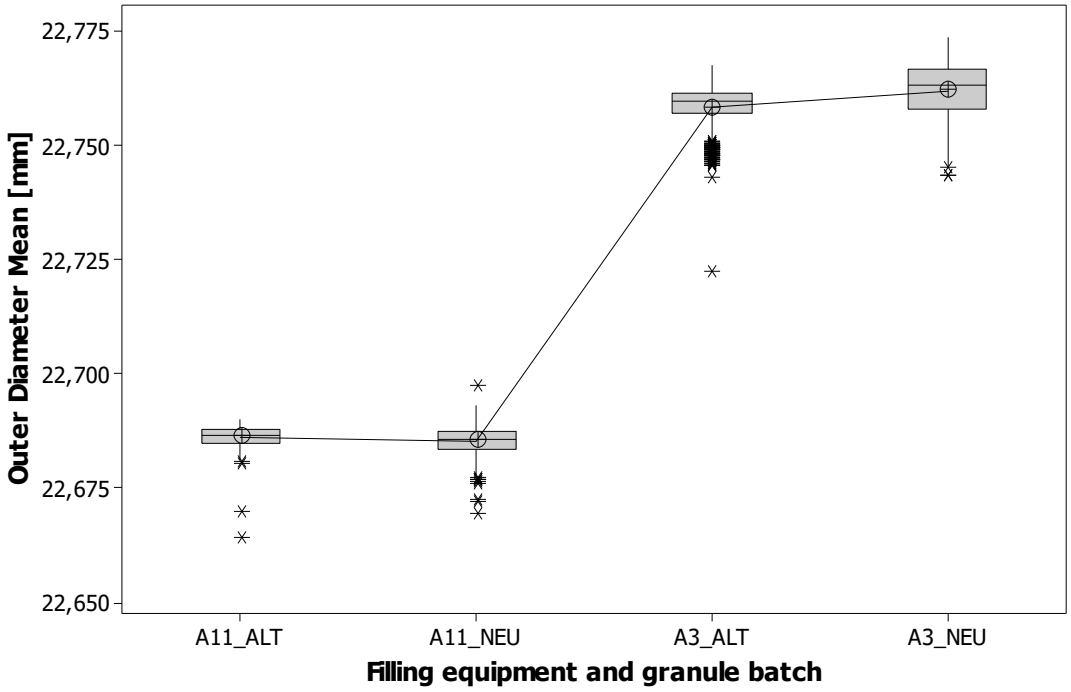

Figure 71: Green part outer diameter data of the powder batches A11 and A03 with different filling equipment (Old vs. New)

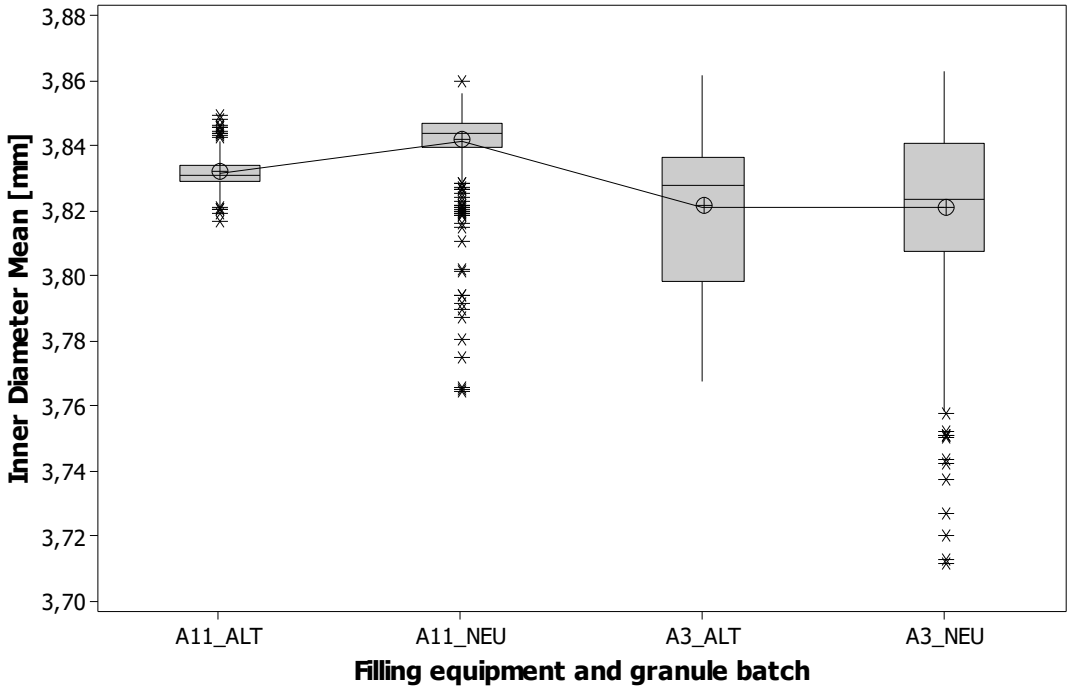

Figure 72: Green part inner diameter data of the powder batches A11 and A03 with different filling equipment (Old vs. New)

7.6. Installation of a mesh inlay in the filling shoe chamber

The sieving of the granular material prior to pressing has already been proven to have a positive influence on the green part result in chapter 7.4. Even though the metal screen (mesh width 200 µm) used had no sizable impact on the particle distribution and yielded no residue, the mechanical strain that impacted the granules by flowing through the mesh had a significant impact on the green parts. This same mechanism of action was tested by directly implementing a metal screen with a mesh size of 2 mm and a rotation of 45° in respect to the filling shoe moving direction into a modified version of the filling shoe "F45". The larger screen size was chosen to not impede the flow of the granular material during the critical stage of die filling. Three different samples of granule batch "A16" were prepared for an experimental comparison do asses the viability of such a mesh inlay. An experimental manufacturing run with the unaltered granule batch "A16" with the unmodified filling shoe "F45" was chosen to establish a baseline. In a second experiment the granule batch "A16" was sieved with the previously employed metal screen with a screen opening width of 200 µm approx. 4 days before pressing and processed with the unmodified filling shoe "F45". The third experimental run employed the unaltered granule batch "A16" but the compaction was carried out by using the modified filling shoe "F45_Mesh_Inlay" with the mesh inlay directly beneath the filling pipe.

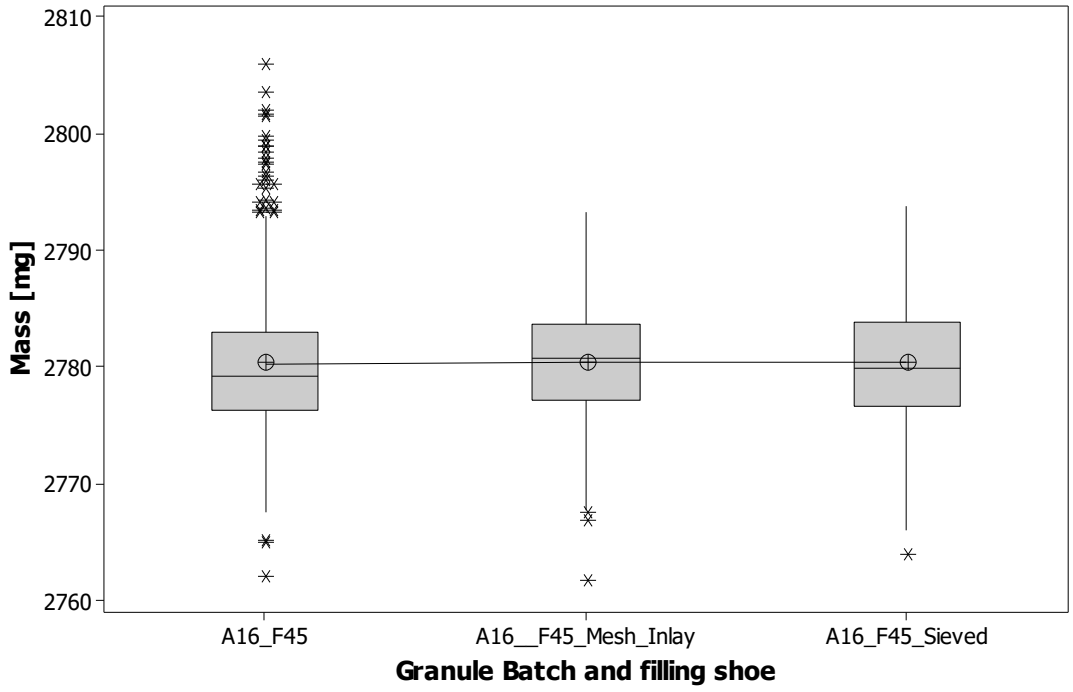

Figure 73: Green part weight data and the comparison between a separate prior sieving and the direct implementation of a mesh in the filling shoe

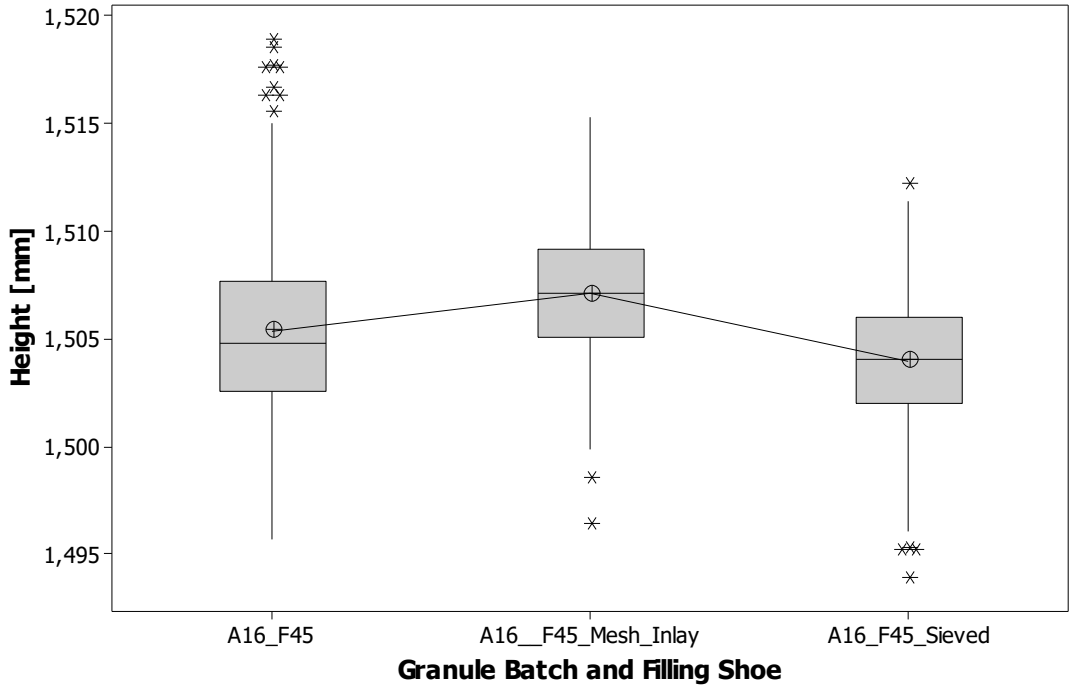

Figure 74: Green part height data and the comparison between a separate prior sieving and the direct implementation of a mesh in the filling shoe

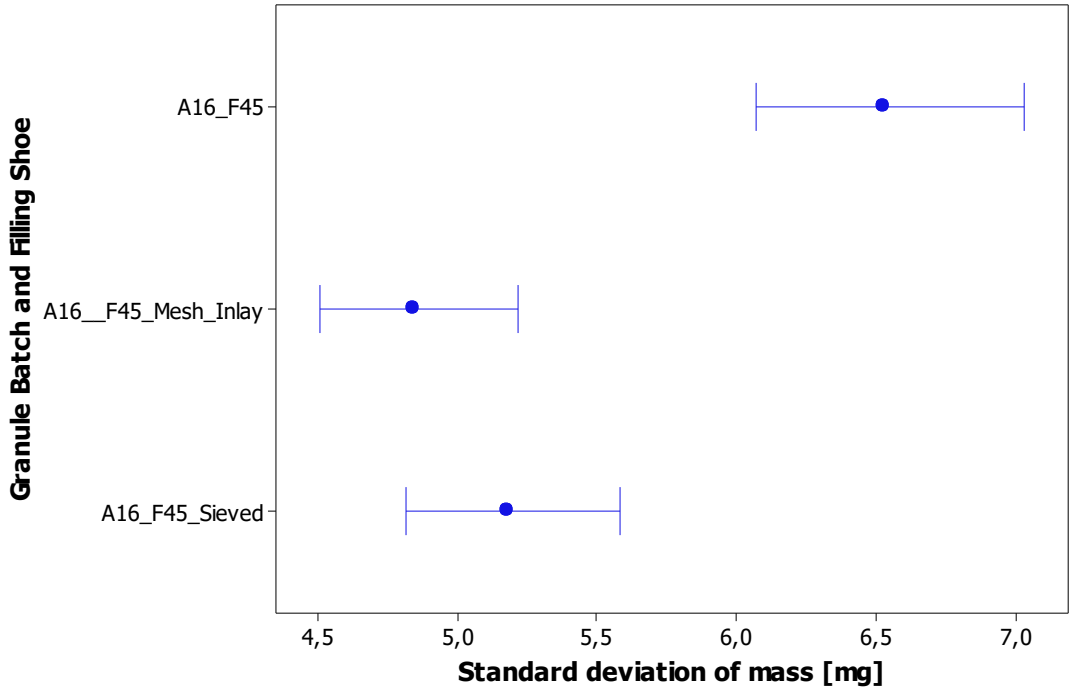

Figure 75: Standard deviation of weight data with their respective confidence intervals and the comparison between a separate prior sieving and the direct implementation of a mesh in the filling shoe

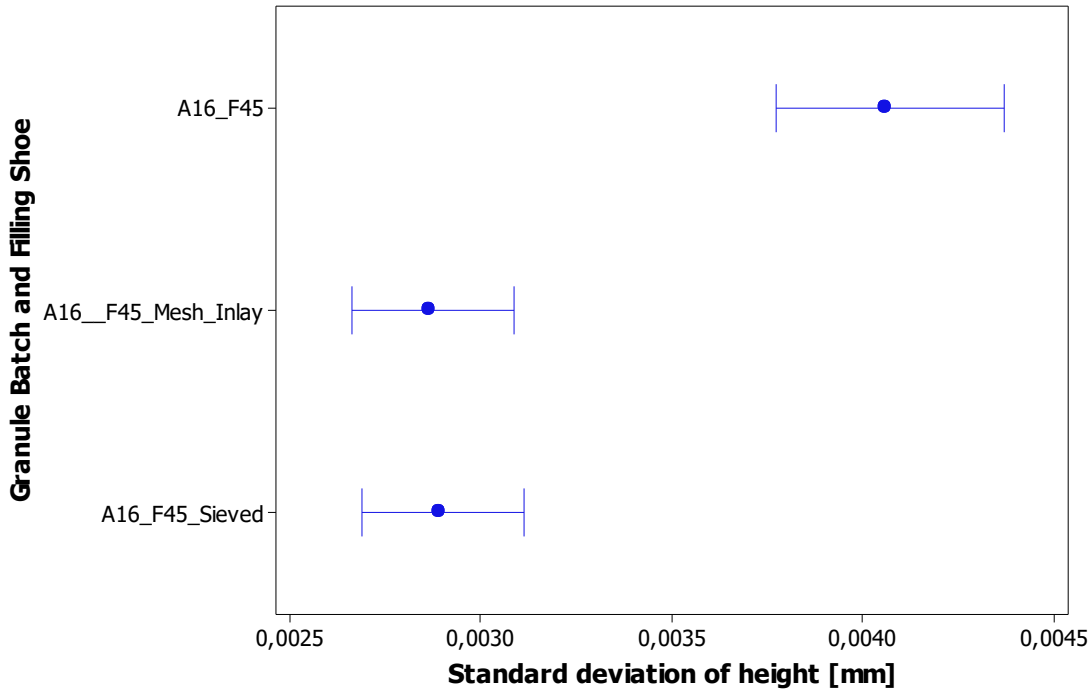

Figure 76: Standard deviation of height data with their respective confidence intervals and the comparison between a separate prior sieving and the direct implementation of a mesh in the filling shoe

There are no clear distinctions in the absolute values of both weight and height, as depicted in Figure 75 and Figure 76, in all three cases the target values of the green parts (2775 mg and 1,5 mm) are held very closely. But in the case of the standard deviations, both the experimental run with the prior sieving of the granular material (A16_F45_Sieved) and the one with the modified filling shoe with a mesh inlay (A16_F45_mesh_Inlay) have shown significant improvement in terms of weight and height. In fact, the tightening of the standard deviation is in both cases very close together with a reduction of about one quarter, as shown in Figure 75 and Figure 76, in comparison to the control experiment. This is true for both weight and height. The experimental results regarding the inner and outer diameter are shown in Figure 77 and Figure 78 and the absolutes values as well as the standard deviations show no clear difference between the three experiments. It could be speculated that the similarity of the experimental results with the mesh inlay and the prior sieving of the granular material, is due to the fact that both interventions seem to eliminate the negative influence that prolonged storing or improper processing seems to have on the granular material. The implementation of a relatively rough mesh directly in between the filling tube outlet and the filling shoe chamber seems to be an effective and simple intervention without the need for additional intermediate process steps.

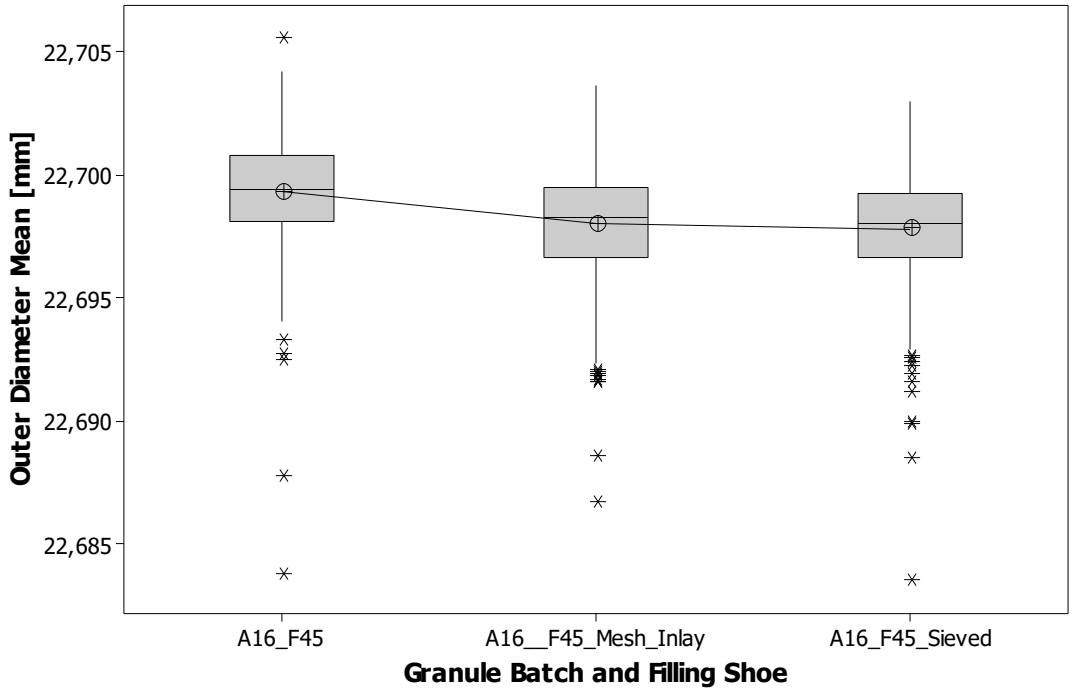

Figure 77: Green part outer diameter data and the comparison between a separate prior sieving and the direct implementation of a mesh in the filling shoe

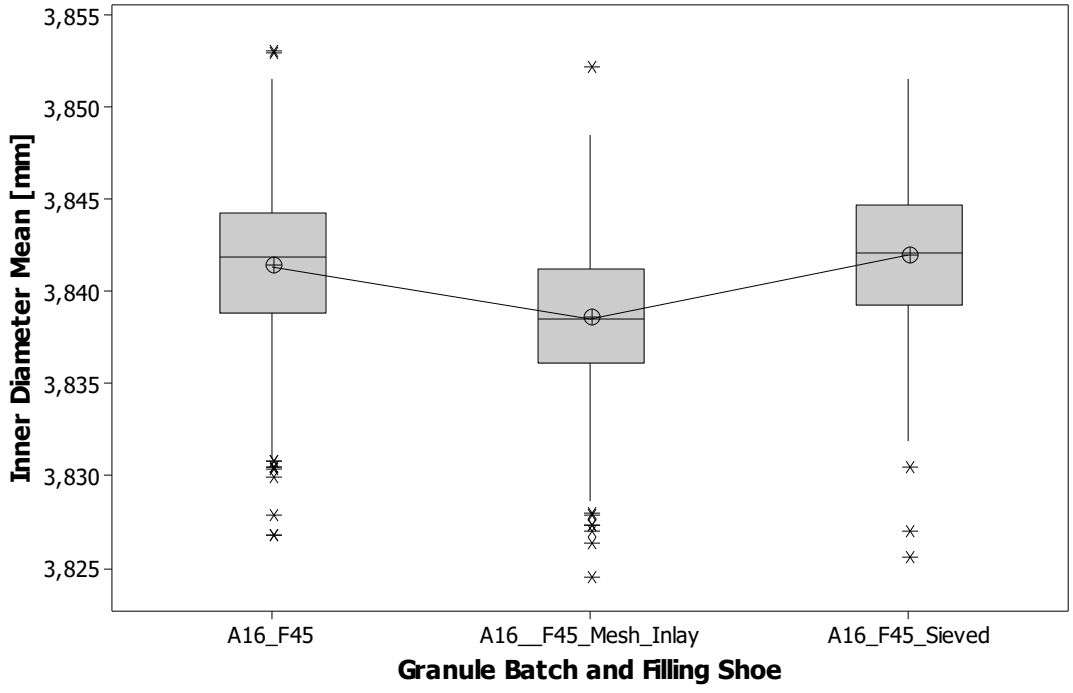

Figure 78: Green part inner diameter data and the comparison between a separate prior sieving and the direct implementation of a mesh in the filling shoe

7.7.Variation of the compaction force and force control on the green parts

The influence of the internal force control mechanism of the DORST TPA6 hydraulic press was assessed by comparing two different manufacturing runs with the granule batch “A16” with the filling shoe “F45” and the hopper “H20” at a machine stroke rate of 15 parts per minute. The only difference was that in one experiment the internal force control was enabled with an intervention threshold of ±0,2 kN. The force curve of the experiment enabled force control is depicted in Figure 80 and shows the individual measured compaction force for each green part along the timeline of the production. The green lines represent the upper and lower threshold for the force control and the violet line represents the arithmetic mean as well as the target value for the compaction force. In comparison with the force curve from the results with a disabled force control, as shown in Figure 79, the impact of the force control near the thresholds is clearly visible. The force control effectively and abruptly manages the fluctuation in compaction force, usually resulting from a fluctuating amount of material in the die. The green part results in terms of weight and height, as depicted in Figure 81 and Figure 82, show no clear sign of the effects of the force control.

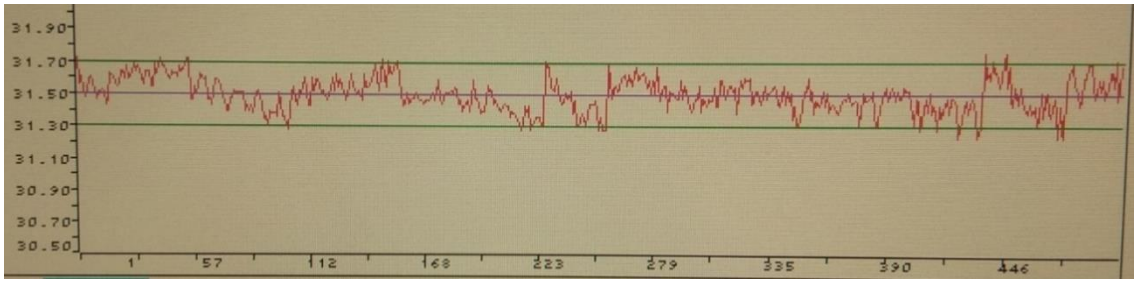

Figure 80: Force curve of an experimental run with granule batch "A16" and enabled force control with an intervention threshold of ±0,2 kN, the abscissa represents the timeline of the 500 compacted parts, the ordinate the corresponding force value in kN for each part

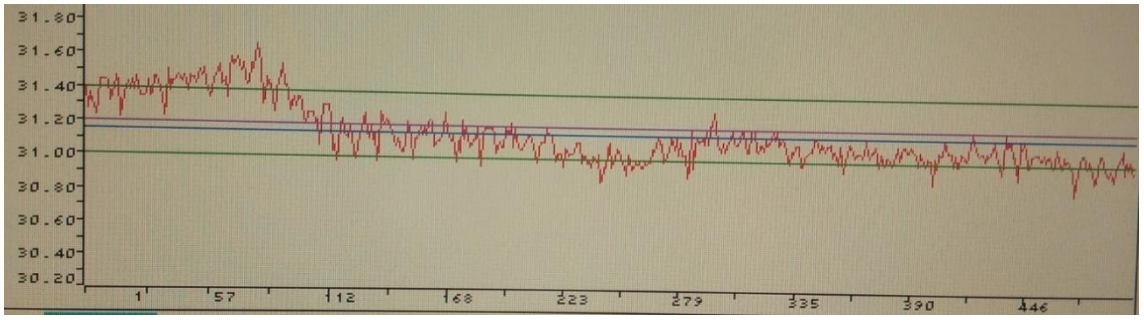

Figure 79: Force curve of an experimental run with granule batch "A16" and disabled force control, the abscissa represents the timeline of the 500 compacted parts, the ordinate the corresponding force value in kN for each part

The same is true for the standard deviations of these parameters. In addition, the green part data regarding the inner and outer diameter, as depicted in Figure 83 and Figure 84, also shows no clear distinction between the two experiments. The sample size of 500 parts that

were manufactured for these experiments may be too small to accurately evaluate the drift of the compaction force and the influence the force control could have on mitigating these fluctuations with the resulting impact on the compacted green parts.

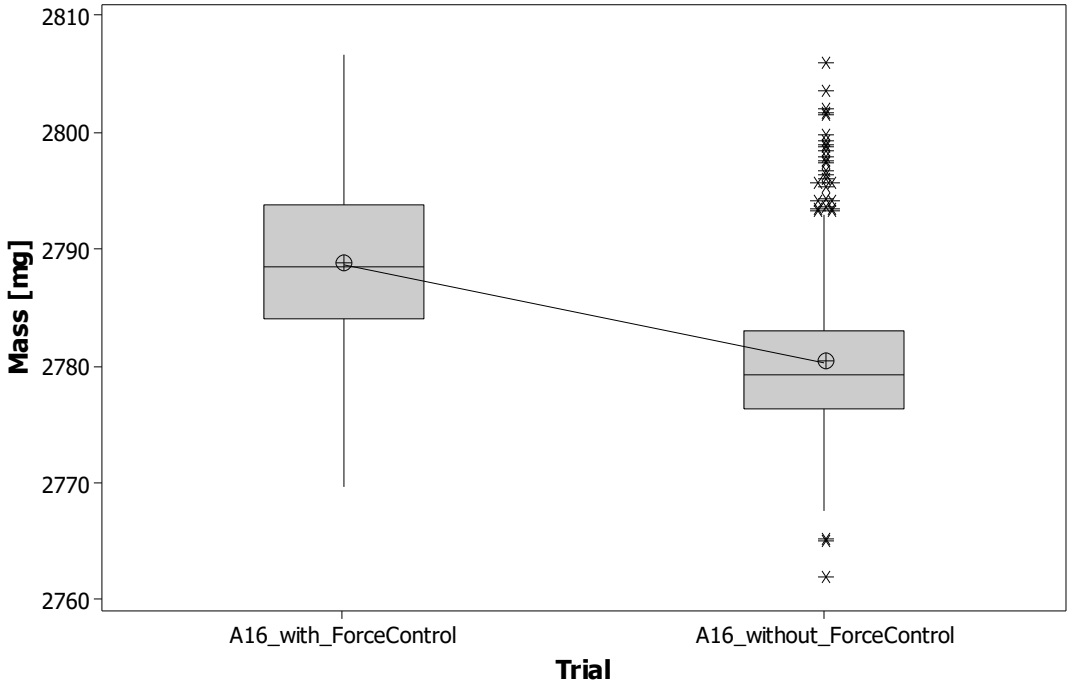

Figure 81: Green part weight data and the comparison between disabled and enabled force control

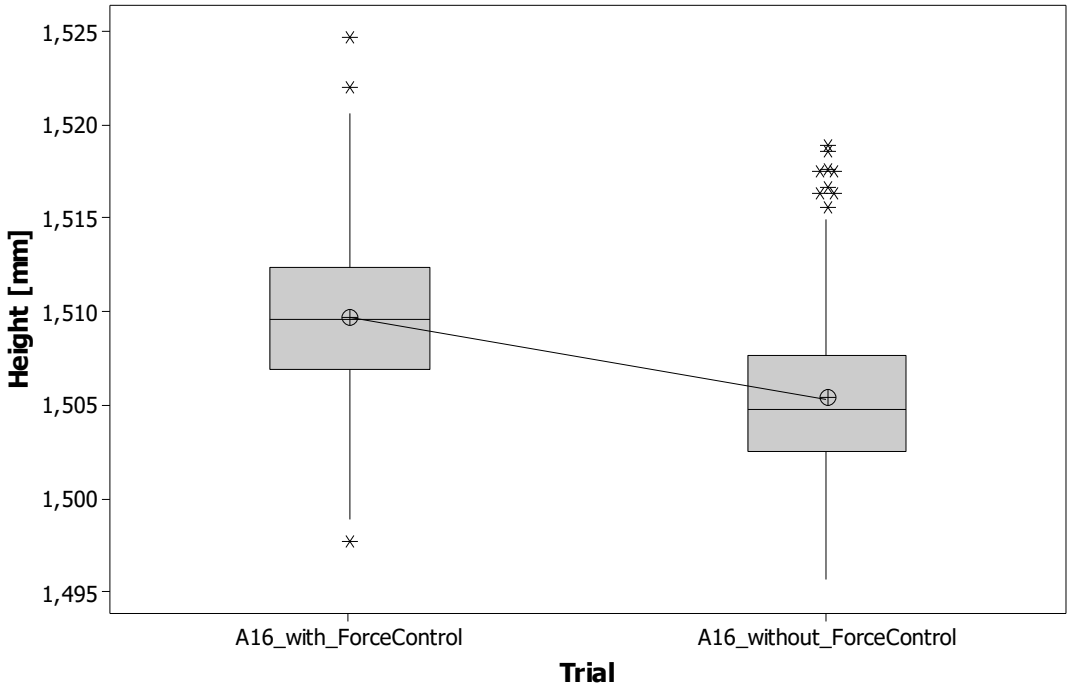

Figure 82: Green part height data and the comparison between disabled and enabled force control

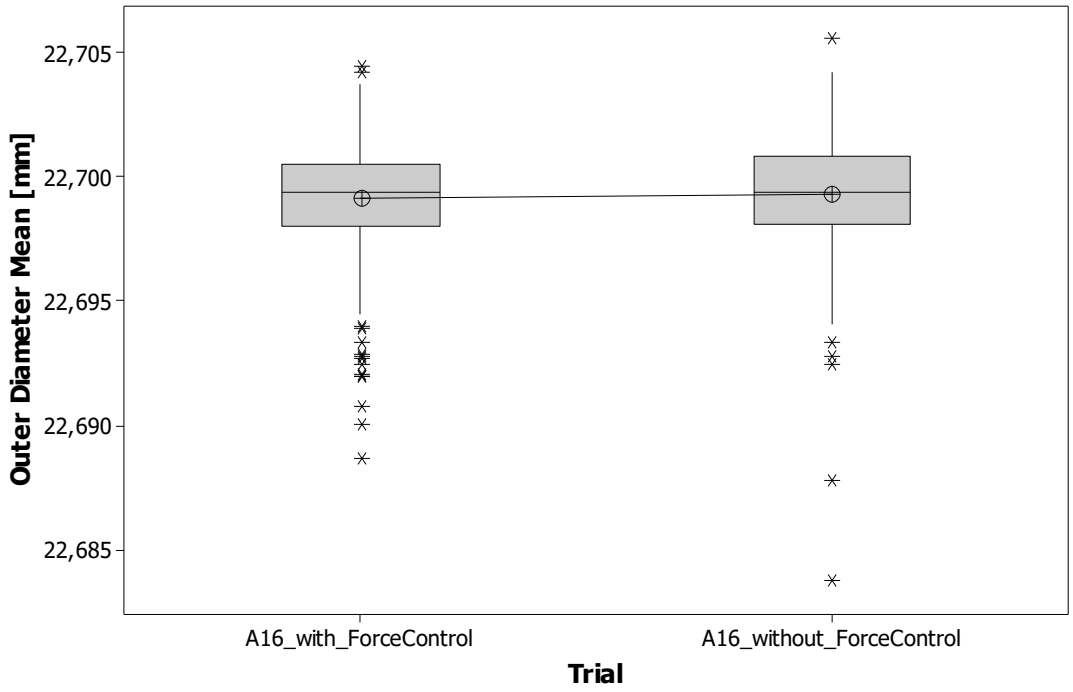

Figure 83: Green part outer diameter data and the comparison between disabled and enabled force control

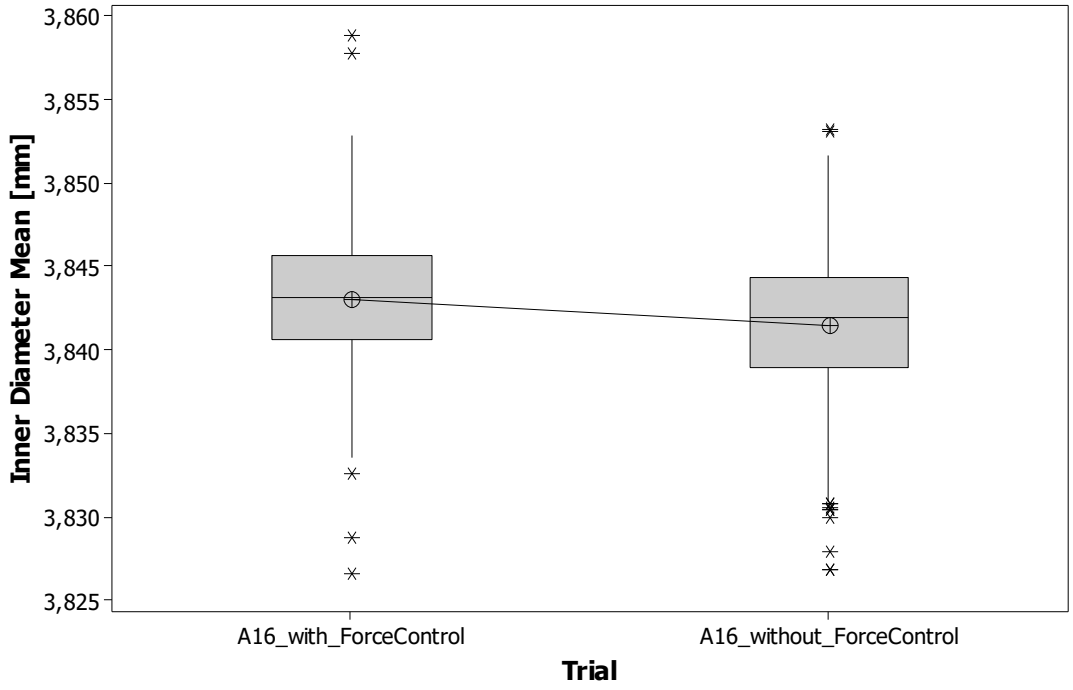

Figure 84: Green part inner diameter data and the comparison between disabled and enabled force control

The importance of the part-to-part variation of the compaction force as a predictor for the part-to-part variation of the green bodies in terms of both weight and thickness is shown in Figure 85 and Figure 86. By analyzing the data of all experimental manufacturing runs that

were conducted over the course of thesis an overall linear correlation of 0,956 for the standard deviation of the weight and the standard deviation of the compaction force could be calculated. A linear correlation 0,981 could be calculated between the standard deviation of the height and the standard deviation of the compaction force.

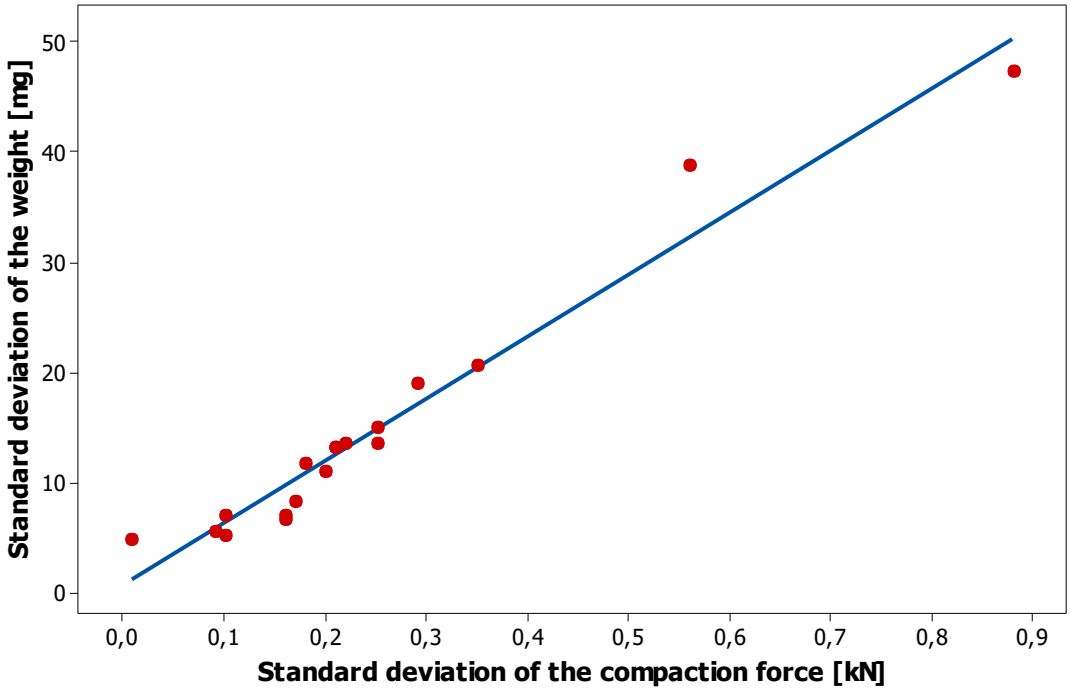

Figure 85: Scatter plot of the standard deviation of the compaction force and standard deviation of the green part weight across all experiments and a linear fit with a correlation of 0,956

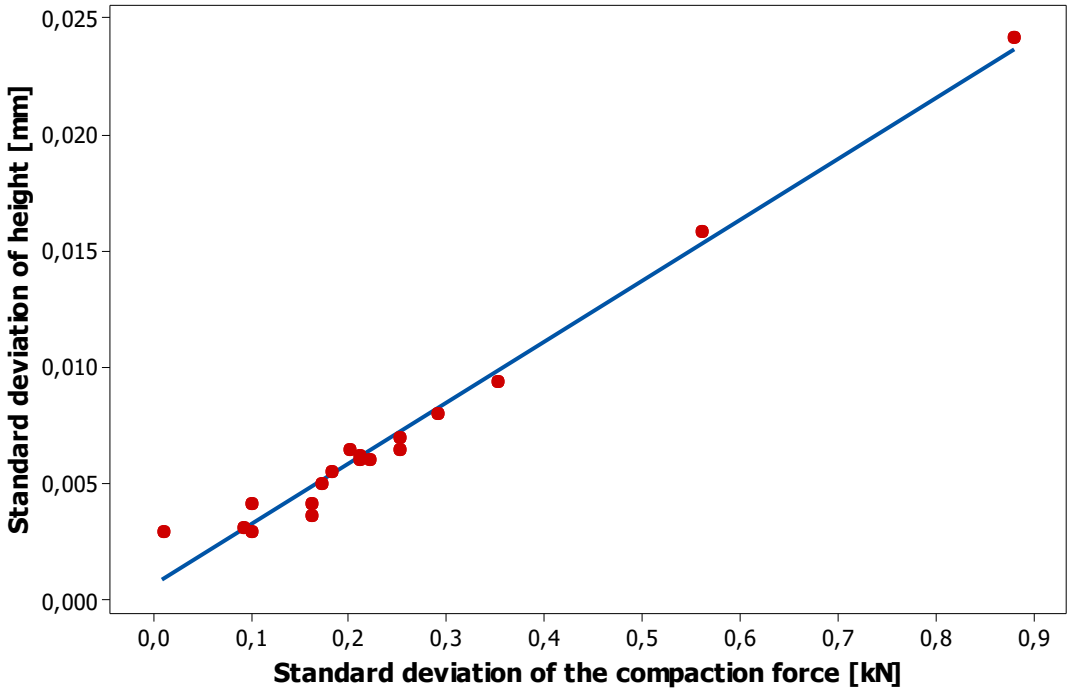

Figure 86: Scatter plot of the standard deviation of the compaction force and standard deviation of the green part height across all experiments and a linear fit with a correlation of 0,981

7.8. Influence of the particle properties on the green parts

The influence of the granule properties on the compaction cycle cannot be understated. Beginning from the flowability and the consequent filling of the cavity, to the establishment of the microstructure and the following densification of the granular material into a solid piece of ceramic, the properties of the particle have a big influence that is then carried further along the entire processing chain until the ceramic product is finished. One of the aims of thesis was to find and establish a relationship between the particle properties and the final results of the compacted green parts. Therefore, the data of all experimental manufacturing runs was analyzed for distinct linear correlations. Several particle properties displayed strong linear correlations, namely a Pearson correlation of at least 0,8 in relation to either the standard deviation of the green part weight or height.

The residual moisture content of the granule batches has shown a strong linear correlation of 0,85 with the standard deviation of the green part weight, as depicted in Figure 87. Even though the mass friction of the moisture is already at a very low level of approx. 0,001 to 0,002, a lower moisture content results in the more consistent filling of the die cavity in regard to material weight. The standard deviation of the green part height strongly correlates (0,8) with the moisture content as well, as depicted in Figure 88 The mass fraction of the organic materials, as measured through the ignition loss (GV) has also shown a strong correlation of 0,8 with the standard deviation of the green part weight, as depicted in Figure 91. The majority of granule batches have a measured ignition loss of 0,029 to 0,031 which is very close to the target of 0,03, yet a slightly lower organic mass fraction is associated with a more consistent result in terms of the green part weight. This effect could be further examined by varying the binder content of the granules. The axial strength of a sample test compact (w_{sa}), that is pressed during the analyzing process of the PTC-03DT powder testing center also shows a strong correlation 0,82 with the standard deviation of the green part weight, as depicted in Figure 90. This pressure represents the maximal pressure that can be applied during the testing procedure before the sample green part is crushed. This is a measure for the green strength that holds the part together and is especially important during ejection from the die. The experimental data however shows that an increased green strength is inversely associated with a more consistent green part result in terms the part weight. Unsurprisingly, the cohesiveness (C) of the test compact, that is pressed during examination with the powder testing center, also displays a strong correlation of 0,83 with the standard

deviation of the green part weight and represents the ratio of the axial strength within the green part to the friction forces that occur between the die and the ceramic material. Cohesiveness (C) values between 1,5 and 2 were common for the granule batches and a lower value is associated with a superior green part result in terms of weight. However a cohesiveness (C) value below 1 is clear indicator for the development of cracks during ejection. [26]

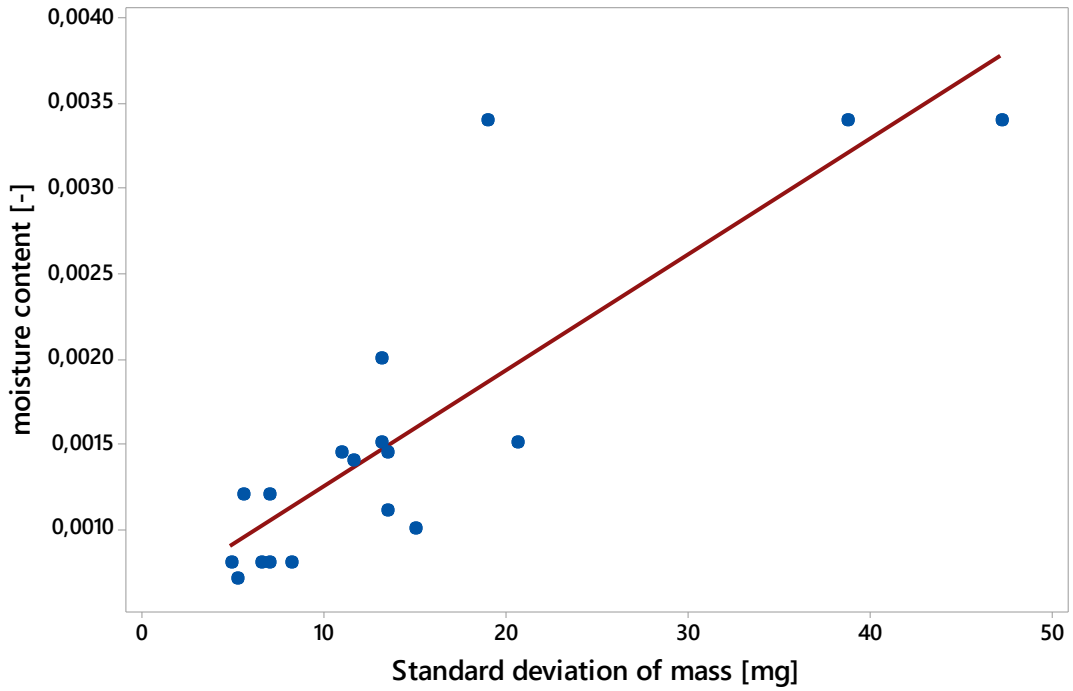

Figure 87: Scatterplot of the particle moisture content and the standard deviation of mass of the green part with a linear correlation of 0,85

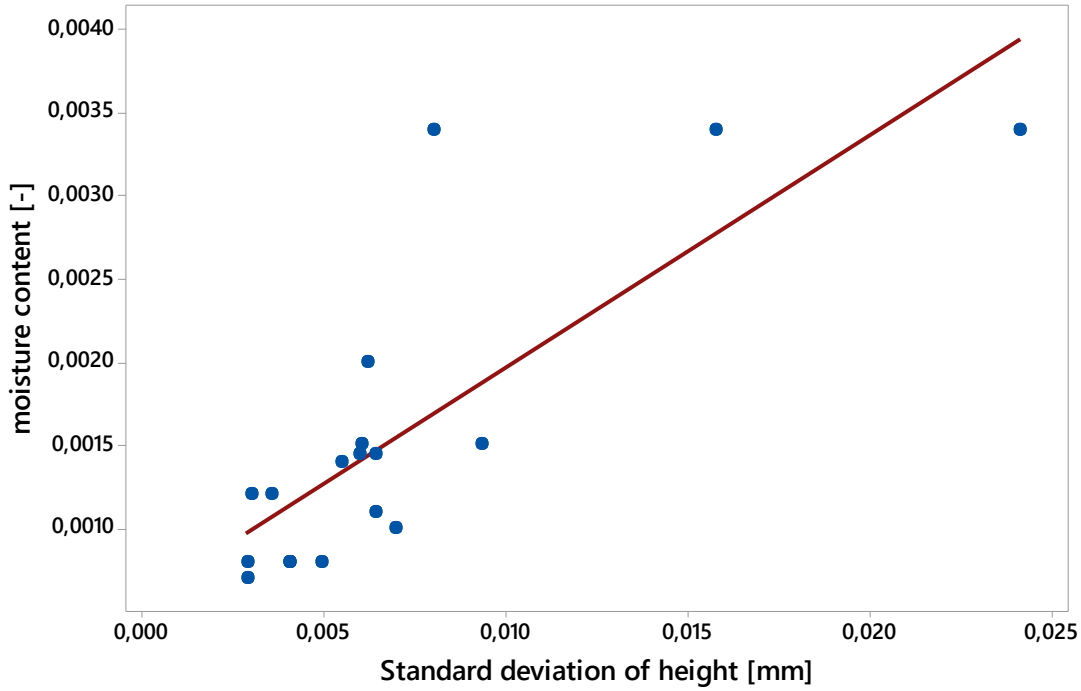

Figure 88: Scatterplot of the particle moisture content and the standard deviation of height of the green part with a linear correlation of 0,8

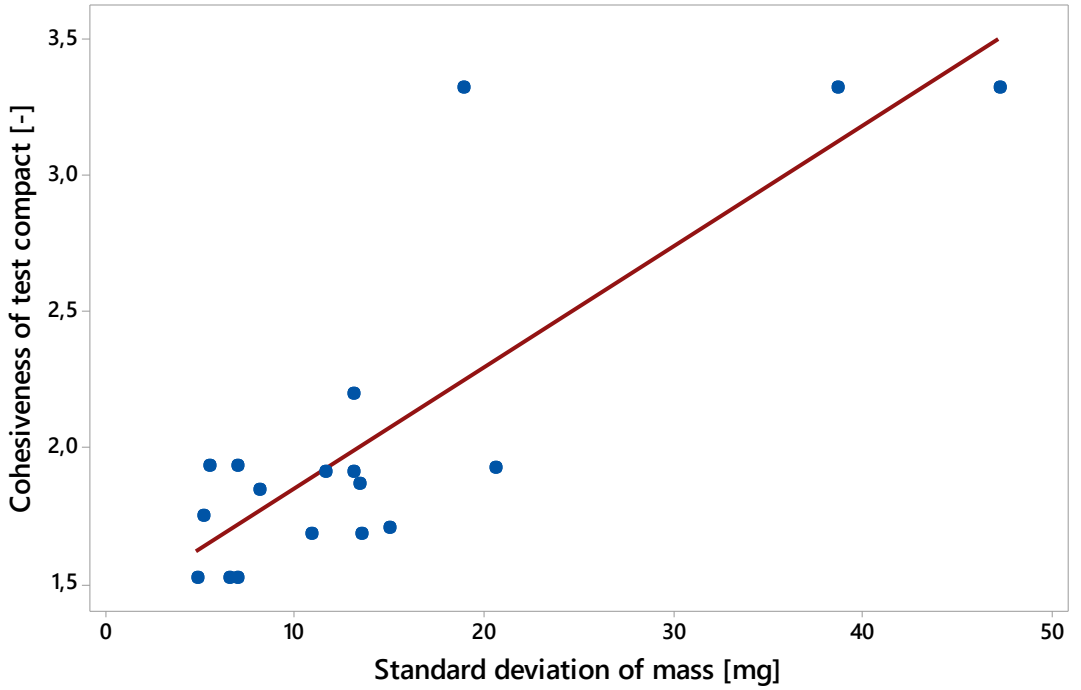

Figure 89: Scatterplot of the cohesiveness of a powder testing center test compact and the standard deviation of mass of the manufactured green part with a linear correlation of 0,83

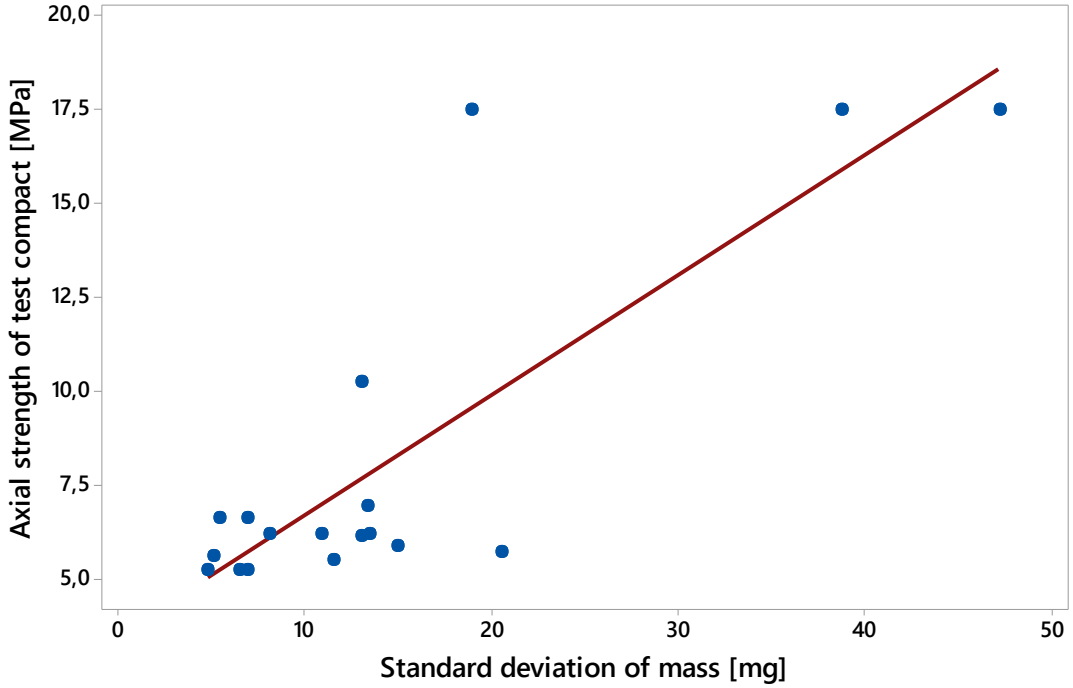

Figure 90: Scatterplot of the axial strength of a powder testing center test compact and the standard deviation of mass of the manufactured green part with a linear correlation of 0,82

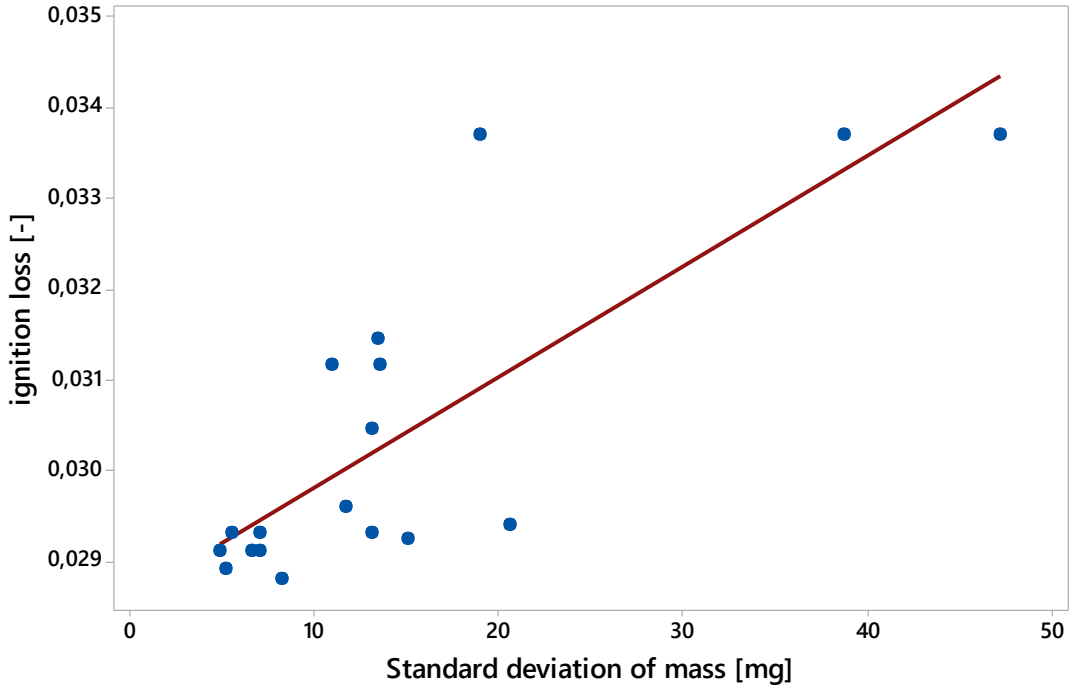

Figure 91: Scatterplot of the ignition loss of the granule batch and the standard deviation of mass of the green part with a linear correlation of 0,8

8. Conclusion

The compaction cycle that occurs during the uniaxial die compaction is a complex process that can be influenced by a variety of different parameters ranging from the granule properties to the die filling equipment and the operating conditions of the hydraulic press. Several process parameters where discovered over the course of this thesis that had significant influence on the green parts.

Because of the experimental manufacturing runs it could be determined that the custom binder system “PTC” should be preferred over the binder “Optapix PAF2”. The “PTC” formulation showed a more consistent part-to-part result in terms of weight and geometry and was not subject to additional geometric expansion after ejection, in comparison with “Optapix PAF2”. The particle size distribution of the used granule batches was examined in an isolated experiment. It was shown that the variation of the disk atomizer speed during spray-drying and the resulting shift in the size distribution has a nonlinear connection with the green part results, as both finer (15000 rpm) and coarser (5000 rpm) particle populations yielded better results than the established default of 12000 rpm. An examination of all the experiments in regard to their particle size distribution and the green part results did not offer further evidence on this connection. However, other particle properties have shown a strong linear correlation with the standard deviation of the green part weight. A slightly lower residual moisture content as well as organic content in the granule batches is associated with a lower part-to-part variation of the green part weight. In addition, a lower axial green strength, as determined with the PTC-03DT powder testing center, is also associated with a lower part-to-part variation of the green part weight.

The variation in the pacing of the compaction cycle has yielded mixed results, depending on the binder system of the granules. In the case of “Optapix PAF2”, the increase of the pacing from 15 to 20 parts per minute has yielded a clear improvement of the part-to-part variation of the green part in terms of weight and height. However, the granule batch with the binder system “PTC” has yielded a negative result in terms of both weight and height variation of the green part results, through the same increase of the pacing.

The impact of the internal force control mechanism of the hydraulic press has yielded no conclusive evidence regarding the produced green parts. Across all experiments however, the standard deviation of the compaction force has a very strong linear correlation with the part-to-part deviation of the green bodies in terms of weight and height.

Two different die filling equipment sets, consisting of the filling shoe and the feeding funnel and their impact on the green parts have been examined. The filling setup with a steeper funneling tapering as well as a steeper filling tube angle has yielded mixed results, depending on the binder system of the used granule batches, in comparison to the initial equipment. In the case of “Optapix PAF2” the steeper angles of the filling equipment resulted in a significant improvement of the green part results in terms of weight and height. In the case of the granule samples with the “PTC” binder, the results did not show such clear improvements, the part-to-part variation of the green part weight, inner and outer diameter has in fact even increased.

The sieving of the granule batches directly after granulation as well as prior to pressing with a conventional metal screen with a screen opening width of 200 µm, large enough to leave no residue on the screen, has also shown a distinct improvement of the green part results in both weight and height. The same improvement in green part results has also been achieved by directly implementing a screen with 2 mm screen opening width into the filling show, directly beneath the filling tube. The sieving of the granule batch prior to pressing as well as the implementation of a mesh directly into the filling shoe have yielded the biggest improvement of part-to-part-variation of all the process parameters and interventions that were experimentally examined over the course of this thesis.

9. Outlook

The uniaxial die compaction is influenced by a plethora of different parameters, beginning with the production of the granules and their resulting properties, to the various technical problems that occur during the compaction cycle and the impact of the equipment and their operating conditions.

The formulation of the binder system that is added prior to the granulation of the raw material has a significant effect on the properties of the green parts and therefore warrants further investigation into the formulation of the binder system as well as the variation of the mass fraction of the binder in relation to the primary material. The influence of the grain size distribution on the green part results could not be resolved sufficiently during this thesis, further investigation with granule samples that possess either a much wider or narrower size distribution can be considered. Small variations in the residual moisture content of the granule batches have also shown to be associated with the properties of the green parts and a controlled increase or decrease of this measured moisture content in an experimental context can also provide additional evidence to substantiate this correlation. Eventually the creation of an accurate prediction model that ties the preparation of the raw material and the granulation of the raw powder and the resulting granule properties with the properties of the compacted green parts could lead to a clear advantage to produce the ceramic disc with minimal part-to-part variation.

Since the pacing of the compaction cycle has a large influence on the economic feasibility of the manufacturing process, further investigation into the increase of the machine stroke rate and the impact on the green parts, well beyond the 20 parts per minute that were examined during this thesis, is warranted. The impact of the force control, especially the parameterization of the force control mechanism, could also not be determined. This can be further investigated as the standard deviation of the compaction force is heavily correlated with the green part properties and a further decrease in this part-to-part variation could yield a superior result. The filling shoe equipment, especially the filling shoe, can be further examined and possibly improved through an extensive computer simulation model, as the

custom fabrication of such an experimental filling shoe is cost prohibitive and therefore changes to the shape and geometry should be well thought out.

The pseudo-sieving of the granule batch prior to pressing or directly in the filling shoe, has yielded the biggest influence on the green part properties of all the experimental interventions over the course of this thesis. However, the mechanism of action behind this procedure is not well understood and could not be objectified with the experimental data. Further investigation into this matter could yield insight on how to counteract this negative influence prior to pressing or eliminate it entirely through various adjustments to the granulation process.

The microstructure of the green part has significant impact on the finished ceramic product, as defects that occur during the compaction cycle are very hard to correct further down the processing chain. A large focus of this thesis was to examine the part-to part variation of the green parts, but the point-to-point variation of each individual green part also provides valuable insight to improve the final properties of the ceramic component. A preliminary qualitative investigation of the radiodensity gradients throughout the green part could not be finished during this work. Further investigation into the actual microstructure, with a scanning electron microscope as well as further computer tomographic assessment to establish a correlation between the radiodensity and the bulk density could possibly yield more insight into the density distribution and possible counteractions.

10. References

[1] H. Salmang and H. Scholze, *Keramik*, 7. Auflage. Berlin: Springer, 2007.

[2] K.-D. Linsmeier, *Technische Keramik*. Landsberg am Lech: Verlag Moderne Industrie, 2013.

[3] A. F. Hottinger, P. Pacheco, and R. Stupp, "Tumor treating fields: A novel treatment modality and its use in brain tumors," *Neuro. Oncol.*, vol. 10, no. 18, pp. 1338–1349, 2016.

[4] David Michael Fanning, "Structure property relations in ferroelectric materials," PhD Thesis, University of Illinois at Urbana-Champaign, 2000.

[5] EPCOS OHG, "Novocure NC-Disc – Process Flow - Update 25/7/2017." Internal Report, Deutschlandsberg, 2017.

[6] P. Frischholz, *Breviary Technical Ceramics*. Selb: Verband der Keramischen Industrie e.V., 2004.

[7] "Sintering Stages." [Online]. Available: http://www.uobabylon.edu.iq/eprints/publication_11_16913_560.pdf. [Accessed: 27-Feb-2018].

[8] R. Oberacker, "Powder Compaction by Dry Pressing," in *Ceramics Science and Technology: Synthesis and Processing*, 1st ed., vol. 3, R. Riedel and I.-W. Chen, Eds. 2012.

[9] P. Beiss, *Pulvermetallurgische Fertigungstechnik*. Berlin: Springer Vieweg, 2013.

[10] "Höganäs Handbook for Sintered Components." [Online]. Available: https://www.hoganas.com/globalassets/media/sharepoint-documents/HandbooksAllDocuments/Handbook2_Production_of_Sintered_Components_December_2013_0675HOG_interactive.pdf. [Accessed: 28-Feb-2018].

[11] A. Sosnik and K. P. Seremeta, "Advantages and challenges of the spray-drying technology for the production of pure drug particles and drug-loaded polymeric carriers," *Adv. Colloid Interface Sci.*, vol. 223, no. 1, pp. 40–54, 2015.

[12] M. Mezhericher, A. Levy, and I. Borde, "Theoretical models of single droplet drying kinetics: A review," *Dry. Technol.*, vol. 28, no. 2, pp. 278–293, 2010.

[13] G. A. Smolenskii and A. I. Agranovskaya, "Dielectric polarization and losses of certain complex compounds," *Zhurnal Tekhnicheskoi Fiz.*, vol. 28, no. 7, pp. 1491–1493, 1958.

[14] A. A. Bokov and Z. G. Ye, "Recent progress in relaxor ferroelectrics with perovskite structure," *J. Mater. Sci.*, vol. 41, no. 1, pp. 31–52, 2006.

[15] Zschimmer & Schwarz, "Dolapix PC 75 - Dispering Agent / Deflocculant." [Online]. Available: http://www.zschimmer-schwarz.com/DOLAPIX_PC_75/simon/zschimmer-schwarz/media/site/downloads/merkblatt/1_K_K_EN_1245_00_1_100.pdf. [Accessed: 15-Nov-2017].

[16] M. Mrksich and M. Whitesides George, "Poly(ethylene glycol)," *ACS Symp. Ser.*, vol. 680, no. 1, pp. 361–373, 1997.

[17] Dow Chemical, "Chemistry of METHOCEL™ Cellulose Ethers - A Technical Review," p. 16, 2013.

[18] Zschimmer & Schwarz, "Contraspum K1012 - Antifoam agent." [Online]. Available:

http://www.zschimmer-schwarz.com/CONTRASPUM_K_1012/simon/zschimmer-schwarz/media/site/downloads/merkblatt/1_K_K_EN_5071_40_3_500.pdf. [Accessed: 15-Nov-2017].

[19] "Mowilith® DN 50 - Celanese - datasheet." [Online]. Available: https://adhesives.specialchem.com/product/p-celanese-mowilith-dn-50. [Accessed: 07-Mar-2018].

[20] Zschimmer & Schwarz, "Optaoix PAF 2 - Temporary Binder." [Online]. Available: http://www.zschimmer-schwarz.com/OPTAPIX_PAF_2/simon/zschimmer-schwarz/media/site/downloads/merkblatt/1_K_K_EN_2515_00_2_800.pdf. [Accessed: 15-Nov-2017].

[21] Retsch Technology, "Particle Analyzer CAMSIZER XT." [Online]. Available: http://www.horiba.com/fileadmin/uploads/Scientific/Documents/PSA/CAMSIZER_XT_flyer.pdf. [Accessed: 15-Nov-2017].

[22] L. Microsystems, "Leica DM4000–6000," 2013. [Online]. Available: https://www.leica-microsystems.com/fileadmin/downloads/Leica DM4000 M LED/Brochures/Leica_DM4000-6000-BrochureTechnical_en.pdf. [Accessed: 16-Nov-2017].

[23] Feeman Technology, "Powder Testing with the FT4 Powder Rheometer." [Online]. Available: http://www.freemantech.co.uk/_powders/ft4-powder-rheometer-universal-powder-tester. [Accessed: 16-Nov-2017].

[24] D. Schulze, "Fließeigenschaften von Schüttgütern," in *Pulver und Schüttgüter. VDI-Buch*, Berlin: Springer, 2009.

[25] "VISCOSITY CUP DIN 53211." [Online]. Available: https://www.tqc.eu/rsrc/artikel_downloads/viscosity-cup-interchangeable-nozzle-vf2020-d44.pdf. [Accessed: 12-Dec-2017].

[26] KZK Powder Tech Corp., "KZK PTC-03DT Manual V27." Monkton, MD, 1998.

[27] Mitutoyo Corporation, "ID-H0530/0560 Digimatic Indicator User's Manual." [Online]. Available: https://www.mitutoyo.co.jp/eng/support/service/manual/pdf/99MAH016B3_ENG.pdf. [Accessed: 12-Dec-2017].

[28] Imaging Source, "DMK 23GM021 - GigE monochrome industrial camera." [Online]. Available: https://www.theimagingsource.com/products/industrial-cameras/gige-monochrome/dmk23gm021/. [Accessed: 21-Nov-2017].

[29] Opto Engineering, "TC13036." [Online]. Available: http://www.opto-telecentric.com/media/pdf/TC13036-datasheet-de.pdf. [Accessed: 21-Nov-2017].

[30] Falcon-Illumination, "FLDR-i90B Lighting Picture Lighting Dimension," 2015. [Online]. Available: http://www.falcon-illumination.com/_datasheet/FLDR-B/DataSheet FLDR-i90B.pdf. [Accessed: 21-Nov-2017].

[31] "Sartorius CUBIS ® Analytical Model MSA225S-000-DU." [Online]. Available: http://balancecanada.com/Documents/MSA225S-000-DU_000.pdf. [Accessed: 21-Nov-2017].

[32] M. Stieß, *Mechanische Verfahrenstechnik - Partikeltechnologie 1*. Berlin: Springer, 2009.

[33] D. E. Niesz, "A review of ceramic powder compaction," *KONA Powder Part. J.*, vol. 14, no. 3, pp. 44–51, 1996.

List of Figures

List of Tables